Control of Crystallization Processes Based on Population Balances

Dissertation
zur Erlangung des akademischen Grades

Doktoringenieur
(Dr.-Ing.)

von Dipl.-Ing. Ulrich Vollmer

geb. am 9. März 1972 in Kirchheim unter Teck

genehmigt durch die Fakultät für Elektrotechnik und Informationstechnik
der Otto-von-Guericke-Universität Magdeburg

Gutachter: Prof. Dr.-Ing. habil. Jörg Raisch
Prof. Dr.-Ing. habil. Andreas Seidel-Morgenstern
Prof. Dr. Doraiswami Ramkrishna

Promotionskolloquium am 20. Mai 2005

Forschungsberichte aus dem Max-Planck-Institut
für Dynamik komplexer technischer Systeme

Band 11

Ulrich Vollmer

Control of Crystallization Processes Based on Population Balances

Shaker Verlag
Aachen 2005

Bibliographic information published by Die Deutsche Bibliothek
Die Deutsche Bibliothek lists this publication in the Deutsche Nationalbibliografie; detailed bibliographic data is available in the internet at http://dnb.ddb.de.

Zugl.: Magdeburg, Univ., Diss., 2005

Printed in Germany.

ISBN 3-8322-4317-8
ISSN 1439-4804

Shaker Verlag GmbH • P.O. BOX 101818 • D-52018 Aachen
Phone: 0049/2407/9596-0 • Telefax: 0049/2407/9596-9
Internet: www.shaker.de • eMail: info@shaker.de

Vorwort

Die vorliegende Arbeit entstand während meiner Tätigkeit als wissenschaftlicher Mitarbeiter am Max-Planck-Institut für Dynamik komplexer technischer Systeme in Magdeburg. Ich hatte das Vergnügen, zu sehen wie das Institut gewachsen ist, von den Anfängen mit einer Hand voll Mitarbeitern in Räumen der Universität Stuttgart bis hin zum beeindruckenden Institutsgebäude an der Elbe, in dem rund 150 Mitarbeiter tätig waren.

Mein Dank gilt an erster Stelle Herrn Prof. Dr.-Ing. habil. Jörg Raisch, der mein Interesse am Thema dieser Dissertation geweckt, mich bei der Bearbeitung stets unterstützt und mir dabei ein außergewöhnliches Maß an Freiraum eingeräumt hat.

Herrn Prof. Dr.-Ing. habil. A. Seidel-Morgenstern danke ich für sein Interesse an meiner Arbeit und die Begutachtung derselben. Weiter danke ich Herrn Prof. Dr. D. Ramkrishna für die freundliche Übernahme eines weiteren Mitberichts.

Darüberhinaus bedanke ich mich beim Gründungsdirektor des Max-Planck-Instituts Herrn Prof. Dr.-Ing. Dr.h.c. mult. E.D. Gilles, der die günstigen Rahmenbedingungen ermöglicht hat, unter denen meine Arbeit entstanden ist.

Den Mitarbeitern am Institut, insbesondere den Kollegen in der Fachgruppe für System- und Regelungstheorie und im Kristallisationsprojekt sowie den „Stuttgartern“ Stefan Motz und Aleksandar Mitrović danke ich für offene Türen, für vielfältige Hilfe und für ebenso anregende wie kurzweilige Diskussionen. Dies gilt in ganz besonderer Weise für meinen (Büro-)Nachbarn Eckart Mayer.

Schließlich danke ich meiner Familie: meinen Eltern, die die Grundlage für alles legten, meiner Frau Elisabeth, die mich begleitet und mir den Rücken gestärkt hat, sowie meinen Kindern, Sophie und Julian, die mir die nötige Ablenkung verschafften.

Bissingen, Juni 2005 Ulrich Vollmer

Contents

Zusammenfassung in deutscher Sprache

Einführung

Modellbasierter Regelungsentwurf für technische Kristallisationsprozesse ist ein hochinteressantes und herausforderndes Thema, auf dem seit vielen Jahren intensiv geforscht wird. Der Grund hierfür liegt in der hohen Komplexität der mathematischen Modelle, die sich wiederum direkt aus der physikalischen Struktur der Kristallisationsprozesse selbst ergibt.

Ein Kristallisationsprozess wird charakterisiert durch die Kristalle, die produziert werden. Diese Partikel unterscheiden sich hinsichtlich einer oder mehrerer *Eigenschaften*, z.B. ihrer Größe. Wenn eine große Anzahl von Teilchen betrachtet wird, ist es günstig nicht die individuellen Partikel zu untersuchen, sondern die gesamte *Partikelpopulation*. Diese Population ist gekennzeichnet durch die *Verteilung* der Teilchen bezüglich ihrer Eigenschaften, z.B. durch die Kristallgrößenverteilung (KGV). Solche Eigenschaftsverteilungen werden auch in der Beschreibung anderer *Partikelprozesse* genutzt. Beispiele hierfür sind Granulation, Polymerisation, Flüssig-flüssig-Extraktion oder biologische Zellfermentation.

Das dynamische Verhalten solcher Partikelprozesse ist im Wesentlichen bestimmt von der zeitlichen Änderung der Eigenschaftsverteilung der betrachteten Teilchenpopulation. Diese Verteilungsfunktion ist Teil des Systemzustands. Folglich sind Partikelprozesse notwendigerweise Systeme mit verteilten Parametern. Im Zentrum des allgemein anerkannten Modellierungsparadigmas für Partikelprozesse steht der Begriff der *Populationsbilanz*. Auf dem Gebiet der Verfahrenstechnik wurde dieser Begriff in den 1960er Jahren eingeführt [40, 85]. Seither wurde eine erhebliche Zahl von Arbeiten zur Modellbildung,

Numerik, Parameteridentifikation und zur Regelung von Populationsbilanzgleichungen veröffentlicht, siehe z.B. [82, 86].

Das Modell eines Kristallisationsprozesses besteht im Allgemeinen aus einer partiellen Integrodifferentialgleichung (der Populationsbilanz) und einer oder mehreren gewöhnlichen Differentialgleichungen (Stoffmengen- und Energiebilanz der Flüssigphase). In der vorliegenden Arbeit werden solche Modelle als Basis für den Regelungs- und Steuerungsentwurf für Kristallisationsprozesse genutzt. Kristallisationsprozesse können auf zwei grundsätzlich unterschiedliche Arten betrieben werden: batchweise oder kontinuierlich. Daraus ergeben sich grundlegend unterschiedliche Regelungsprobleme. Lösungen für beide Problemstellungen werden in dieser Arbeit mit Hilfe aktueller Methoden der Regelungstheorie auf Basis von populationsdynamischen Modellen erarbeitet.

Kontinuierliche Kristallisation

Kontinuierlich betriebene Kristallisationsprozesse arbeiten üblicherweise über lange Zeit in einem stationären Zustand. Die Qualität des erzeugten Produkts wird folglich von der stationären KGV bestimmt. Um sie günstig zu beeinflussen ist es üblich, kleine Kristalle gezielt abzutrennen und aufzulösen (Feinkornauflösung). Neben dem erwünschten Effekt auf die KGV beeinflusst diese Maßnahme jedoch die Dynamik in unerwünschter Weise. Dies kann zu Instabilität des stationären Zustands führen. Die Dynamik des Systems beschränkt also die Einsetzbarkeit der Feinkornauflösung und damit die erreichbare Produktqualität. Ziel einer Regelung ist die Stabilisierung der Ruhelage bei hohen Feinkornauflösungsraten und damit die Verbesserung der erzielbaren Produktqualität.

In der verfahrenstechnischen Forschung steht das Ziel im Vordergrund, populationsdynamische Modelle immer genauer und detaillierter zu machen. Ein solches detailliertes Modell eines kontinuierlichen Kristallisators wird in Kapitel 2 vorgestellt [66]. Es beinhaltet physikalisch begründete Beschreibungen des Kristallwachstums und des Abriebs aufgrund von Kristall-Rührer-Kollisionen. Außerdem wird die Ruhezone, die zur Abtrennung kleiner Kristalle für die Feinkornauflösung dient, mit einer separaten Populationsbilanz beschrieben.

Um dieses Modell einer regelungstechnischen Nutzung zugänglich zu machen werden in Kapitel 3 gezielte Vereinfachungen vorgenommen, so dass das vereinfachte Modell stationär lösbar wird. Dann kann für das um diese Ruhelage linearisierte Modell eine Übertragungsfunktion von der Stellgröße (Feinkornauflösungsrate) zur Messgröße (Gesamt-

kristallmasse) aufgestellt werden. Diese Übertragungsfunktion ist transzendent, sie hat also unendlich viele Pole und Nullstellen und spiegelt damit die verteilte Natur des betrachteten Systems wider. Die Modellvereinfachungen umfassen: Approximation der nichtlinearen Längenabhängigkeit der Wachstumsrate durch eine stückweise lineare Funktion, Approximation der nichtlinearen Konzentrationsabhängigkeit der Wachstumsrate durch ein einfaches Potenzgesetz, Ersetzen des Abriebs durch „negatives Wachstum“, quasistationäre Betrachtung der Ruhezone und Beschreibung der Feinkornabtrennung durch eine einfache Klassierfunktion.

In Kapitel 4 werden auf Basis des vereinfachten Modells stabilisierende H_∞-Regler entworfen. Die H_∞-Theorie ermöglicht den Entwurf von Reglern, die robust gegen Modellfehler sind. Es werden Reglerentwürfe für multiplikative Modellfehler und für koprim faktorisierte Modellfehler durchgeführt. Für die Berechnung der Regler wird die in [24] entwickelte Methode zur Lösung des gemischten Sensitivitätsproblems für verteilte Systeme genutzt. Daraus ergeben sich transzendente Reglerübertragungsfunktionen, die schließlich mittels Fourier-Entwicklung und balancierter Reduktion durch rationale Übertragungsfunktionen approximiert werden. Die sich ergebenden Regler werden in Simulationen mit dem vereinfachten Modell (aus Kapitel 3) und mit dem detaillierten Modell (aus Kapitel 2) getestet. Dabei zeigt sich, dass nur der für koprim faktorisierte Modellfehler entworfene Regler robust genug ist, um das detaillierte Modell zufriedenstellend zu regeln. Mit diesem Regler wird die Ruhelage des Referenzmodells stabil und der Grenzzyklus liegt im Einzugsbereich dieser Ruhelage.

Die hier vorgestellte Vorgehensweise zeichnet sich im Vergleich zu anderen Untersuchungen dadurch aus, dass die Regler auf Basis eines *verteilten Modells* entworfen werden. Das Populationsmodell wird vor dem Reglerentwurf nicht diskretisiert. Ein weiteres Merkmal dieser Arbeit bezieht sich auf einen Mangel, der bereits im Übersichtsartikel [87] beklagt wird. Dort wird festgestellt, dass die moderne *robuste Regelungstheorie* bislang keine Anwendung im Bereich der Kristallisation gefunden hat. Ein Schritt zur Behebung dieses Mangels wird in dieser Arbeit gemacht.

Batch-Kristallisation

Der zweite Teil der Arbeit beschäftigt sich mit einem batchweise betriebenen Kristallisationsprozess. Für Batchprozesse stellen sich ganz andere Regelungs- bzw. Steuerungsprobleme. Der Prozess muss über die gesamte Batchdauer so geführt werden, dass am Ende

ein Produkt mit gewünschten Eigenschaften erreicht wird. Speziell für die hier betrachtete Batch-Kühlungskristallisation bedeutet dies, dass der Temperaturverlauf während des gesamten Prozesses so geführt werden soll, dass am Ende eine bestimmte KGV erreicht wird.

Dazu wird in Kapitel 5 ein relativ einfaches Standard-Populationsmodell aus der Literatur vorgestellt [65], das die Herleitung eines endlich-dimensionalen Momentenmodells erlaubt. Eine sehr nützliche Systemeigenschaft für Trajektorienplanung und Regelungsentwurf ist die *differentielle Flachheit* [20]. Es wird gezeigt, dass das Momentenmodell nicht flach ist, aber durch eine geeignete zustandsabhängige Zeitskalierung flach gemacht werden kann. Solche Systeme heißen *orbital flach* [21, 35, 89].

In Kapitel 6 wird gezeigt, dass das gegebene Populationsmodell invertiert werden kann, d.h. für eine vorgegebene KGV, die am Batchende erreicht werden soll, kann der zugehörige Temperaturverlauf direkt berechnet werden. Dazu wird einerseits die orbitale Flachheit des Systems ausgenutzt und zum anderen die Tatsache, dass die Populationsbilanz durch die eingeführte Zeitskalierung in eine einfache Transportgleichung mit geraden Charakteristiken überführt wird. Damit lässt sich das Steuerungsproblem sehr viel eleganter lösen als mit der häufig verwendeten dynamischen Optimierung. Wenn man jedoch trotzdem an einer Optimierung der KGV interessiert ist, kann das resultierende Optimierungsproblem durch die hier hergeleitete Systeminversion erheblich vereinfacht werden. Aufgrund der Parametrierung des flachen Systems durch den flachen Ausgang kann das dynamische Optimierungsproblem so formuliert werden, dass keine numerische Lösung des Systemmodells nötig ist. Schließlich sind flache Systeme durch Zustandsrückführung exakt linearisierbar. Diese Eigenschaft wird ausgenutzt, um eine Trajektorienfolgeregelung zu entwerfen, die den Batch-Kristallisationsprozess auch in Gegenwart von Unsicherheiten entlang gewünschter Trajektorien der Momente führt.

Das entscheidende Merkmal dieser Systeminversions-Methode ist die Möglichkeit, einen Temperaturverlauf zu berechnen, der auf *eine* bestimmte KGV führt anstatt nur eine skalare Kenngröße der KGV zu optimieren. Außerdem wird die Steuerung bei dieser Vorgehensweise *analytisch* berechnet, während sonst üblicherweise numerische Methoden zum Einsatz kommen.

Chapter 1

Introduction

1.1 Population Balance Modelling

Model based design of control strategies for crystallization processes is a very exciting and challenging topic and has been an area of active research since many years. This is mainly due to the fact that meaningful models for crystallization processes are of high complexity and therefore are difficult to handle mathematically. The model complexity, in turn, is caused by the physical structure of the process itself.

A crystallization process is characterized by the particles which it produces. These particles may be distinguished by *individual properties*, e.g. crystal size. If a large number of particles is involved it is convenient not to consider the individual particles but an entire *population*. This population is characterized by the *distribution* of its particles with respect to their properties, e.g. by the crystal size distribution. Crystallization shares this feature with other processes such as granulation, polymerization, liquid-liquid extraction or cell cultures. They form the class of *particulate processes* or dispersed phase processes.

Describing the dynamic behaviour of particulate processes essentially involves specifying the temporal change of the particle property distribution. This distribution function is part of the system state. Hence, particulate processes inherently are distributed parameter systems. From a system theoretic point of view these systems are infinite-dimensional. The modelling paradigm commonly accepted for this class of systems is the framework of *population balances*. In the field of chemical engineering this methodology was introduced in 1964 in [40] and [85]. In the four decades since then a vast amount of publications has appeared covering modelling, numerics, identification and control of population balance

equations. Some of the milestones on this way are [86], [81] and [82].

In this framework, the state of an individual particle is represented by a particle state vector containing *external* coordinates (position of a particle in physical space) and *internal* coordinates (properties of the particle, e.g. particle size). A population of particles is characterized by its particle property distribution, which is described mathematically by a *number density function*. This function represents the (average) number of particles per volume of particle state space. It is understood that this deterministic approach is only reasonable if large populations are considered. It is further assumed that the number density function is sufficiently smooth to be differentiated with respect to its arguments. The actual number of particles in a certain area of the particle state space is determined by the integral of the number density function over this area.

The temporal change of the number density function is described by the *population balance equation*, which is a partial differential equation (PDE). It describes the change due to continuous "transport" of particles in their state space, e.g. by particle growth, as well as the effect of "birth" and "death" events such as nucleation, breakage or agglomeration. The two last-mentioned processes represent *nonlocal* effects: a particle of a certain size breaking into two parts causes two particles to be formed at distant points in particle state space. These phenomena distinguish systems described by population balance equations from spatially distributed systems. Concerning the mathematical formulation, these effects may lead to integral terms in the partial differential equation. Apart from those particle-particle interactions the dispersed phase usually also interacts with its environment, e.g. the continuous liquid phase in crystallization. The state of the continuous phase may influence rates of growth, birth and death processes and thus affects the particle population. In the other direction, the dispersed particle phase generally affects the continuous phase, e.g. by mass transfer from liquid to solid due to growth in crystallization or by heat transfer due to the heat of crystallization. Therefore, in general a model for a particulate system consists of a population balance equation, which describes the dispersed phase, coupled with a mass (or mole) balance and an energy balance, which describe the continuous phase.

1.2 Control of Crystallization Processes

In this dissertation, population balance models describing crystallization processes are used as a basis for the design of control strategies. Crystallization processes are used in

the chemical and pharmaceutical industry for the production of solid materials. In the following only crystallization from solution is considered. Crystallization is frequently used because in many cases chemical reactions take place in liquid phase whereas products often are solid materials. Furthermore, crystallization can be used for purification and separation.

The basic concept of crystallization is simple and well known. A solution can be supersaturated, e.g. by cooling or by evaporation of solvent. In a supersaturated solution, solute molecules from the solution are built into the crystal lattice. Hence, the crystal is growing. Furthermore, new crystals can emerge from the solution. Consequently, solute mass is transfered from liquid solution to solid crystals. Supersaturation is the driving force for these processes. The most significant property of crystals is their size. Crystal size distribution (CSD) is the crucial variable in industrial crystallizers. This is, on the one hand, due to the fact that the dynamics of crystallization plants can only be understood when regarding the CSD. On the other hand, the CSD is important because it heavily influences product quality and down-stream processability. It influences properties such as filterability, the ability to flow or the dissolution rate of crystalline material.

Industrial crystallization plants can be operated in basically two different ways: continuous or batch. These two modes of operation result in two different control problems, which are both addressed in this dissertation. Therefore, the thesis is composed of two major parts corresponding to the two fundamentally different control problems arising in crystallization. It is the aim of this work to demonstrate that sophisticated up-to-date control synthesis methods can be applied to crystallization processes on the basis of population balance models.

The first part of the thesis comprises Chapters 2 to 4. It deals with continuously operated crystallization plants, where clear solution is continuously fed to the crystallizer and product is continously withdrawn. Continuous processes run for very long periods of time and serve for the production of large amounts of bulk materials. They are desired to be operated at a steady state. Hence, product quality is determined by the steady state CSD. This quantity can be influenced by fines dissolution, i.e. the continuous removal and dissolution of small particles. Unfortunately, apart from the desired effect on the CSD this also affects the dynamics of the system in an undesirable way. Extensive fines dissolution may lead to instability of the steady state. In Chapter 2, a detailed population balance model introduced in [66] is presented, which describes a continuous crystallizer. This model considers nucleation, growth and attrition of crystals. It captures the destabilizing effect of fines dissolution and predicts the resulting sustained oscillations of CSD and so-

lute concentration. In Chapter 3, this detailed model is simplified to obtain a population balance model which can be represented in the form of a transcendental transfer function. In Chapter 4, this transfer function serves as a basis for the design of stabilizing feedback controllers. The controllers are synthesized using H_∞-theory for infinite-dimensional systems [24]. What distinguishes this approach from most other contributions in the area of continuous crystallizer control is that controllers are designed on basis of a distributed parameter model. The population balance model is *not* discretized prior to controller design.

The second part of the thesis comprises Chapters 5 and 6. In batch cooling crystallization the product quality is determined by the CSD at the end of the batch, which can be influenced by the cooling profile, i.e. the temperature trajectory during the batch run. In Chapter 5, a relatively simple standard population balance model [65] is presented. It allows the derivation of a finite-dimensional model describing the temporal behaviour of the moments of the CSD. The notion of differential flatness [20] is introduced and it is shown that the moment model is not flat but can be rendered flat by an appropriate state dependent time scaling. In Chapter 6, this property of the model is exploited to design feedforward control strategies for the production of desired CSDs. The flatness property is further used to simplify the optimization of CSD properties. Finally, nonlinear feedback tracking controllers are designed, which control the system along desired trajectories of the moments. The distinctive feature of this part is that the temperature trajectory which achieves a desired CSD is determined *analytically* rather than by numerical optimization. By doing so, this approach also makes it possible to decide whether a specific CSD can be produced under given conditions or not.

Detailed introductions and literature overviews on industrial crystallization, control of continuous and control of batch crystallization processes are given in the respective chapters.

Chapter 2

Population Balance Model for a Continuous Crystallizer

2.1 Introduction to Continuous Crystallization

Crystallization in continuous mode is widely used as a purification and separation process in the chemical industry. It mainly serves for the production of large amounts of bulk commodity chemicals, e.g. ammonium sulphate, adipic acid [30]. Different types of crystallizer designs are used in industrial practice. The selection of a crystallizer type, on the one hand, depends on the physical properties of the combination of solute and solvent, such as solubility and its temperature dependence. On the other hand the choice is determined by the product requirements, such as desired mean crystal size. There are three main types of crystallizers. *Fluidized suspension crystallizers*, also called Oslo crystallizers, are especially useful for the production of coarse material. *Forced circulation crystallizers* are relatively inexpensive and best suited where large amounts of solute have to be evaporated. Finally, *draft tube baffled (DTB) crystallizers* are flexible in use and they are very well-studied. Detailed population balance models, such as the one presented in this chapter, have been set up. A motivation for this interest is to gain a better understanding of the cyclic behaviour that is frequently observed in the operation of DTB crystallizers. The three types of crystallizer designs basically differ with respect to the way in which the slurry is mixed and the crystals are kept suspended. In addition, there are several possibilities to generate supersaturation, the driving force of crystallization. The solution can be supersaturated either by cooling or by evaporation of solvent (or a combination of both). Further possibilities are *drowning-out*, i.e. the addition of an anti-

solvent or *reaction crystallization.* For further details on questions of design and selection of crystallizers see one of the reference works [62, 69, 71, 103].

The process considered in the following is an evaporative DTB crystallizer. For a sketch see Figure 2.1. The crystallizer is operated as follows. Crystal-free solution is fed to the

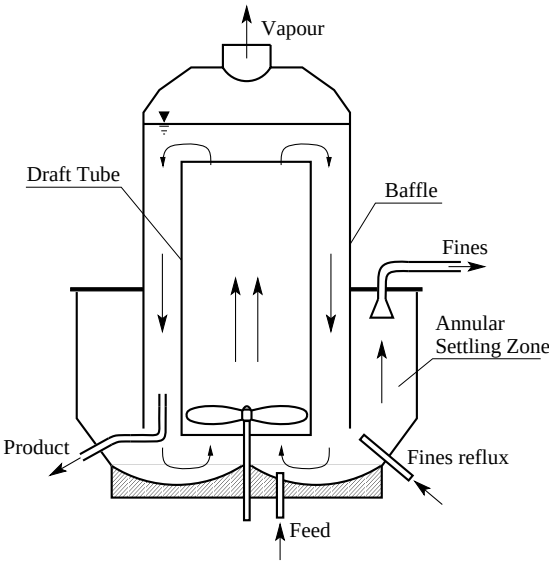

Figure 2.1: Sketch of DTB crystallizer

vessel from the bottom. Solvent is evaporated such that the solution in the crystallizer becomes supersaturated. Hence, new crystals form and existing crystals grow. The particles are prevented from settling by a propeller which, in combination with a draft tube, generates a loop flow. Inside the draft tube the suspension is forced to rise and outside it comes down. Suspension containing product crystals and solution is continuously withdrawn from the process.

In many applications, a coarse product is desired. A possibility to shift the CSD towards larger crystals is the systematic dissolution of small crystals (fines). This can be achieved as follows. A baffle separates an annular settling zone from the suspended magma. At the top of this zone, suspension is pumped off. This causes a vertical upward flow. But only

small crystals are dragged along, due to gravitation large particles settle at the bottom. Thus, at the top of the baffled zone, solution containing only small crystals is discharged. This solution is heated in an external heat exchanger such that the fines are dissolved. The clear hot solution is then fed back to the crystallizer at the bottom of the settling zone.

One of the major problems arising in the operation of continuous crystallizers are undamped oscillations of CSD and supersaturation. Cyclic behaviour of DTB crystallizers is a phenomenon which has been encountered in industrial practice [83]. It has been studied intensely by quite a number of researchers. Experimental studies in laboratory scale have been carried out [83, 100]. Mathematical models of different levels of detail have been formulated and examined numerically by simulation [6, 16, 49, 68, 80]. Furthermore, mathematical models have been analytically investigated [2, 7, 18, 45, 50, 53, 86, 99] to find stability results for crystallization processes. A commonly accepted result is that fines dissolution and classified product removal significantly promote cycling in continuous crystallizers. Consequently, the improvement of CSD properties obtained by the application of fines dissolution is being paid for by a deterioration of the dynamic process behaviour. In many cases, it is impossible to choose the fines dissolution rate as high as it would be necessary to achieve the desired CSD quality, because the process shows sustained oscillations and therefore the desired steady state is never attained.

2.2 Population Modelling

In this chapter, a detailed population balance model derived in [66] and [68] for an evaporative DTB crystallizer is presented. It comprises physically founded kinetic models for the two main processes which influence the CSD, crystal growth and attrition due to crystal stirrer collisions. Similar population models have been developed in [6] and [30]. A model using similar kinetic models but considering two independent parameter properties, crystal length and internal lattice strain, has been reported in [29].

What distinguishes these models from others presented in the literature is their *predictiveness* and *scalability*. There are no empiric relations involved in the kinetic expressions. All parameters have clear physical meaning and can be directly measured or determined in separate experiments. They do not have to be fitted to measurement data from the specific plant to be modelled. Therefore, these models can be used to predict the dynamic behaviour of different design variants or the effects of modifications in the operating conditions. This makes the models very useful for planning and design of crystallization plants.

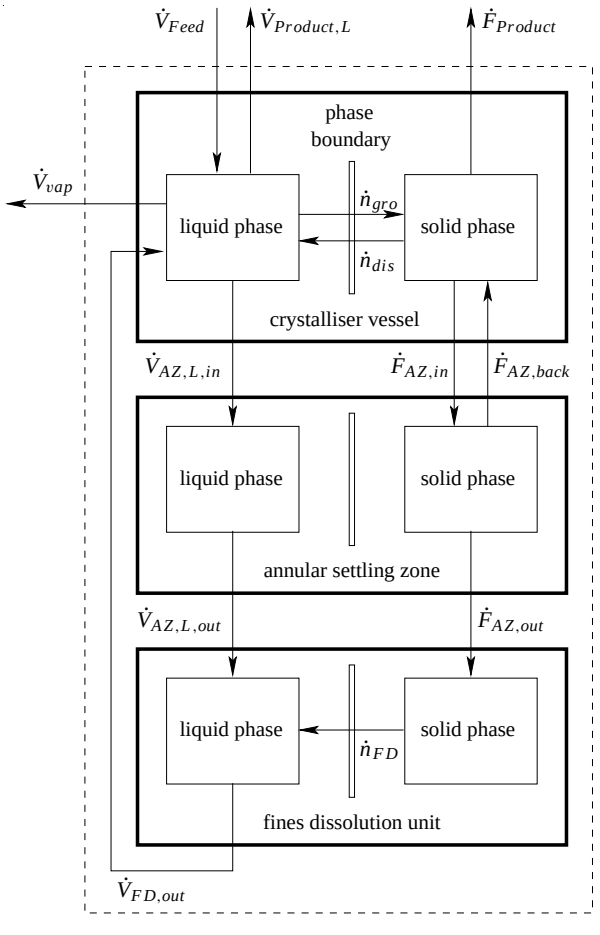

Figure 2.2: Schematic representation of crystallizer with annular settling zone and fines dissolution unit

The crystallizer content consists of two phases, the dispersed solid phase and the surrounding liquid phase, which have to be modelled separately. Furthermore, the content of the crystallizer itself, the annular settling zone and the fines dissolution unit are treated individually. Figure 2.2 illustrates the material exchange between the single pieces of process equipment, i.e. the crystallizer, the annular settling zone and the fines dissolution unit, and across the liquid-solid phase boundary. Volumetric flows, molar fluxes (across the phase boundary) and particle number fluxes are denoted by $\dot{V}_i$, $\dot{n}_i$ and $\dot{F}_i$, respectively.

2.2.1 Modelling of the Dispersed Solid Phase in the Crystallizer

Population Balance

The distribution of the crystals with respect to crystal size is described by the number density function $F(L,t)$ which represents the number of particles per crystal size at time t. The size of a particle is represented by a characteristic length L, e.g. edge length in the case of cubic particles. It is assumed that the shape of crystals is sufficiently constant, such that the volume of an individual particle can be determined by $V_P = k_V L^3$ with a constant volume shape factor k_V.

In modelling the crystallization process, it is further assumed that the overall volume of suspension in the crystallizer V is kept constant, that the process is operated isothermally at temperature T and that there are no crystals in the feed. Finally, secondary nucleation and more specifically attrition due to crystal stirrer collisions is presumed to be the predominant source of small crystals such that primary nucleation, homogeneous and heterogeneous, is negligible. Hence, the model cannot describe the startup of the crystallizer from a crystal-free solution. However, once a continuous crystallizer is in operation there is always a large amount of crystals present in the process generating reasonably many attrition fragments. Furthermore, solute is consumed by growing crystals such that supersaturation is relatively low and stays within the so-called metastable zone. Under these conditions, it is very well justified to disregard primary nucleation.

The dynamic behaviour of the CSD $F(L,t)$ is described by the population balance equation

$$\begin{aligned}\frac{\partial F(L,t)}{\partial t} &= -\frac{\partial (G(\sigma(t),L)F(L,t))}{\partial L} - \dot{F}_{dis}(L,t) - \dot{F}_{Product}(L,t) \\ &\quad + \dot{F}_{AZ,back}(L,t) - \dot{F}_{AZ,in}(L,t) + \dot{F}_{attr}(L,t) \end{aligned} \tag{2.1}$$

with initial and boundary conditions

$$F(L,0) = F_0(L) \tag{2.2}$$

$$F(0,t) = 0. \tag{2.3}$$

Deviating from usual notation, *absolute* supersaturation is denoted by σ. The common notation (Δc) is prohibited here because Δ is used later on to denote deviations from steady state. *Relative* supersaturation, for which the symbol σ is used oftentimes, does not occur in this thesis. Further, note that symbols of the form $\dot{F}_i$ do *not* denote time derivatives but they represent number density fluxes due to different effects influencing the number density function $F(L,t)$. The CSD changes in time due to crystal growth with growth rate $G(\sigma, L)$, dissolution of small crystals with number density flux $\dot{F}_{dis}$, product removal $\dot{F}_{Product}$, exchange with the annular zone $\dot{F}_{AZ,back}$ and $\dot{F}_{AZ,in}$, and attrition due to crystal stirrer collisions $\dot{F}_{attr}$. An overview on these individual phenomena is given in the following. Only the principal ideas are presented here. The technical details as well as parameter values can be found in Appendix A or in [66].

Crystal Growth

The growth rate expression

$$G(\sigma,L) = 2k_d(L)\left(\frac{\sigma}{c_S} + \frac{k_d(L)}{2k_r c_S} - \sqrt{\left(\frac{k_d(L)}{2k_r c_S}\right)^2 + \frac{k_d(L)\sigma}{k_r c_S^2}}\right) \tag{2.4}$$

is reported in [63]. It takes into account the effect of diffusion of solute molecules towards the crystal surface and the integration of these molecules into the crystal lattice. The driving force for crystallization due to [27] is

$$\sigma = c_{L,A} - c_{L,A,sat} = c_{L,A} - c_{L,A,sat,ideal}\, e^{\frac{\Gamma_S}{RTL}}, \tag{2.5}$$

where $c_{L,A}$ is the concentration of solute (component A) in the liquid phase and $c_{L,A,sat}$ is the concentration at saturation. Saturation concentration is defined to be exactly the condition under which a particle does not grow and is not dissolved. This concentration depends on the particle itself. The length dependence described in equation (2.5), which was proposed in [27], is due to internal lattice strain in crystal fragments. As primary nucleation is neglected, it is assumed that all crystals have originally been generated by attrition. The collision causes a strain in the crystal lattice of attrition fragments, which, in turn, causes them to dissolve more easily. This effect decreases with the crystal becoming

bigger. Consequently, small crystals have a higher solubility than big ones. The saturation concentration for an ideal crystal with no internal lattice strain, e.g. generated by primary nucleation, is denoted by $c_{L,A,sat,ideal}$.

Because of the length dependence of saturation concentration $c_{L,A,sat}$ in equation (2.5) the driving force σ is negative for small crystals. This leads to a negative growth rate, which means that the very small crystals are not growing but are becoming smaller and will finally disappear. For negative growth, surface integration is, of course, irrelevant. Therefore, the growth rate for negative driving force $\sigma < 0$ is given only by the diffusion limited part, i.e. the first addend, of equation (2.4).

Dissolution of Small Crystals

Crystals are not stable below a certain length L_{crit}. Small crystals with negative growth rate finally become smaller than L_{crit} and, hence, disappear from the population. This is described by the number flux

$$\dot{F}_{dis}(L,t) = (1 - h(L - L_{crit}))D_{dis}F(L,t) \tag{2.6}$$

with dissolution rate D_{dis} and the Heaviside step function $h(\bullet)$. If particles are assumed to disappear immediately when reaching the critical size, the dissolution rate has to be infinite.

Product Removal

Product removal is assumed to be representative, i.e. the product slurry discharged from the crystallizer has the same composition and in particular the same CSD as the suspension inside the crystallizer. Therefore, the number flux due to product removal is

$$\dot{F}_{Product}(L,t) = \frac{\dot{V}_{Product}}{V}F(L,t) \tag{2.7}$$

where $\dot{V}_{Product}$ is the volumetric flow rate of product removal.

Exchange with the settling zone

The conditions inside the settling zone are treated in detail in Chapter 2.2.3. The number fluxes due to exchange of crystals between crystallizer and annular zone are described there.

Attrition Due to Crystal Stirrer Collisions

A detailed investigation of fragment formation due to collisions of crystals with the stirrer has been reported in [26] and is briefly summarized in this paragraph. Attrition effects can be described by a sum of three number fluxes

$$\dot{F}_{attr}(L,t) = -\dot{F}^{-}_{attr}(L,t) + \dot{F}^{+}_{attr,1}(L,t) + \dot{F}^{+}_{attr,2}(L,t). \tag{2.8}$$

This accounts for the three effects of a collision event. First, a crystal of a certain size disappears because of being abraded. Second, a crystal slightly smaller than the original one is generated instead and, third, a couple of small attrition fragments are produced. See Figure 2.3 for an illustration. The sink term is expressed as

$$\dot{F}^{-}_{attr}(L,t) = \int_0^{R_{st}} \bar{\beta}(L,r)F(L,t)\, dr = \beta(L)F(L,t). \tag{2.9}$$

The attrition rate $\beta(L)$ is defined as an integral over the stirrer radius based attrition rate $\bar{\beta}(L,r)$, where r represents the radial position where a crystal hits the stirrer and R_{st} is the stirrer radius. The attrition rate depends on the geometry and speed of the stirrer and physical properties of the liquid phase, see Appendix A.1 or the original work [26].

The source term accounting for the formation of abraded crystals is

$$\begin{aligned} \dot{F}^{+}_{attr,1}(L,t) \;=\; & \int_0^{R_{st}} \left(\bar{\beta}\left(L'_{edge}(L,r),r\right) F(L'_{edge}(L,r),t) + \right. \\ & \left. \bar{\beta}\left(L'_{blade}(L,r),r\right) F(L'_{blade}(L,r),t)\right)\, dr \end{aligned} \tag{2.10}$$

where $L'_{edge/blade}(L,r)$ is the length of an original crystal that produces an abraded crystal of length L when colliding with the edge/blade of the stirrer at radial position r. Due to the conservation of volume during an attrition event, the length $L'_{edge/blade}(L,r)$ can be obtained from

$$k_V L'^3_{edge/blade} - k_V L^3 - V_{attr,edge/blade}(L'_{edge/blade}, r) = 0 \tag{2.11}$$

where the volume abraded from a crystal of length L' colliding with the stirrer edge/blade at radial position r is $V_{attr,edge/blade}(L',r)$. This volume depends on the geometry and speed of the stirrer and physical properties of the crystalline material.

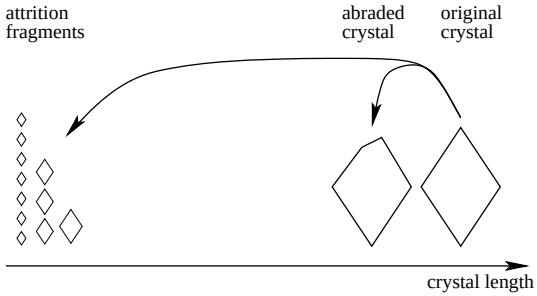

Figure 2.3: Attrition of crystal colliding with the stirrer

Finally, the source term describing the generation of small attrition fragments is given by

$$\dot{F}^{+}_{attr,2}(L,t) = \int_0^{R_{st}} \int_L^{\infty} \big(N_{frag,edge}(L',r) f_{frag,edge}(L',L,r) \bar{\beta}(L',r) F(L',t) + N_{frag,blade}(L',r) f_{frag,blade}(L',L,r) \bar{\beta}(L',r) F(L',t) \big)\, dL'\, dr, \quad (2.12)$$

where $f_{frag,edge/blade}(L',L,r)$ represents the size distribution of fragments with respect to length L generated from a crystal of length L' colliding with the stirrer edge/blade at r. The integral over crystal size L' reflects the fact that attrition fragments of length L can be produced from attrition events at any size $L' > L$. The number of fragments $N_{frag,edge/blade}(L',r)$ generated from a crystal of length L' colliding with the stirrer at position r has to satisfy the volume condition

$$V_{attr,edge/blade}(L',r) = N_{frag,edge/blade}(L',r) k_V \int_{L_{frag,min}}^{L_{frag,max,edge/blade}(L')} L^3 f_{frag,edge/blade}(L',L,r)\, dL. \quad (2.13)$$

This CSD, again, depends on the geometry and speed of the stirrer and on physical properties of the crystalline material. For explicit expressions for all quantities used in this paragraph see Appendix A.1. For further details on the physical background the reader is referred to [26].

2.2.2 Modelling of Liquid Phase in the Crystallizer

The liquid phase in the crystallizer can be described by two differential equations, one for the amount of moles of solution n_L and one for the amount of moles of solute $n_{L,A}$

$$\begin{aligned}\frac{dn_L(t)}{dt} &= c_{Feed,L}\dot{V}_{Feed} - c_L(t)\dot{V}_{Product,L}(t) + c_{FD,L}(t)\dot{V}_{FD,out}(t) \\ &\quad -c_L(t)\dot{V}_{AZ,L,in}(t) - c_B\dot{V}_{vap} - (\dot{n}_g(t) - \dot{n}_{dis}(t)) \qquad (2.14)\\ \frac{dn_{L,A}(t)}{dt} &= x_{Feed,L,A}c_{Feed,L}\dot{V}_{Feed} - x_{L,A}(t)c_L(t)\dot{V}_{Product,L}(t) \\ &\quad +x_{FD,L,A}(t)c_{FD,L}(t)\dot{V}_{FD,out}(t) - x_{L,A}(t)c_L(t)\dot{V}_{AZ,L,in}(t) \\ &\quad -(\dot{n}_g(t) - \dot{n}_{dis}(t)) \qquad (2.15)\end{aligned}$$

with appropriate initial conditions

$$n_L(0) = n_{L,0}, \quad \text{and } n_{L,A}(0) = n_{L,A,0}, \qquad (2.16)$$

where $x_{L,A}$, $x_{Feed,L,A}$ and $x_{FD,L,A}$ are the mole fractions (moles of solute per moles of solution) in the crystallizer, in the feed and the fines dissolution reflux. The volumetric flow rates and molar concentrations (moles of solution per m^3 of solution) of feed, fines dissolution reflux and vapour stream are denoted by $\dot{V}_i$ and c_i, respectively, with the corresponding indices. The mole fluxes between solid and liquid phase due to crystal growth and dissolution of small crystals are denoted by $\dot{n}_g$ and $\dot{n}_{dis}$, respectively. The expressions for these mole fluxes can be easily derived

$$\dot{n}_g(t) = \frac{3k_V\rho_A}{M_S}\int_0^\infty L^2 G(\sigma(t), L)F(L,t)\,dL \qquad (2.17)$$

$$\dot{n}_{dis}(t) = \frac{k_V\rho_A}{M_S}\int_0^{L_{crit}} L^3 D_{dis}(L)F(L,t)\,dL. \qquad (2.18)$$

Due to the volume constraint $V = const.$ the two differential equations (2.14) and (2.15) can be replaced by a single equation for the mole fraction $x_{L,A}$ describing the composition of the liquid phase

$$\begin{aligned}n_L(t)\frac{dx_{L,A}(t)}{dt} &= c_{Feed,L}\dot{V}_{Feed}(x_{Feed,L,A} - x_{L,A}(t)) \\ &\quad +c_{FD,L}(t)\dot{V}_{FD,out}(t)(x_{FD,L,A}(t) - x_{L,A}(t)) \\ &\quad +x_{L,A}(t)c_B\dot{V}_{vap} - (1 - x_{L,A}(t))(\dot{n}_g(t) - \dot{n}_{dis}(t)) \qquad (2.19)\end{aligned}$$

with initial condition

$$x_{L,A}(0) = x_{L,A,0}. \tag{2.20}$$

Assuming an ideal mixture, the number of moles of solution n_L can then be calculated from the volume of the liquid phase

$$n_L(t) = \frac{V_L(t)\rho_A\rho_B}{x_{L,A}(t)M_A\rho_B + (1 - x_{L,A}(t))M_B\rho_A}. \tag{2.21}$$

The liquid phase volume is given by

$$V_L(t) = V - V_S(t) = V - k_V \int_0^\infty L^3 F(L,t)\, dL. \tag{2.22}$$

The feed rate $\dot{V}_{Feed}$ is adjusted such that the volume condition (2.22) is satisfied, i.e. the liquid volume is varied in order to keep the overall volume of slurry constant. Besides the mole fraction $x_{L,A}$, an alternative way to describe the composition of the liquid phase is the molar concentration

$$c_{L,A} = \frac{n_L}{V_L} x_{L,A}, \tag{2.23}$$

which is used in the definition of supersaturation σ in equation (2.5).

2.2.3 Modelling of the Dispersed Solid Phase in the Settling Zone

It is assumed that the volume of slurry in the annular settling zone is constant and that crystal growth, dissolution and attrition can be neglected [66]. Then, the CSD in the annular zone $F_{AZ}(L,t)$ only changes due to in- and outflow terms. Therefore, its temporal behaviour can be described by the simple population balance equation

$$\frac{\partial F_{AZ}(L,t)}{\partial t} = \dot{F}_{AZ,in}(L,t) - \dot{F}_{AZ,out}(L,t) - \dot{F}_{AZ,back}(L,t) \tag{2.24}$$

with initial and boundary conditions

$$F_{AZ}(L,0) = F_{AZ,0}(L) \tag{2.25}$$

$$F_{AZ}(0,t) = 0. \tag{2.26}$$

The particle number flux from the crystallizer to the settling zone is

$$\dot{F}_{AZ,in}(L,t) = \frac{\dot{V}_{AZ,in}}{V} F(L,t) \tag{2.27}$$

where $\dot{V}_{AZ,in}$ is the volumetric flow rate entering the annular zone. Due to the discharge of slurry at the top of the settling zone, a vertical flow from bottom to top is generated with velocity $\dot{V}_{AZ,out}/A_{AZ}$ where A_{AZ} is the cross sectional area of the settling zone. However, due to gravitation the particles are forced in the opposite direction with a settling velocity $v_s(L, \varepsilon_{AZ,S})$ depending on particle size and the solids content of the slurry $\varepsilon_{AZ,S} = V_{AZ,S}/V_{AZ}$ inside the baffle zone. Superposing the upwards and downwards motion yields the effective particle velocity in the annular settling zone [66]

$$v_{AZ}(L, \varepsilon_{AZ,S}(t)) = \frac{\dot{V}_{AZ,out}(t)}{A_{AZ}} - v_s(L, \varepsilon_{AZ,S}(t)). \tag{2.28}$$

Small particles are dragged along with the upward flow, leave the annular zone and enter the fines dissolution unit. This results in the particle number flux

$$\dot{F}_{AZ,out}(L,t) = \frac{\max(0, v_{AZ})}{h_{AZ}} F_{AZ}(L,t), \tag{2.29}$$

with height of the annular zone h_{AZ}. For large particles the resulting velocity $v_{AZ}(L, \varepsilon_{AZ,S})$ is negative. Therefore, these particles settle and finally return to the crystallizer with the particle number flux

$$\dot{F}_{AZ,back}(L,t) = -\frac{\min(0, v_{AZ})}{h_{AZ}} F_{AZ}(L,t). \tag{2.30}$$

2.2.4 Modelling of the Liquid Phase in the Settling Zone

From a mole balance for the liquid phase in the settling zone the differential equation

$$n_{AZ,L}(t)\frac{dx_{AZ,L,A}(t)}{dt} = c_L(t)\dot{V}_{AZ,L,in}(t)x_{L,A}(t) - c_{AZ,L}(t)\dot{V}_{AZ,L,out}(t)x_{AZ,L,A}(t) \tag{2.31}$$

with initial condition

$$x_{AZ,L,A}(0) = x_{AZ,L,A,0} \tag{2.32}$$

for the mole fraction in the annular zone $x_{AZ,L,A}$ can be derived. It accounts for inflow from the crystallizer and outflow to the fines dissolution unit. The overall volumetric flow rate leaving the annular zone

$$\dot{V}_{AZ,out}(t) = \dot{V}_{AZ,L,out}(t) + \dot{V}_{AZ,S,out}(t) = \dot{V}_{AZ,L,out}(t) + k_V \int_0^\infty L^3 \dot{F}_{AZ,out}(L,t)\, dL \tag{2.33}$$

to the fines dissolution unit is equivalent to the fines dissolution flow rate that can be chosen by the operator of the crystallizer. The flow rate to the settling zone $\dot{V}_{AZ,in}$ is adjusted such that the overall volume of slurry in the annular zone is kept constant

$$V_{AZ} = V_{AZ,L}(t) + V_{AZ,S}(t) = const. \tag{2.34}$$

2.2.5 Modelling of the Fines Dissolution Unit

It is assumed that crystals entering the fines dissolution unit are completely dissolved and clear solution with an increased solute content is returned to the crystallizer after a delay time τ_{FD}. The mole fraction entering the crystallizer from the fines dissolution loop, therefore, is

$$x_{FD,L,A}(t) = \frac{x_{AZ,L,A}(t-\tau_{FD})c_{AZ,L}(t-\tau_{FD})\dot{V}_{AZ,L,out}(t-\tau_{FD}) + \dot{n}_{FD}(t)}{c_{AZ,L}(t-\tau_{FD})\dot{V}_{AZ,L,out}(t-\tau_{FD}) + \dot{n}_{FD}(t)}. \quad (2.35)$$

with the mole flux from solid to liquid phase due to fines dissolution

$$\dot{n}_{FD}(t) = c_S k_V \int_0^\infty L^3 \dot{F}_{AZ,out}(t-\tau_{FD})\, dL. \quad (2.36)$$

2.3 Comparison to Real Plant

The Laboratory for Process Equipment at Delft University of Technology operates a 1000 litre evaporative DTB crystallizer. A detailed description, operating conditions and parameter values of this plant can be found in [43, 61, 75]. All necessary parameter values are collected in Appendix A.2. In experiments, it was found that this crystallizer exhibits sustained oscillations when operated at high fines dissolution rates, see [6, 14].

It was shown in [66, 68] that the model presented in Chapter 2.2 does *not* predict the oscillatory behaviour which was observed in the real plant. In [6] a model with the same growth and attrition kinetics was presented, which, in addition, accounts for spacial non-homogeneity of the system states by decomposing the crystallizer into several spacial compartments. Although it correctly predicts some aspects of the crystallizer behaviour, this model also fails to predict the sustained oscillations correctly.

Therefore, in [66, 68] an additional effect was incorporated into the fines dissolution model. As depicted in Figure 2.1 and described in Chapter 2.1 the hot reflux stream from the fines dissolution unit reenters the crystallizer at the lower part of the settling zone, the region where mainly large crystals accumulate before they return to the well mixed part of the crystallizer vessel. It is argued that the hot, undersaturated solution entering from the fines dissolution unit generates a local undersaturation in an area where mainly large crystals are present. This leads to the dissolution of large crystals. This effect is incorporated into the model by formally modifying the rise/sink velocity of particles

v_{AZ} in the settling zone as if large particles were also dragged into the fines dissolution unit. In the range of 0.8 mm $\leq L \leq$ 1.3 mm a linear slope is added, starting from 0 for $L = 0.8$ mm rising up to 50% of the maximum velocity of small particles at $L = 1.3$ mm. For a graphical illustration, see Figure 2.4.

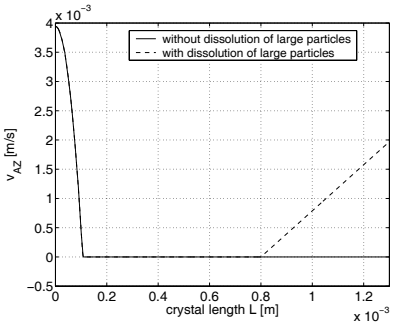

Figure 2.4: Rise/sink velocity v_{AZ} of particles, at $\varepsilon_{AZ,S} = 5.17\%$.

With this extension the model produces sustained oscillations for values of the fines dissolution rate where oscillations actually occur in the real plant. In [6], measurements of the mass median crystal size L_{50} are reported. The mass median crystal length L_{50} is defined such that half of the overall crystal mass $m_S(t)$ is contributed by crystals smaller than L_{50}, i.e.

$$k_V \rho_A \int_0^{L_{50}(t)} L^3 F(L,t)\, dL = \frac{k_V \rho_A \int_0^{\infty} L^3 F(L,t)\, dL}{2} = \frac{m_S(t)}{2}. \tag{2.37}$$

In [68] it is shown that the period of oscillations in the simulation matches almost perfectly with experimental data. The amplitude of the oscillations of the mass median crystal size L_{50} are also matched fairly well.

2.4 Discussion

A detailed population balance model has been presented, which takes into account crystal growth, attrition due to crystal stirrer collisions and dissolution of the very small imperfect

attrition fragments. Furthermore, the model comprises a separate population balance for the annular settling zone describing the classifying effect of the settling zone which is exploited for fines dissolution.

The intention when developing this model clearly was to gain a more thorough understanding of the crystallization process under consideration and to obtain a model which is scalable and predictive. To achieve this, the physical and chemical phenomena taking place on a microscopic level were modelled in detail and incorporated in the overall process model. Great effort has been taken to make the model as physically meaningful as possible. All parameters in the model are either measurable directly or can be obtained from separate experiments. But the determination of parameters does *not* require any experiments on the actual plant to be modelled. The only point that deviates from this modelling principle is the last part. The dissolution of large particles due to the undersaturated fines reflux is only considered qualitatively but has not yet been modelled in its physical details.

Nevertheless, with respect to the objectives of scalability, predictiveness and physical meaning this model is excellent. These features make the model well suited for process design purposes. The effects of different crystallizer design variants and operating conditions can be tested in simulation studies *before* the actual plant is set up. However, accuracy and predictiveness do not come for free. The price to be paid is model complexity. For further *analytic* investigations such as computation of steady states and the testing of their stability or as a basis for controller design, the model presented in this chapter is too complex. For the latter purpose, in the following a simplified population balance model is derived from the detailed one presented so far.

Chapter 3

Model Simplification

3.1 Introduction

As already Aristotle asserted, precision is not a value-in-itself but the adequate degree of precision depends on the subject to be studied ”for it is the mark of an educated man to look for precision in each class of things just so far as the nature of the subject admits”[3].

If the purpose of a process model is to assist the design of a new crystallization plant, then the model necessarily needs to be *predictive* as discussed in Section 2.2. High model accuracy, for this application, is indispensable. The model described in the previous chapter would very well serve that purpose. However, as a basis for controller synthesis it is sufficient to use a model which is capable of *describing* the behaviour of a particular existing plant - the plant to be controlled. For control purposes other aspects are of importance. On the one hand, the purpose of incorporating a feedback controller into a system is to make the process more robust with respect to uncertainties. Hence, the underlying model does not have to capture the real process in complete detail. But, on the other hand, based on a more accurate process model it is, in many cases, possible to design controllers with superior performance. Furthermore, any model based controller synthesis method is only able to handle a specific class of models, such as e.g. continuous-time, linear, finite-dimensional, time-invariant single-input-single output models, for which controller synthesis has been studied most extensively. Consequently, there is an interplay between the control objective which can be reached, the structure (and a potential reduction or simplification) of the process model and the choice of a controller synthesis method. Based on these considerations, in this chapter a simpler model is derived.

The original model is distributed with respect to a property coordinate and, hence, from a system theoretic point of view it is infinite-dimensional. This is an essential characteristic of the system which, therefore, is to be conserved during the model simplification procedure.

Because the objective of the subsequent controller design is the stabilization of an unstable steady state, it can be argued that the process will be kept close to a steady state and, therefore, a linearized process model is adequate to describe the system's behaviour within the operating region. Hence, linearization of the system will be part of the model simplification. A representation of linear systems which is particularly useful for controller design purposes is a transfer function. Since the system is infinite-dimensional the transfer function derived in this chapter is transcendental. Further simplification could be achieved by lumping the distributed system. However, as described in Chapter 4 there exist appropriate controller synthesis methods for plants described by transcendental transfer functions. Hence, lumping of the system can be avoided.

To enable the derivation of a transfer function the Laplace transformed linearized partial differential equations involved in the model have to be solvable analytically. To achieve this, the particle number fluxes due to attrition, nucleation and dissolution of particles, the crystal growth rate expression and the description of annular settling zone and fines dissolution unit are reformulated based on physical considerations. In this step, parameters are introduced which have to be determined by fitting steady state values of the simplified model to results obtained from simulation of the original model or, alternatively, to measurement data acquired from experiments with the plant to be modelled. Hence, predictiveness of the model is sacrificed in this step for the sake of model simplicity.

More precisely, parameter values are obtained in three different ways. Some of them, e.g. overall volume of the crystallizer content, can be taken directly from the description of the physical system, i.e. they can be copied from the detailed model. Some parameters are determined by curve fitting to approximate the kinetics used in the detailed model with simpler expressions. The third way parameters are chosen is to match certain steady state simulation results of the detailed model. Since the detailed model exhibits sustained oscillations the steady state is not reached in simulations. Analytic determination of the steady state is also not possible, as already mentioned before. Hence, steady state values are taken from simulations of the detailed model disregarding the dissolution of large particles due to the reflux of undersaturated solution from the fines dissolution unit, which was discussed in Chapter 2.3. This model is stable and so a steady state is achieved in simulations. Parameters of the simplified model are chosen such that the overall crystal

mass, the supersaturation and the maximum crystal length of the simple model derived in this chapter are in agreement with the detailed model, where in both cases the dissolution of large particles is disregarded. Then, adding the dissolution of large crystals makes both models oscillate. Note that for the simplified model the steady state can be determined analytically, such that this procedure does not involve simulation of the simplified model. All parameter values for the simplified model are listed in Appendix A.3.

In the following, the original complex model presented in the previous chapter is referred to as the *reference model*. The simplified model to be derived in this chapter is called *design model* as it will, later on, serve as a basis for controller design.

The remainder of the chapter is organized as follows. First, the particle number fluxes are reformulated to obtain a simpler population balance model. Second, this model is linearized around a desired operating point. Then, the system is in a form such that an irrational transfer function can be obtained by Laplace transformation.

3.2 Simplified Population Balance Model

3.2.1 Dispersed Solid Phase in the Crystallizer

To start with, the same population balance equation (2.1) as in the reference model is used. However, the number fluxes occurring in this equation are simplified.

Crystal Growth

The growth rate $G(\sigma, L)$ in the reference model, (2.4), is a complex nonlinear function of crystal length L and the driving force for crystal growth σ. This function is approximated by an expression where a piecewise linear dependence on L is multiplied by a simple power law of σ

$$\begin{aligned} G(\sigma, L) &= k_g \sigma^g \cdot \left(\frac{L(1 - h(L - L_{growth}))}{L_{growth}} + h(L - L_{growth}) \right), \\ &= \begin{cases} k_g \sigma^g \frac{L}{L_{growth}}, & L < L_{growth} \\ k_g \sigma^g, & L \geq L_{growth} \end{cases} \end{aligned} \tag{3.1}$$

where $h(L)$ is the Heaviside step function. The driving force for crystallization (2.5) is redefined using the ideal saturation concentration $c_{L,A,sat,ideal}$

$$\sigma = c_{L,A} - c_{L,A,sat,ideal}$$

neglecting effects of non-ideal crystal structure. Values for the length L_{growth} and the exponent g are obtained by curve fitting, see Figure 3.1. The parameter k_g is chosen such that the third moment of the CSD at steady state determined with the simplified model matches the corresponding value obtained with the reference model.

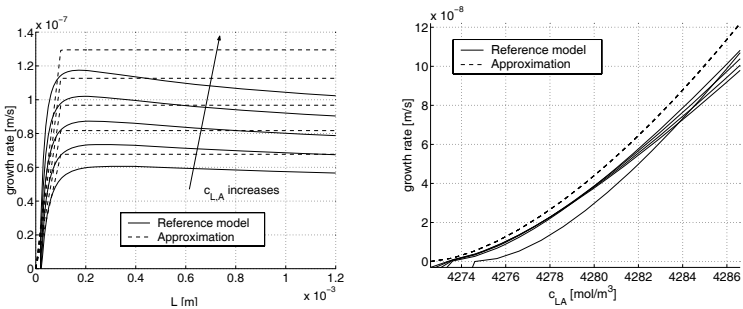

Figure 3.1: Original and approximated growth rates versus crystal length L at values of $c_{L,A}$ from $4,282\frac{\text{mol}}{\text{m}^3}$ to $4,287\frac{\text{mol}}{\text{m}^3}$ (left) and versus concentration $c_{L,A}$ at values of L from 0.1 mm to 1.1 mm (right).

Dissolution of Small Crystals

Since the correction of the ideal saturation concentration accounting for crystal imperfection is neglected, dissolution of small fragments, (2.6), is also disregarded

$$\dot{F}^{-}_{dis} = 0. \tag{3.2}$$

Attrition due to crystal-stirrer collisions

In the reference model, attrition is described by three terms: a sink term $\dot{F}^{-}_{attr}$ due to large crystals that collide with the stirrer, (2.9), a source term $\dot{F}^{+}_{attr,1}$ due to the generation of abraded large crystals with a characteristic length somewhat smaller than the length of the

original crystal, (2.10), and finally a source term $\dot{F}^{+}_{attr,2}$ for the production of N_{frag} small fragments with the size distribution f_{frag}, see equation (2.12).

For the design model, the combination of the sink term $\dot{F}^{-}_{attr}$ and the source term $\dot{F}^{+}_{attr,1}$ accounting for the generation of slightly smaller crystals is replaced by a negative growth expression with the rate

$$\begin{aligned} G_{attr}(L) &= k_{g,attr}\left(L + 3(L - L_{g,attr})h(L - L_{g,attr})\right) \\ &= \begin{cases} k_{g,attr}L, & L < L_{g,attr} \\ k_{g,attr}(4L - 3L_{g,attr}), & L \geq L_{g,attr} \end{cases}. \end{aligned} \tag{3.3}$$

This qualitatively captures the fact that crystals become smaller due to attrition. The piecewise linear shape of $G_{attr}(L)$ (see Figure 3.2) reflects the fact that large particles are abraded at a higher rate than small ones. This determines the reformulation of the first two number fluxes due to attrition

$$\dot{F}^{+}_{attr,1}(L,t) - \dot{F}^{-}_{attr}(L,t) = -\frac{\partial[G_{attr}(L)F(L,t)]}{\partial L}. \tag{3.4}$$

The length $L_{g,attr}$ where the corner occurs in the shape of $G_{attr}(L)$ is chosen in the middle of the possible size range. The growth coefficient $k_{g,attr}$ is determined such that the effective growth rate at steady state conditions is zero for the maximum crystal length L_{end}

$$G_{eff}(L_{end}, \sigma_{ss}) = 0,$$

where G_{eff} is the sum of the physical growth rate G and the negative growth rate due to attrition G_{attr}

$$G_{eff}(L, \sigma) = G(\sigma, L) + G_{attr}(L).$$

This means that for a crystal which is larger than L_{end} the decrease in size due to attrition is faster than the size increase due to growth. In effect, the crystal becomes smaller. Hence, at steady state no crystals larger than L_{end} exist according to the simplified model. The maximum steady state crystal length L_{end} and the steady state concentration $c_{L,A,ss}$ are obtained from simulation of the reference model.

The remaining source term $\dot{F}^{+}_{attr,2}$ describing the production of small crystal fragments in the reference model is defined in equation (2.12). For the simplified model it is assumed that all attrition fragments are produced with the same length L_0 where $L_{frag,min} < L_0 < L_{frag,max}$. This means, that the size of attrition fragments is assumed to be independent of the size of the original large crystal L' and independent of the radial position r at which the crystal hits the stirrer. Hence, the distribution of the fragments $f_{frag}(L', L, r)$ in (2.12)

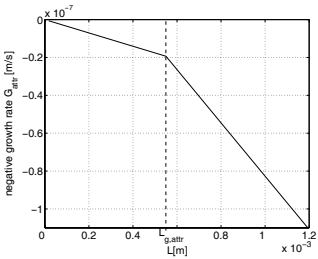

Figure 3.2: Negative growth rate due to attrition.

is replaced by a Dirac impulse $\delta(L - L_0)$. Since this function is independent of L' and r, the corresponding source term can be rewritten as

$$\dot{F}^{+}_{attr,2}(L,t) = \delta(L - L_0) \int_{L}^{\infty} \underbrace{\left(\int_{0}^{R_{st}} N_{frag}(L',r)\bar{\beta}(L',r)\, dr \right)}_{\beta_{frag}(L')} F(L',t)\, dL' \,. \tag{3.5}$$

where $\beta_{frag}(L')$ is the rate of fragment formation due to attrition. Since attrition is assumed to be the only source of nuclei and dissolution of small fragments is neglected, L_0 is the smallest length where crystals occur. Inserting the modified attrition expressions (3.4) and (3.5) into the population balance equation (2.1) and integrating it over the size domain from $L = 0$ to $L = L_0+$ (where L_0+ is an abbreviation for the right hand side limit $\lim_{L \to L_0} L, \quad L > L_0$) yields

$$\begin{aligned} \int_{0}^{L_0+} \frac{\partial F(L,t)}{\partial t}\, dL = \int_{0}^{L_0+} \Bigg(& - \frac{\partial (G_{eff}(\sigma,L)F(L,t))}{\partial L} - \dot{F}_{Product} \\ & + \delta(L - L_0) \int_{L}^{\infty} \beta_{frag}(L')F(L',t)\, dL' + \dot{F}_{AZ,back} - \dot{F}_{AZ,in} \Bigg)\, dL. \end{aligned} \tag{3.6}$$

Since there are no crystals smaller than L_0, i.e. $F(L,t) = 0, \quad L < L_0$, this equation can be simplified as follows

$$0 = -G_{eff}(\sigma, L_0)F(L_0,t) + \int_{L_0}^{\infty} \beta_{frag}(L')F(L',t)\, dL'. \tag{3.7}$$

If the size range on which the population balance equation (2.1) is defined is confined to $L > L_0$, then the left boundary condition is defined by the formation of attrition

$$F(L_0, t) = \frac{\int_{L_0}^{\infty} \beta_{frag}(L) F(L, t)\, dL}{G_{eff}(\sigma, L_0)}. \tag{3.8}$$

In the reference model, the production rate of fragments $\beta_{frag}(L)$ is a complex nonlinear function depending on the geometry and speed of the stirrer and physical properties of the crystalline material and the liquid phase [26]. For the use in the simplified model, this function is approximated by a power law of the form $k_b L^b$. Finally, the boundary condition for the simplified model is defined as

$$F(L_0, t) = \frac{B(t)}{G_{eff}(\sigma, L_0)}, \tag{3.9}$$

where

$$B(t) = k_b \int_{L_0}^{\infty} L^b F(L, t)\, dL \tag{3.10}$$

is the rate of particle formation due to attrition. The minimum crystal length L_0 is chosen such that

$$c_{L,A,sat,ideal} e^{\frac{\Gamma_S}{RTL_0}} = c_{L,A,ss}, \tag{3.11}$$

i.e. the driving force for crystallization at steady state conditions according to (2.5) is zero for crystals of size L_0. This means, L_0 is the size at which the steady state growth rate is 0. Crystals smaller than L_0 observe a negative growth rate and, therefore, vanish eventually. The nucleation coefficient k_b in (3.9) is chosen such that the steady state solute concentrations $c_{L,A,ss}$ obtained with the simplified model and the reference model are equal. For a graphical illustration of the simplified attrition model see Figure 3.3, which is to be compared to the original version in Figure 2.3.

3.2.2 Reformulation of Solute Mole Balance for the Crystallizer

The process under consideration is an evaporative crystallizer where solvent is evaporated at a constant vapour flow rate $\dot{V}_{vap}$. Instead of including the evaporation explicitly in the model it can be captured equivalently by decreasing the value of the inlet flow rate $\dot{V}_{Feed}$ by the amount of the vapour outflow $\dot{V}_{vap}$ and increasing the feed concentration $c_{Feed,L,A}$ accordingly, such that the inlet mole flux of solute $\dot{V}_{Feed} \cdot c_{Feed,L,A}$ is maintained.

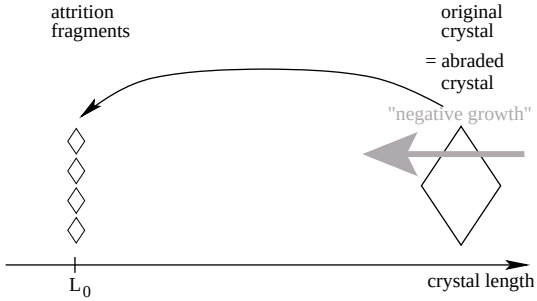

Figure 3.3: Attrition of crystal colliding with the stirrer, simplified version. (Compare to Figure 2.3)

Assuming that the mixture of solute and solvent is ideal and the volume change due to crystallization is negligible, the requirement of constant total volume $V = const.$ implies that the volumetric in- and outflow rates are equal $\dot{V}_{Feed} = \dot{V}_{Product}$. Under these assumptions, the solute mole balance describing the liquid phase (2.15) can be expressed in terms of the solute concentration $c_{L,A}$ by the following ODE

$$\begin{aligned} \frac{dn_{L,A}}{dt} &= V\frac{d(\varepsilon_L c_{L,A})}{dt} = (c_{Feed,L,A} - c_{L,A}\varepsilon_L)\,\dot{V}_{Feed} + \dot{n}_{FD,out} \\ &\quad -c_{L,A}\varepsilon_L \dot{V}_{AZ,in} - \frac{3\rho_A k_V}{M_A}\int_{L_0}^{L_\infty} L^2 G(\sigma, L) F(L,t) dL, \end{aligned} \tag{3.12}$$

with liquid volume fraction ε_L

$$\varepsilon_L = \frac{V_L}{V} = 1 - \frac{k_V}{V}\int_{L_0}^{L_\infty} L^3 F(L,t) dL. \tag{3.13}$$

The molar flux entering the crystallizer from the fines dissolution unit $\dot{n}_{FD,out}$ is defined in the following chapter where fines dissolution is treated in more detail.

3.2.3 Settling Zone and Fines Dissolution Loop

In the reference model it is assumed that no nucleation, growth or attrition occurs in the annular settling zone. Consequently, the dynamics are only determined by the in- and outflow terms from the crystallizer to the settling zone, from there to the fines dissolution

unit and from the annular zone back to the crystallizer due to backmixing, see equation (2.24).

The settling zone exerts two effects on the crystallizer. First, it is responsible for the separation of fines. Second, the annular zone represents an additional volume for the crystallizer. In order to simplify the crystallizer model, in the following these two effects are treated completely separately and independent of each other.

First, to incorporate the volume of the annular zone into the crystallizer model it is assumed that the suspension inside this zone is ideally mixed. Hence, the settling zone can be regarded as a dead volume which is connected to the crystallizer. In a first step, the

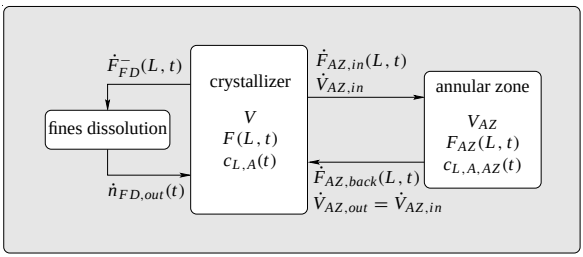

Figure 3.4: Illustration of simplified model.

separation effect is not considered. Consequently, at this point the flux of small crystals from the annular zone to the fines dissolution unit is neglected

$$\dot{F}_{AZ,out} = 0. \tag{3.14}$$

Furthermore, it is assumed that the solids content in the flow going back to the crystallizer is representative

$$\dot{F}_{AZ,back}(L,t) = \frac{\dot{V}_{AZ,out}(t)}{V_{AZ}} F_{AZ}(L,t). \tag{3.15}$$

Under these assumptions it follows from the requirement of constant volume of slurry in the annular zone (2.34) that the volumetric in- and outflow rates are equal

$$\dot{V}_{AZ,out}(t) = \dot{V}_{AZ,in}(t). \tag{3.16}$$

Consequently, the incoming particle flux from the crystallizer to the settling zone (2.27) is

$$\dot{F}_{AZ,in}(L,t) = \frac{\dot{V}_{AZ,out}(t)}{V} F(L,t). \tag{3.17}$$

The purpose of this model is to study a crystallizer under operating conditions which lead to sustained oscillations. These operating conditions are primarily characterized by extensive fines dissolution. This means, the volumetric flow rate to the fines dissolution unit $\dot{V}_{AZ,out}$ is large. Under this condition it is justified to assume that the residence time in the annular zone is small compared to the time constants of crystal growth and attrition. Consequently, the settling zone can be regarded quasi-stationary, i.e. the time derivative in (2.24) is set to zero. This leads to

$$\dot{F}_{AZ,in}(L,t) - \dot{F}_{AZ,out}(L,t) - \dot{F}_{AZ,back}(L,t) = 0 \tag{3.18}$$

and with the simplified expressions for the number fluxes entering and leaving the annular zone (3.14), (3.15) and (3.17) it follows that

$$\frac{F_{AZ}(L,t)}{V_{AZ}} = \frac{F(L,t)}{V}. \tag{3.19}$$

This means that the volume based CSDs (number of crystals per crystal length and volume of slurry) in the crystallizer and the settling zone are equal. To check if the model simplification derived for the settling zone, cumulating in equation (3.19), is justified, in Figure 3.5 the volume based mass density functions in the crystallizer, $\frac{k_V \rho_A L^3 F(L,t)}{V}$, and the annular zone, $\frac{k_V \rho_A L^3 F_{AZ}(L,t)}{V_{AZ}}$, obtained from a simulation of the reference model are plotted. The mass density representation of the CSD (mass of crystals per crystal length) is shown rather than the number density function because it illustrates the shape of the CSD more intuitively. The CSDs are plotted at four time instances during one period of oscillation. It can be seen that both curves are very similar except for a sharp peak around $L = 0.1$ mm in the CSD in the annular zone. This peak is due to the fact that small particles are dragged along with the flow in the upward direction to the fines dissolution unit and large particles have a downward velocity due to gravitational settling. For particles around 0.1 mm both effects cancel out such that these particles accumulate in the settling zone. This effect is not captured in the simplified model. However, for physical reasons the existence of this accumulation effect is questionable anyway - particles with zero (or downward) velocity probably do not enter the settling zone in the first place.

The dynamics of the liquid phase composition in the annular zone is also completely determined by the in- and outgoing flows. Hence, with the same argument as above, the mole balance can be treated as quasi-stationary. From (2.31) it follows with (3.16) that

$$0 = c_L(t) x_{L,A}(t) - c_{AZ,L}(t) x_{AZ,L,A}(t) \tag{3.20}$$

which is equivalent to

$$c_{L,A}(t) = c_{AZ,L,A}(t). \tag{3.21}$$

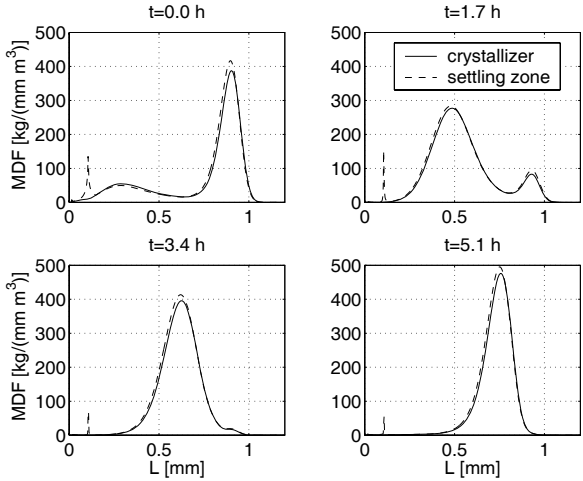

Figure 3.5: Comparison of $\frac{k_V \rho_A L^3 F(L,t)}{V}$ and $\frac{k_V \rho_A L^3 F_{AZ}(L,t)}{V_{AZ}}$.

i.e. the solute concentrations in the settling zone and the crystallizer are equal. Again, to verify whether this simplification is justified, in Figure 3.6 the concentrations in the crystallizer $c_{L,A}(t)$ and in the annular zone $c_{L,A,AZ}(t)$ are plotted for the time of one period of oscillation. These are results obtained with the reference model. Obviously, both concentrations are very similar during the entire time. Hence, the quasi-stationary treatment of the annular zone appears to be reasonable.

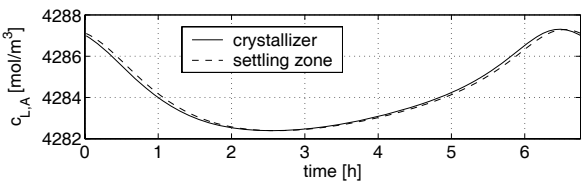

Figure 3.6: Comparison of solute concentration in the crystallizer and in the settling zone.

Up to this point only the additional volume provided by the settling zone was considered, the separation of small crystals has been disregarded. To capture the effect of fines

dissolution, an additional term $\dot{F}_{FD}$ is introduced in the population balance (2.1). Fines separation is modelled by a simple piecewise constant classification function $h_{FD}(L)$, see Figure 3.7. This function approximates the separation effect of the annular zone. In addition, it captures the fact that large particles are dissolved due to the local undersaturation produced by the hot reflux stream from the fines dissolution unit. The residence time in

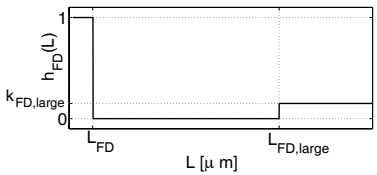

Figure 3.7: Piecewise constant classification function $h_{FD}(L)$.

the fines dissolution loop τ_{FD} is neglected. Hence, the particle number flux due to fines dissolution is

$$\dot{F}_{FD}(L,t) = \frac{\dot{V}_{AZ,out}}{V} h_{FD}(L) F(L,t) \tag{3.22}$$

and the mole flux from the fines dissolution unit to the crystallizer is

$$\dot{n}_{FD,out}(t) = c_{L,A}\varepsilon_L \dot{V}_{AZ,out} + \frac{\rho_A k_V}{M_S} \int_{L_0}^{L_\infty} L^3 \dot{F}_{FD}(L,t) dL. \tag{3.23}$$

To justify the use of the simple classification function $h_{FD}(L)$, in Figure 3.8 the effective classification function in the reference model $\frac{\dot{F}_{AZ,out}}{F(L,t)}$ is plotted for four different times during a cycle period along with the classification function $\frac{\dot{F}_{FD}}{F(L,t)} = \frac{\dot{V}_{AZ,out}}{V} h_{FD}(L)$ used in the design model. The very large values occurring in the reference model around $L = 0.1mm$ in the top right and the lower left plot of Figure 3.8 are a result of the sharp peaks seen in Figure 3.5, which have been discussed before. Apart from this rather questionable effect, the simple classification function $h_{FD}(L)$ matches the results of the reference models fairly well.

3.2.4 Summary of Simplified Model

Adding the population balances for the crystallizer (2.1) and the annular zone (2.24), taking into account (3.19) and (3.4), the final population balance equation for the crystallizer

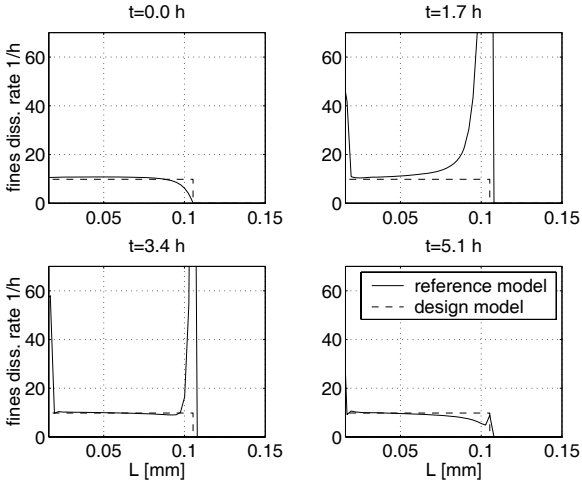

Figure 3.8: Classification functions in reference and design model

is obtained

$$\begin{aligned} \frac{V+V_{AZ}}{V}\frac{\partial F(L,t)}{\partial t} &= -\frac{\partial (G(\sigma,L)+G_{attr}(L))F(L,t)}{\partial L} \\ &\quad -\dot{F}_{Product}(L,t)-\dot{F}_{FD}(L,t) \end{aligned} \tag{3.24}$$

where the number flux due to product removal is the same as in the reference model (2.7) and the fines dissolution flux $\dot{F}_{FD}^{-}$ is given in (3.22). The corresponding boundary condition is

$$F(L_0,t)=\frac{k_b}{G_{eff}(\sigma,L_0)}\int_{L_0}^{\infty} L^b F(L,t)dL. \tag{3.25}$$

The growth rates G and G_{attr} (see (3.1) and (3.3)) are given by

$$\begin{aligned} G(\sigma,L) &= k_g\sigma^g\cdot\left(\frac{L(1-h(L-L_{growth}))}{L_{growth}}+h(L-L_{growth})\right) \\ G_{attr}(L) &= k_{g,attr}\left(L+3(L-L_{g,attr})h(L-L_{g,attr})\right). \end{aligned}$$

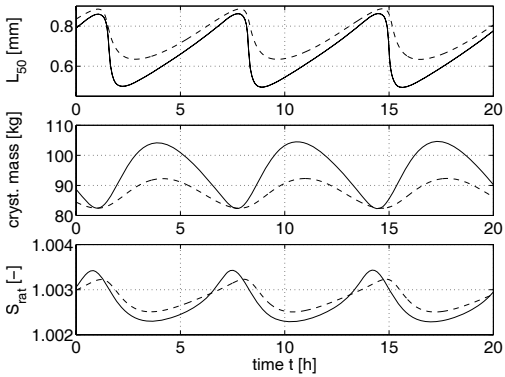

Figure 3.9: Comparison of mass median crystal size L_{50}, crystal mass and supersaturation S_{rat}: reference model (solid line) and simplified design model (dashed).

Similarly, the final solute mole balance is obtained from (3.12) with (3.21) and (3.23)

$$\begin{aligned}(V+V_{AZ})\frac{d(\varepsilon_L c_{L,A})}{dt} &= \dot{V}_{Product}\left(c_{Feed,L,A}-\varepsilon_L c_{L,A}\right)\\ &\quad+\frac{\rho_A k_V}{M_S}\int_{L_0}^{L_\infty} L^3\frac{\dot{V}_{AZ,out}}{V}h_{FD}(L)F(L,t)dL\\ &\quad-\frac{3\rho_A k_V}{M_S}\int_{L_0}^{L_\infty} L^2 G(\sigma,L)F(L,t)dL. \end{aligned} \tag{3.26}$$

The parameters used in the design model are listed in Appendix A.3.

In order to check the validity of the model simplifications presented in this chapter, simulation results of the reference model and the design model are compared. Figure 3.9 shows the mass median crystal size L_{50}, the overall mass of crystals and the relative supersaturation

$$S_{rat}(t)=\frac{c_{L,A}(t)}{c_{L,A,sat}}, \tag{3.27}$$

the driving force for crystallization, while the system is on its limit cycle. Obviously, the period of the limit cycle is matched almost perfectly although relatively simple kinetic expressions were chosen in the design model. Also, the shape of the signals and their phase is matched quite well. However, there is a notable difference in the amplitude

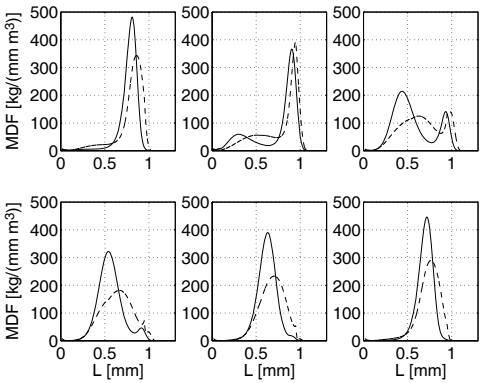

Figure 3.10: Comparison of mass density function during one oscillation period: reference model (solid line) and simplified design model (dashed).

of the oscillations for all three variables. In Figure 3.10, additionally, the mass density function is presented at six equally spaced instances of time during one oscillation period. In principle, the shapes of the mass density function match quite well. With both models it can be observed how a peak grows through the size range and that a new peak of small crystals is only formed when there is a significant amount of large crystals present. This is the basic mechanism causing the oscillatory behaviour. However, also for the mass density function there is a quantitative difference between the results obtained from the reference and the design model.

Recapitulating, it can be stated that the simplified model *reproduces* the basic dynamic behaviour of the process fairly well, which is important for controller design, but it is *not* expected to *predict* the behaviour if, e.g., operating conditions were changed significantly.

3.2.5 Derivation of Transfer Function

In contrast to the reference model, for the simplified design model a steady state solution can be derived analytically. The steady state size distribution

$$F_{ss}(L) \;=\; C \cdot \exp\left(-\int_{L_0}^{L} \frac{\frac{\dot{V}_{Product} + h_{FD}(\xi)\dot{V}_{AZ,out}}{V} + \frac{\partial G_{eff}(\xi,\sigma_{ss})}{\partial \xi}}{G_{eff}(\xi,\sigma_{ss})} \right) d\xi \qquad (3.28)$$

is the solution of the ordinary differential equation (ODE) obtained from (3.24) by setting the time derivative equal to 0. The constant C represents the steady state value of the number density function at the lower boundary, i.e. $F_{ss}(L_0) = C$. Usually, it would be expected that this constant could be determined by inserting the steady state solution (3.28) into the boundary condition (3.9). However, since the boundary condition involves an integral over the size distribution $F(L,t)$ the constant C cancels. Instead, the resulting nonlinear equation

$$G_{eff}(\sigma_{ss}, L_0) = k_b \int_{L_0}^{\infty} L^b \exp\left(- \int_{L_0}^{L} \frac{\frac{\dot{V}_{Product} + h_{FD}(\xi)\dot{V}_{AZ,out}}{V} + \frac{\partial G_{eff}(\xi,\sigma_{ss})}{\partial \xi}}{G_{eff}(\xi,\sigma_{ss})} \, d\xi \right) dL \qquad (3.29)$$

determines the steady state driving force σ_{ss} and thus the solute concentration $c_{L,A,ss}$. The constant C is obtained from the steady state version of the mole balance for the liquid phase (3.26). Consequently, the steady state solute concentration $c_{L,A,ss}$ is independent of the steady state solute concentration in the feed $c_{Feed,L,A}$. If the inlet concentration is set to a higher value, the steady state concentration does not change, but the constant C and therefore the overall amount of crystals increases.

This unexpected qualitative behaviour which can be deduced easily from the simplified model cannot be recognized so easily from the reference model. However, if the model simplifications carried out in this chapter are reasonable, similar behaviour should be found in the reference model. As the steady state cannot be calculated analytically the effect can only be verified by simulations. In Figure 3.11 simulation results of the reference model are shown resulting from two different feed concentrations. First, the feed solution is chosen to be saturated $c_{Feed,LA} = c_{L,A,sat}$. In a second simulation run the feed solution is undersaturated by 1%, i.e. $c_{Feed,LA} = 0.99 c_{L,A,sat}$. For this investigation the steady state is to be inspected. Hence, the dissolution of large crystals due to the hot reflux stream from the fines dissolution unit is neglected such that the model is stable and a steady state is reached. From Figure 3.11 it is obvious that the change in feed concentration has virtually no effect on steady state concentration. But, as expected from the analytic results for the simplified model, the overall number of crystals (zeroth moment of the CSD) settles at a lower value. This underlines the usefulness of the simplified model for analyzing the qualitative system behaviour.

Besides the steady state (3.28), the simplified model also possesses a trivial steady state $F(L,t) \equiv 0$, $c_{L,A} = c_{Feed,L,A}$, corresponding to $C = 0$. This would mean that no crystals are formed at all if the process is started with a crystal-free solution – regardless of the

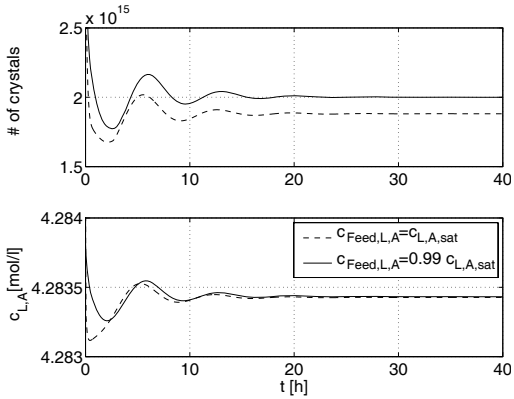

Figure 3.11: Number of crystals and solute concentration $c_{L,A}$ for different values of feed concentration.

level of supersaturation in the crystallizer. This, of course, is *not* a characteristic of the real process but a result of neglecting primary nucleation. As mentioned in section 2.2.1 the model is not meant to describe the process under conditions where only very few or very small crystals are present because in this case attrition is *not* the dominating source of nuclei.

For controlling the process a manipulated variable is needed. In this thesis the volumetric flow rate to the fines dissolution unit $\dot{V}_{AZ,out}(t)$ is used to act on the process. The third moment of the size distribution

$$m_3(t) = \int_{L_0}^{L_\infty} L^3 F(L,t)\, dL \tag{3.30}$$

is assumed to be measured. The third moment can be calculated from an online measurement of the particle size distribution, e.g. by Focused Beam Reflectance Measurement [44, 97].

The model equations (3.24), (3.26) and (3.9) with $\dot{V}_{AZ,out}(t)$ as the system input are linearized with respect to the desired steady state (3.28). Via Laplace-transformation an ODE with independent variable L is obtained from the linearized population balance equation. The particle number fluxes in (3.24) are such that this ODE can be solved analytically. From this solution $F(L,s)$ together with the linearized and Laplace-transformed

mole balance (3.26), a transfer function $P(s)$ from manipulated variable $\dot{V}_{AZ,out}$ to measured variable m_3 can be obtained

$$\Delta m_3(s) = P(s)\Delta\dot{V}_{AZ,out}(s) = \frac{QP_1(s)}{QP_2(s)}\Delta\dot{V}_{AZ,out}(s), \tag{3.31}$$

where the Δ-expressions denote deviations from the steady state. For the technical details on linearization and Laplace-transformation of the model and derivation of the transfer function $P(s)$ see Appendix C.

Both numerator $QP_1(s)$ and denominator $QP_2(s)$ of the plant transfer function $P(s)$ are *quasi-polynomials* of the form

$$QP_i(s) = \sum_k P_k(s)e^{-\tau_k s}, \quad i = 1, 2 \tag{3.32}$$

with polynomials $P_k(s)$. Quasi-polynomials are transcendental functions and therefore they have an infinite number of zeros [4]. Consequently, the plant transfer function $P(s)$ has infinitely many poles and zeros. This reflects the infinite-dimensional nature of the system. The transfer function $P(s)$ involves rather lengthy expressions, which were computed using a computer algebra system. Although the expression for $P(s)$ is not really handy it can, of course, be evaluated numerically. Instead of stating the transfer function explicitly it is more instructive to represent it graphically. Standard graphic representations of transfer functions are Bode and Nyquist plots of the corresponding frequency responses. The Bode amplitude and phase plots of $P(j\omega)$ are shown in Figure 3.12. The Nyquist plot in the complex plane is given in Figure 3.13.

Furthermore, poles and zeros of $P(s)$ can be computed numerically. The poles and zeros lying in a section of the complex plane are shown in Figure 3.14. It can be seen that there is one pair of unstable poles and two pairs of right half plane zeros. This implies that the steady state considered here is unstable - as expected. Furthermore the system is non-minimum phase. Based on this model, a stabilizing controller for the crystallization process is synthesized in the following chapter.

3.3 Discussion

In this chapter, the detailed population balance model presented in the previous chapter has been simplified based on physical considerations. The objective of this model simplification was to obtain a model which is in a more suitable form for controller design.

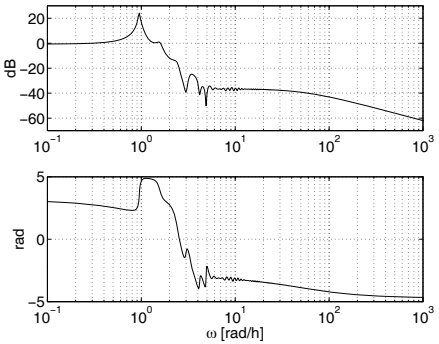

Figure 3.12: Bode plot of frequency response $P(j\omega)$.

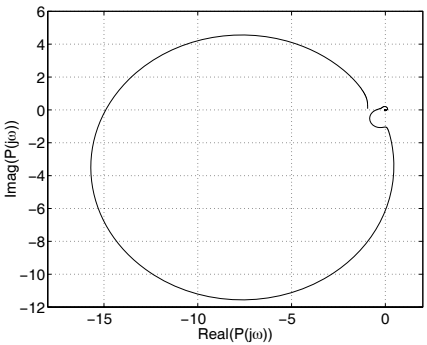

Figure 3.13: Nyquist plot of frequency response $P(j\omega)$.

Specifically, the model was reformulated such that a transfer function could be derived describing the relation of fines flow rate and third moment of the CSD, which will serve as manipulated and measured variable, respectively.

The simplifications involved

- replacing the kinetic expressions for crystal growth and attrition by simpler ones
- neglecting effects of crystal imperfection on saturation concentration
- quasi stationary treatment of the annular zone

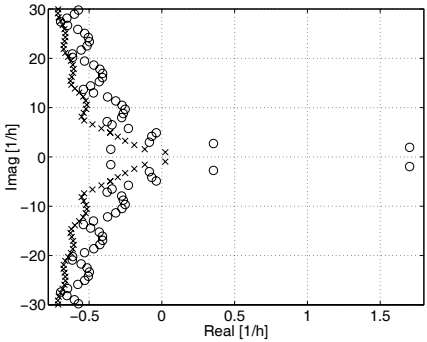

Figure 3.14: Poles $\times$ and zeros $\circ$ of the plant transfer function $P(s)$.

- description of fines separation by a simple classification function.

In these simplifications, predictiveness of the model was sacrificed for model simplicity. However, the resulting simplified model was shown in simulations to qualitatively reproduce the dynamic behaviour of the reference model. In a second step, the nonlinear model equations were linearized and Laplace-transformed. The simplified kinetic expressions introduced in the first simplification step had been chosen such that the ODE resulting from the linearized, Laplace-transformed population balance equation could be solved analytically. With this condition, it is possible to derive a transfer function for the crystallization process. This transfer function is irrational and, therefore, has infinitely many poles, which reflects the infinite-dimensional nature of the process. Based on this irrational transfer function, feedback controllers are developed in the following chapter.

Chapter 4

Controller synthesis

4.1 Introduction to Continuous Crystallizer Control

Research activities on feedback control of continuous crystallization are very much focused on processes exhibiting sustained oscillations. In this context, the purpose of feedback control is to stabilize an open-loop unstable steady state surrounded by a stable limit cycle. This is an area of active research, see [87] for a profound review. There are several open problems which have to be resolved for effective crystallizer control [39].

Any feedback controller needs on-line measurement information. Measuring the most important variables involved in crystallization, supersaturation and CSD, is not trivial. For on-line measurement of supersaturation *Fourier transform infra red spectroscopy* (FTIR) has been reported to be useful especially in combination with *attenuated total reflection* (ATR) probes, see e.g. [13, 54]. For an overview on supersaturation measurement techniques see [55]. For on-line CSD measurement, several approaches are under investigation including techniques based on ultrasonic wave extinction, laser light diffraction and focused beam reflectance (FBRM), [76, 97]. Several measurement devices are available commercially. The main drawback of these techniques is that the CSD is not *directly* measured but has to be calculated from the measurement signals. These calculations are often ill-conditioned and, therefore, difficult to do. They implicitly assume a certain fixed shape of crystals, which in some cases may lead to corrupted results. Furthermore, image analysis can be applied for the determination of CSDs. Imaging has the advantage that also the shape of crystals can be determined. However, image analysis needs a lot of computation time which makes it difficult to use as an on-line measurement. For all

the techniques which can not be applied directly in the process ("in-line") the problem of drawing samples has to be solved. Comparability of CSDs obtained with different measurement principles is an open problem as well. The influence of the choice of measurement devices on controllability of the process is addressed in [15].

Apart from the need of on-line measurements, a further prerequisite for model based control is a process model. As has been seen in the previous chapters, models for crystallization processes are rather complex. Population balance models are of distributed nature and they are usually nonlinear, which makes model based controller synthesis for crystallization processes a challenging task. This is the problem addressed in this chapter. In the literature, several different ways to deal with the model complexity problem have been reported.

First, simple PID-type controllers can be used, where the tuning of the controller parameters does not require an explicit plant model, see e.g. [5, 52, 84, 88, 101]. In [87], the major shortcoming of these simple controller designs is identified to be their lack of explicit consideration of the issue of robustness with respect to uncertainty.

A second way to deal with the problem of model complexity is to use a relatively simple population balance model for which a closed set of moment equations can be derived. Hence, the moment equations together with mass and energy balances form a finite-dimensional model, which exactly reproduces the trajectories of the moments, the solute concentration and the crystallizer temperature. Based on a moment model, in [72] a multivariable controller is designed optimizing a quadratic cost functional. In [37], controllability and observability of crystallization processes is investigated on the basis of moment models. The main drawback of this approach is that it is not applicable to processes with fines dissolution because in this case a term in the population balance equation is needed which cannot be expressed as a function of moments. Furthermore, for the method of moments to be applicable all variables of interest – in particular the measured and controlled variables – have to be functions of the state variables of the moment model, i.e. the moments, solute concentration and crystallizer temperature.

Third, it is possible to base controller design on a finite-dimensional model obtained by system identification methods or by training of an artificial neural network, see [14, 90]. Following this approach, no first principles model is needed. However, an identified model does not provide as much insight into the system and does not promote the understanding of the process as a model derived from first principles does. Yet, understanding the process to be controlled is of importance for an appropriate controller design.

Fourth, it is possible to start with an infinite-dimensional population balance model, approximate it by a finite-dimensional system, and design a controller using finite-dimensional theory. In [17, 104], a population balance model is linearized and lumped using the method of lines. Using the LQG approach, a linear, finite-dimensional SISO controller is designed in [17]. In [9], a general method for the approximation of nonlinear infinite-dimensional systems by finite-dimensional ones is presented. This approach makes use of the method of weighted residuals in combination with the concept of approximate inertial manifold. Subsequently, an input-output-linearizing controller can be designed based on the nonlinear, finite-dimensional approximated model. Unfortunately, in the continuous crystallizer example presented in [9] this approximation method is not applied but a simple population balance is used from which a moment model is derived. In [10, 11] these ideas are extended by considering model uncertainty issues. In [102], a multiple input - multiple output predictive control is developed employing a discretized population model. More specifically, a nonlinear quadratic dynamic matrix control is implemented using state estimation by an extended Kalman filter.

Results on the application of infinite-dimensional control theory to population balance systems are rare. Approximate controllability of a population balance model for a continuous crystallization process was proven in [98]. Recently, controller design for an oscillatory crystallizer using H_∞-theory for infinite-dimensional systems [24] was reported in [108] for a relatively simple population balance model. In [110], this approach has been applied to the population balance model developed in Chapter 3. Both [108] and [110] have been co-authored by the author of this thesis. This controller design procedure is described in the remainder of this chapter.

4.2 Choice of Controller Synthesis Method

In the two previous chapters, a model of a crystallization plant has been derived which, on one hand, captures the essential dynamic behaviour and represents the infinite-dimensional nature of the plant. On the other hand it is in a form which is useful for controller design. Namely, a transfer function from manipulated input to measured output has been derived. Hence, Bode and Nyquist plots can be produced and the location of poles and zeros of the system can be computed. This is standard information on which classical linear controller design is based. Thus, control engineers' intuition can be applied, although dealing with an infinite-dimensional model. In particular, us-

ing the Nyquist stability criterion a PID-type controller could be designed. However, the transfer function $P(s)$ represents the linearized version of an already simplified model. If the controller is desired to work also with the original reference model the controller has to be robust with respect to model uncertainties. H_∞-theory provides a framework for the systematic synthesis of controllers which guarantee stability and a certain level of performance not only for the nominal model underlying the controller design process but for a whole set of models containing the nominal design model. Thus, H_∞-theory is well suited for the design of robust controllers. H_∞-theory is well established for linear, time-invariant, finite-dimensional systems, see e.g. [116] for an excellent textbook. But it has long been known that the basic considerations on robustness and performance carry over to the infinite-dimensional case [25]. However, the computational methods used for finite-dimensional systems are not applicable any more. The state space methods usually employed for solving the H_∞ minimization problem, i.e. the actual computation of a controller, cannot be used in infinite dimensions since the system state is not a vector in $\mathbb{R}^n$. State space methods for infinite-dimensional systems were developed in [106]. This approach involves the solution of operator Riccati equations and is therefore not applicable easily. An alternative frequency domain approach was taken in [24, 78]. This method is more easily implementable and is therefore employed here to synthesize controllers for the crystallization process. It allows the solution of the mixed sensitivity problem, which will be defined later on, for infinite-dimensional single-input-single-output (SISO) plants with finite-dimensional weighting functions. In this approach, the idea of *late lumping* is pursued. Controller design is based on the linearized distributed parameter model. This results in a controller which is itself infinite-dimensional. For implementation, the controller is approximated by a finite-dimensional transfer function. Thus, the system's distributed nature is preserved as long as possible in the controller design process.

Alternatively, an *early lumping* approach could be taken. This would involve the approximation of the plant transfer function by a rational, i.e. finite-dimensional, transfer function. Then, finite-dimensional controller design techniques, e.g. standard H_∞ theory, could be applied. The advantage of this approach is that finite-dimensional H_∞ controller design is computationally simpler and more flexible than the infinite-dimensional design. However, the infinite-dimensional problem can also be solved using a computing environment such as Matlab. Furthermore, the early lumping approach is also not free of problems. Care has to be taken in the approximation of the unstable infinite-dimensional plant transfer function. The unstable poles of the plant transfer function $P(s)$ are very close to the imaginary axis, see Figure 3.14. If the exponential terms in $P(s)$ are simply

approximated by Padé-terms these poles could easily be shifted into the left half plane. An uncertain number of poles, however, can potentially cause problems in a robust controller design.

The main advantage of the late lumping approach is related to the achievable controller quality. Since H_∞ controller design is based on the minimization of a certain cost function a clear measure for the quality of a controller is defined – the value of the cost function. In an early lumping approach, the cost function would be minimized with respect to the approximated finite-dimensional model. Hence, the controller would, of course, be optimal for controlling the finite-dimensional model. For the infinite-dimensional plant, however, it would be sub-optimal and it is not obvious how far it would be from the optimum. In contrast, with the late lumping approach, first, the optimal controller is synthesized. The optimal controller is irrational and, therefore, not readily implementable. In the subsequent approximation of the controller, quality is certainly sacrificed. But, as the optimum is known, also the quality loss associated with the approximation is known. Hence, an explicit trade off between quality and simplicity of the controller is possible.

4.3 H_∞-Control for Infinite-Dimensional Systems

The primary reason for controlling the process is to stabilize the unstable steady state (3.28). Furthermore, the controller can be designed to attenuate the effects of unknown disturbances acting on the process such as changes in feed concentration or temperature. The controller design will be based on the simplified linear model derived in Chapter 3. Hence, the controller needs to be *robust* with respect to mismatch between the design model and the reference model. H_∞-theory provides a framework for the rigorous formulation of such robustness issues by making use of the H_∞ norm for transfer function matrices. For a stable $G(s)$ the H_∞ norm is defined as

$$\|G(s)\|_\infty := \sup_\omega \bar{\sigma}[G(j\omega)] \,, \tag{4.1}$$

where $\bar{\sigma}$ denotes the maximum singular value. In this context, a transfer function is said to be stable if it has no poles in the closed right half of the complex plane. The H_∞ norm can be interpreted as the maximum gain of the transfer function matrix $G(s)$. H_∞ controller design is based on the minimization of the H_∞ norm of certain closed loop transfer functions under the constraint of closed loop stability. In this framework, a controller $C(s)$ can be explicitly designed to guarantee closed loop stability and a certain level of

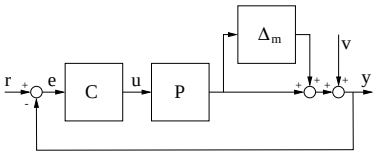

Figure 4.1: System with multiplicative uncertainty.

disturbance attenuation not only for the nominal design model $P(s)$ but for a set of transfer functions containing $P(s)$. This set of transfer functions is defined by the type of model uncertainty which is considered. The controller is then called robust with respect to this model uncertainty. There are many different ways to formulate model uncertainty. Two standard formulations are presented in the following. As we are dealing with a SISO plant this exposition is not given for the general case but in a formulation specific for SISO systems.

4.3.1 Multiplicative Model Uncertainty

One way to describe plant model mismatch is *multiplicative model uncertainty*. This concept is illustrated in Figure 4.1. The controller $C(s)$ is required to stabilize not only the nominal model $P(s)$ but all transfer functions in the set

$$\begin{aligned}\mathcal{P}_m = \{&(1+\Delta_m(s))P(s) : |\Delta_m(j\omega)| < |W_m(j\omega)|,\\ &P(s) \text{ and } (1+\Delta_m(s))P(s) \text{ have the same}\\ &\text{number of right half plane poles}\}.\end{aligned} \tag{4.2}$$

The weighting function $W_m(s)$ is a degree of freedom which has to be specified during the design process. $W_m(s)$ is an asymptotically stable transfer function which, without loss of generality, can be restricted to be minimum phase. It can be shown that a controller $C(s)$ stabilizes all elements of the set $\mathcal{P}_m(s)$ if and only if it stabilizes the nominal plant model $P(s)$ and

$$\left|\left| W_m(s)\frac{P(s)C(s)}{1+P(s)C(s)} \right|\right|_\infty < 1. \tag{4.3}$$

The influence of disturbances v on the measured output y is given by the *sensitivity transfer function*

$$S_\Delta(s) = \frac{1}{1+P_\Delta(s)C(s)}, \tag{4.4}$$

where $P_\Delta(s) = (1 + \Delta_m(s))P(s)$. Of course, it is desired to make the effect of disturbances small. Hence, the requirement of disturbance attenuation can be formulated using the sensitivity function

$$|S_\Delta(j\omega)| < \left| \frac{1}{W_d(j\omega)} \right| , \quad \forall\omega \tag{4.5}$$

or equivalently

$$||W_d(s)S_\Delta(s)||_\infty < 1 \tag{4.6}$$

where $W_d(s)$ is a stable frequency dependent weighting function which, again, can be restricted to be minimum phase. It determines how good disturbance attenuation is required to be at which frequency. It is the other degree of freedom besides $W_m(s)$ which has to be chosen in the design process.

It can be shown [116] that a controller $C(s)$ guarantees disturbance attenuation (4.6) and closed loop stability (4.3) for all $P_\Delta(s) \in \mathcal{P}_m$ if it stabilizes the nominal model $P(s)$ and

$$\gamma_m(C) = \left\| \begin{bmatrix} W_d(s)\frac{1}{1+P(s)C(s)} \\ W_m(s)\frac{P(s)C(s)}{1+P(s)C(s)} \end{bmatrix} \right\|_\infty < \frac{1}{\sqrt{2}} . \tag{4.7}$$

A controller $C_{opt}(s)$ with the highest possible degree of disturbance attenuation and robustness with respect to multiplicative uncertainty is obtained by minimizing the performance index γ_m over all controllers stabilizing the nominal model $P(s)$

$$\min_{C \text{ stabilizes } P} \left\| \begin{bmatrix} W_d(s)\frac{1}{1+P(s)C(s)} \\ W_m(s)\frac{P(s)C(s)}{1+P(s)C(s)} \end{bmatrix} \right\|_\infty . \tag{4.8}$$

This is called the *mixed sensitivity problem*. As mentioned above, this minimization problem has been solved in [24, 78] for infinite-dimensional SISO plants $P(s)$ with finite-dimensional weighting functions $W_d(s)$, $W_m(s)$.

4.3.2 Coprime Factor Uncertainty

An alternative formulation of plant model mismatch is *coprime factor uncertainty* [32]. In this context the perturbed plant is defined as

$$P_\Delta(s) = (M(s) + \Delta_M(s))^{-1}(N(s) + \Delta_N(s)), \tag{4.9}$$

where $(M(s), N(s))$ is a coprime factorization of $P(s)$, i.e.

$$P(s) = M^{-1}(s)N(s) \tag{4.10}$$

with stable transfer functions $M(s)$ and $N(s)$ having no common right half plane zeros. Since both $M(s)$ and $N(s)$, have to be stable the unstable poles of the plant transfer function $P(s)$ have to be right half plane zeros of the factor $M(s)$.

The concept of coprime factor uncertainty is illustrated in Figure 4.2. More formally, the set of all transfer functions which are required to be stabilized is expressed as follows

$$\begin{aligned} \mathcal{P}_{cf} &= \{(M(s)+\Delta_M(s))^{-1}(N(s)+\Delta_N(s)) : |||[\Delta_N\ \Delta_M]|||_\infty < \epsilon, \\ &\quad \Delta_N, \Delta_M \text{ stable}\}. \end{aligned} \tag{4.11}$$

This formulation of model uncertainty is, in some sense, more powerful than the multi-

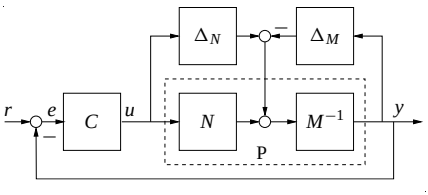

Figure 4.2: System with coprime factor uncertainty.

plicative uncertainty description (4.2) because it does not require that the nominal and the perturbed plant have the same number of unstable poles.

It can be shown that a controller $C(s)$ stabilizes all $P_\Delta \in \mathcal{P}_{cf}$ if and only if it stabilizes the nominal model $P(s)$ and

$$\gamma_{cf}(C) = \left\| \begin{bmatrix} C(s) \\ I \end{bmatrix} \frac{1}{1+P(s)C(s)} M^{-1} \right\|_\infty \leq \frac{1}{\epsilon} \tag{4.12}$$

see e.g. [116]. Hence, by minimizing γ_{cf} over all stabilizing $C(s)$ a controller is obtained which achieves the maximum possible degree of robustness with respect to coprime factor uncertainty

$$\min_{C \text{ stabilizes } P} \left\| \begin{bmatrix} C(s) \\ I \end{bmatrix} \frac{1}{1+P(s)C(s)} M^{-1} \right\|_\infty . \tag{4.13}$$

As will be seen in the following, unfortunately the H_∞ controller synthesis method for infinite-dimensional plants given in [24, 78] only solves the mixed sensitivity problem (4.8) but not the optimization problem resulting from coprime factor uncertainty (4.13). However, (4.13) can be reformulated to obtain a problem of the form (4.8) with a specific

choice of weighting functions W_d and W_m. To achieve this, the plant transfer function $P(s)$ is factorized according to (4.10) with the specific choice

$$M(s) = \frac{\prod_{k=1}^{m}(s - s_k)}{\prod_{k=1}^{m}(s + s_k)}\,, \tag{4.14}$$

where s_k, $k = 1, \ldots, m$ are the unstable poles of the plant $P(s)$. With this choice, the factor $M(s)$ is all-pass, i.e.

$$\begin{aligned} |M(j\omega)| &= 1 \\ \text{and hence} \quad |P(j\omega)| &= |N(j\omega)|\,. \end{aligned} \tag{4.15}$$

Consequently, (4.13) simplifies to

$$\min_{C \text{ stabilizes } P} \left\| \begin{bmatrix} C(s) \\ I \end{bmatrix} \frac{1}{1 + P(s)C(s)} \right\|_\infty . \tag{4.16}$$

This is equivalent to (4.8) with the weighting functions chosen as follows

$$\begin{aligned} W_d(s) &= 1 \\ W_m(s) &= N_m^{-1}(s)\,, \end{aligned} \tag{4.17}$$

where $N_m(s)$ is the minimum-phase part of $N(s)$, i.e. $N(s) = N_m(s)N_a(s)$, and $N_a(s)$ is all-pass. The frequency response $N_m(j\omega)$ has the same amplitude plot as $N(j\omega)$, i.e. $|N_m(j\omega)| = |N(j\omega)|, \quad \forall\omega$.

4.3.3 Computation of Optimal Controller

Once the weighting functions are chosen, a controller has to be computed, i.e. the minimization problem (4.8) has to be solved. A method for the solution of the mixed sensitivity problem for infinite-dimensional SISO plants was developed by C. Foias, H. Özbay and A. Tannenbaum using operator theoretic methods in the frequency domain, for details see [24, 78] and the references therein. It has been shown that this problem can be reduced to an eigenvalue-eigenvector problem for a Hankel+Toeplitz type operator. If certain assumptions hold, the solution to the problem can be computed from a finite number of linear equations exploiting a special inner-outer factorization of the plant transfer function. Results from the above references which are necessary for the actual design procedure are briefly summarized in the following, as also presented in [108].

The synthesis method is applicable if the following assumptions are met:

1. The plant transfer function can be decomposed as

$$P(s) = \frac{M_n(s)N_1(s)N_2(s)}{M_d(s)}, \tag{4.18}$$

where

- $M_d \in H_\infty$ is rational inner
- $M_n \in H_\infty$ is arbitrary inner
- $N_1 \in H_\infty$ is outer and $N_1^{-1} \in H_\infty$
- $N_2 \in H_\infty$ is rational outer.

A transfer function is in H_∞ if and only if it is stable and proper. An H_∞-function M is called *inner* if $|M(j\omega)| = 1$. All pass transfer functions and pure delays are inner. An H_∞-function N is called *outer* if it has no zeros in the open right half plane. Minimum phase transfer functions are outer.

In particular, this has two consequences.

- Since all the plant factors are in H_∞, i.e. they are stable, the unstable poles of $P(s)$ represent the (right-half-plane) zeros of $M_d(s)$. The plant factor $M_d(s)$ is required to be finite-dimensional, which means that the plant $P(s)$ is only allowed to have finitely many unstable poles.
- $M_n(s)$ and $M_d(s)$ are inner, i.e. they are proper but not strictly proper. $N_1(s)$ is also proper, because $N_1(s) \in H_\infty$, but not strictly proper, because $N_1^{-1}(s) \in H_\infty$. Hence, for $\omega \to \infty$ any roll of in the Bode magnitude plot of $P(s)$ is produced by the rational factor $N_2(s)$. For $\omega \to \infty$ the Bode magnitude plot of $P(s)$ "looks like" that of a finite-dimensional transfer function. In particular, it has a constant roll off rate, which is an integer multiple of -20 dB per decade

$$\frac{\mathrm{d}\log_{10}|P(j\omega)|}{\mathrm{d}\log_{10}\omega} = -20k, \quad k \in \mathbb{N}_0$$

2. The weighting functions $W_m(s)$, $W_d(s)$, $W_d^{-1}(s) \in H_\infty$ are rational. Furthermore, $(W_m(s)N_2(s))^{-1} \in H_\infty$. This implies that if $P(s)$ is strictly proper, $W_m(s)$ has to be improper.

If the above assumptions are met an optimal controller solving the minimization problem (4.8) can be computed from the inner and outer factors of the plant transfer function

(4.18), two finite-dimensional transfer functions $E_\gamma(s)$, $F_\gamma(s)$ obtained from the weighting functions $W_d(s)$, $W_m(s)$ and another rational transfer function $L(s)$ satisfying a set of interpolation equations. An optimal controller is given by

$$\begin{aligned} C_{opt}(s) &= \frac{E_{\gamma_{opt}}(s)M_d(s)F_{\gamma_{opt}}(s)L(s)}{N_1(s)N_2(s)(1+M_n(s)F_{\gamma_{opt}}(s)L(s))}, \\ \text{with} \quad E_\gamma(s) &= \frac{W_d(-s)W_d(s)}{\gamma^2} - 1, \\ F_\gamma(s) &= H_\gamma(s)\prod_{i=1}^{n_1}\frac{s+\eta_i}{s-\eta_i}, \end{aligned} \tag{4.19}$$

where $\eta_1 \cdots \eta_{n_1}$ are the poles of $W_d(s)$, and $H_\gamma(s)$ is the stable, minimum-phase transfer function determined by the spectral decomposition

$$H_\gamma(s)H_\gamma(-s) = \left(1 - \left(\frac{W_d(s)W_d(-s)}{\gamma^2} - 1\right)\left(\frac{W_m(s)W_m(-s)}{\gamma^2} - 1\right)\right)^{-1}.$$

$L(s) = \frac{L_2(s)}{L_1(s)}$ is a rational transfer function satisfying the following interpolation conditions:

$$0 = L_1(\beta_k) + M_n(\beta_k)F_\gamma(\beta_k)L_2(\beta_k) \tag{4.20-a}$$

$$0 = L_1(s_k) + M_n(s_k)F_\gamma(s_k)L_2(s_k) \tag{4.20-b}$$

$$0 = L_2(-\beta_k) + M_n(\beta_k)F_\gamma(\beta_k)L_1(-\beta_k) \tag{4.20-c}$$

$$0 = L_2(-s_k) + M_n(s_k)F_\gamma(s_k)L_1(-s_k) \tag{4.20-d}$$

where $\beta_1, \cdots, \beta_{n_1}$ are the right half plane zeros of $E_\gamma(s)$ and $s_0, \cdots, s_{k-1}$ are the unstable poles of the plant $P(s)$. The transfer function $L(s)$ is of $(n_1+k-1)th$ order where k is the number of right half plane poles of $P(s)$ and n_1 is the number of right half plane zeros of $E_\gamma(s)$, i.e. the order of the weighting function $W_d(s)$. The conditions (4.20-a) - (4.20-d) make sure that the right half plane zeros of the $M_d(s)$ term in the numerator of C_{opt} are cancelled by the $(1 + M_n(s)F_{\gamma opt}L(s))$ expression within the controller and therefore do not cancel the unstable poles of the plant. The largest value for γ such that (4.20-a) - (4.20-d) has a non-trivial solution is the minimal performance cost γ_{opt}. Lower and upper bounds for γ_{opt} can also be computed [24]. The conditions (4.20-a) - (4.20-d) form a set of linear equations with the coefficients of $L_1(s)$ and $L_2(s)$ as unknown variables. It can be written in matrix form: $0 = A_\gamma \cdot l$, with vector l containing the unknown coefficients. A nontrivial solution is obtained if and only if matrix A_γ is singular. Therefore, γ_{opt} is found, for example, by searching the largest value of γ such that the minimum singular

value of A_γ is 0. Once the optimal performance cost γ_{opt} is known, it is straightforward to determine the corresponding controller C_{opt} from equation (4.19).

The procedure described in this section is readily implementable on a computer. In fact, a Matlab implementation is available [79] for the computation of C_{opt}, γ_{opt} if $P(s)$ is already decomposed according to (4.18). Also, factorization of the plant has been done in Matlab.

4.3.4 Reduction of Controller Dimension

The expression for $C_{opt}(s)$ (4.19) involves the possibly irrational transfer functions $M_n(s)$ and $N_1(s)$. Therefore, the optimal controller itself can be irrational. For practical implementation, it needs to be approximated by a rational transfer function. This is achieved using an approximation technique based on Fourier transform and balanced model reduction developed in [34]. To approximate a stable possibly infinite-dimensional transfer function $G(s)$ the following steps are taken.

1. Define the discrete counterpart $G_d(z) := G(\lambda(1-z)/(1+z))$ using the bilinear transform $s = \lambda(1-z)/(1+z)$. This transform maps the imaginary axis in the s-plane to the unit circle in the z-plane.

2. Discretize $G_d(z)$ on the unit circle:
$$G_{dk} = G_d(z_k) \text{ with } z_k = e^{j\frac{2\pi k}{M}}, \quad k = 1, \ldots, M. \tag{4.21}$$

3. Compute the discrete Fourier transform (DFT) coefficients for G_{dk}:
$$c_n = \frac{1}{M} \sum_{k=0}^{M-1} G_{dk} z_k^n, \quad n = 0, \ldots, M-1 \; . \tag{4.22}$$

4. The inverse DFT yields: $G_d(z_k) = \sum_{n=0}^{M-1} c_n z_k^n$, $k = 1, \ldots, M$. This expression is used to approximate $G_d(z)$ by $G_{d,appr}(z) = \sum_{n=0}^{N} c_n z^n$, with some $N < M$.

5. Using the inverse bilinear transform $z = (\lambda - s)/(\lambda + s)$ the approximation of $G(s)$ in the s-domain is obtained:
$$G_{appr}(s) = \sum_{n=0}^{N} c_n \left(\frac{\lambda - s}{\lambda + s} \right)^n \tag{4.23}$$
with coefficients c_n according to (4.22).

Convergence of this approximation in the H_∞ sense, i.e.

$$||G(s) - G_{appr}(s)||_\infty \to 0, \quad \text{for } (N, M) \to (\infty, \infty)$$

is established in [34] under certain mild conditions. However, for sufficiently close approximation, usually, very high approximation orders N are needed. Therefore, in a further step the order is reduced via balanced realization truncation. The discrete approximation $G_{d,appr}(z)$ obtained from the Fourier series can be realized in a special state space form for which the observability and controllability Gramians needed for balanced order reduction are especially easy to compute. Therefore, the combination of Fourier transform and balanced model reduction yields a fast and numerically robust approximation procedure. This procedure has been implemented in Matlab.

Note that the procedure described here is only applicable for stable transfer functions. If the controller $C_{opt}(s)$ is unstable, the (stable) infinite-dimensional factors in (4.19) need to be approximated separately. Namely, these factors are $N_1(s)$ and $M_n(s)$. If in (4.19) they are replaced by rational approximations a finite-dimensional approximation for the controller $C_{opt}(s)$ is obtained.
An alternative way to deal with an unstable controller is to factorize it with stable factors and subsequently approximate the infinite-dimensional factors. Any controller stabilizing the plant $P(s)$ can be represented in the form of the Youla parameterization [114]

$$C(s) = \frac{X(s) + M_d(s)Q(s)}{Y(s) - M_n(s)N_1(s)N_2(s)Q(s)} \tag{4.24}$$

where $M_d(s)$ and $M_n(s)N_1(s)N_2(s)$ are coprime factors of the plant $P(s)$ and the transfer functions $X(s)$ and $Y(s)$ are chosen such that they satisfy the Bezout identity

$$Y(s)M_d(s) + M_n(s)N_1(s)N_2(s)X(s) = 1. \tag{4.25}$$

All transfer functions occurring in (4.24) are stable. The factors $Y(s)$, $M_n(s)N_1(s)$ and $Q(s)$ are infinite-dimensional and, therefore, need to be approximated using the procedure presented in this Chapter. A rational approximation of the controller is obtained by replacing the infinite-dimensional factors in (4.24) by their respective approximations.

4.4 H_∞-Controller Design for the Crystallizer Model

4.4.1 Factorization of Plant Transfer Function

In this chapter, the H_∞-technique described so far is applied to the simplified continuous crystallizer model derived in Chapter 3. Two different designs are presented corresponding to two different choices of weighting matrices in the mixed sensitivity problem (4.8).

To obtain the factorization (4.18) of the plant transfer function $P(s)$, the right half plane poles and zeros of $P(s)$ have to be computed, i.e. the right half plane zeros of the quasi-polynomials $QP_1(s)$ and $QP_2(s)$ in (3.31) have to be determined. This problem can be solved numerically using the Nelder-Mead simplex search algorithm [73] implemented, e.g., in Matlab. The zeros of the plant transfer function $P(s)$ are computed by searching for minima of the absolute value $|P(s)|$, the poles are determined by searching minima of the inverse $1/|P(s)|$. Appropriate starting values for the search can e.g. be provided based on the visual inspection of a three dimensional magnitude plot of the transfer function's absolute value $|P(s)|$ over the complex plane. The unstable pair of poles is found to be

$$s_{0/1} = (0.0236 \pm 0.952j)1/\text{h}, \tag{4.26}$$

the right half plane zeros are

$$\begin{aligned} z_{0/1} &= (1.70 \pm 1.95j)1/\text{h} \\ z_{2/3} &= (0.354 \pm 2.73j)1/\text{h}. \end{aligned} \tag{4.27}$$

See also Figure 3.14 for a plot of the locations of poles and zeros. In the Bode plot given in Figure 3.12, it can be seen that the magnitude of the plant frequency response $P(j\omega)$ has a constant roll off rate of 20 dB per decade of ω for $\omega \to \infty$. With this roll off rate and with a finite number of unstable poles it is possible to factorize the plant transfer function $P(s)$ according to (4.18):

- $M_n(s)$ is an all-pass function with the right half plane zeros $z_i,\ i = 0, \ldots, 3$ given in (4.27).
- $M_d(s)$ is an all-pass function with the unstable poles of the plant s_0, s_1 given in (4.26) as its right half plane zeros.
- $N_2(s)$ has to produce the roll off of 20 dB per decade, because the other factors are all proper but not strictly proper (the inner functions $M_n(s)$ and $M_d(s)$ have

constant magnitude, the outer function $N_1(s)$ is required to be invertible in H_∞). Therefore, $N_2(s)$ is chosen to be a first order transfer function with one stable pole s_{N2} and no zero.

Consequently, the plant factors in (4.18) are given by the following expressions

$$M_n(s) = \frac{\prod_{i=0}^{3}(s - z_i)}{\prod_{i=0}^{3}(s + z_i)} \tag{4.28-a}$$

$$M_d(s) = \frac{(s - s_0)(s - s_1)}{(s + s_0)(s + s_1)} \tag{4.28-b}$$

$$N_2(s) = \frac{1}{s - s_{N2}} \tag{4.28-c}$$

$$N_1(s) = \frac{P(s)M_d(s)}{M_n(s)N_2(s)}. \tag{4.28-d}$$

4.4.2 Controller Design for Multiplicative Uncertainty

The next step in the H_∞ controller design is the choice of weighting functions $W_d(s)$ and $W_m(s)$ involved in the mixed sensitivity problem (4.8).

For a first design, the weighting functions will be chosen according to the considerations presented in Chapter 4.3.1, i.e. the controller is designed to guarantee stability and a certain level of disturbance attenuation in the presence of multiplicative model uncertainty.

Often, models are quite accurate at low frequencies but are rather uncertain in the high frequency range. In particular, several parameters for the simplified model derived in Chapter 3 were adapted to meet requirements at steady state, i.e. for $\omega \to 0$. In addition, the annular settling zone was considered quasi-stationary, neglecting fast dynamics. Therefore, the simplified model is expected to be "good" for low frequencies but rather inaccurate in the high frequency range. This is reflected by the choice of the multiplicative uncertainty weighting function

$$W_m(s) = \frac{(100s + 1)^2}{2(s + 1)} \tag{4.29}$$

which is small in the low frequency range and large for high frequencies. Furthermore, this transfer function has two zeros but only one pole (i.e. it is not proper) and hence satisfies the condition that $(W_m(s)N_2(s))^{-1} \in H_\infty$, see Chapter 4.3.3.

Disturbances acting on the process are usually varying relatively slowly. Therefore, disturbance attenuation is desired to be good in the low frequency range and one does not care for high frequencies. The corresponding weighting function is chosen such that $|W_d(s)|$ is large at low frequencies

$$W_d(s) = 10\frac{(s+1)^3}{(500s+1)^3}. \tag{4.30}$$

For a Bode magnitude plot of both weighting functions see Figure 4.3. As is to be expected, the choice of these specific functions involves some trial-and-error.

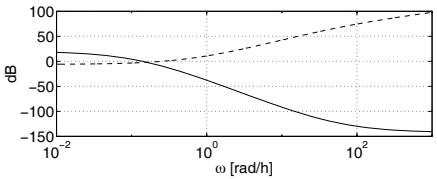

Figure 4.3: Magnitude of weighting functions $W_d(j\omega)$ (solid line) and $W_m(j\omega)$ (dashed) for mixed sensitivity problem .

Following the procedure given in Chapter 4.3.3, it is straightforward to compute an irrational optimal controller $C_{m,opt}(s)$ as given in (4.19). $C_{m,opt}$ turns out to be stable. For approximation, the controller transfer function is discretized with $M = 4096$ sampling points, see equation (4.21) and a Fourier series with $N = 500$ addends is computed according to equation (4.23) with the parameter $\lambda = 1.2$. Then, the resulting transfer function is reduced to 15^{th} order by balanced reduction, which yields a reasonable approximation error.

A Bode plot of the frequency responses of both optimal controller $C_{m,opt}(s)$ and approximated 15^{th} order controller $C_m(s)$ is presented in Figure 4.4. Nyquist plots of the open loop frequency responses with both controllers, i.e. $P(j\omega)C_{m,opt}(j\omega)$ and $P(j\omega)C_m(j\omega)$ are shown in Figure 4.5. The open loop system has one pair of unstable poles. According to the Nyquist stability criterion the Nyquist plot has to encircle the critical point -1 once to make the closed loop stable.

The controller was designed to be robust with respect to multiplicative plant uncertainty. However, its robustness can also be evaluated in terms of classical robustness measures such as gain and phase margins. These measures are also included in Figure 4.5. Relations

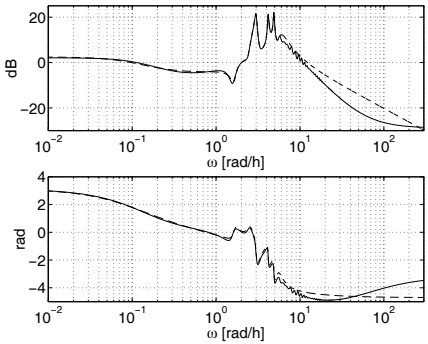

Figure 4.4: Bode plot of irrational optimal controller controller $C_{m,opt}(j\omega)$ (solid line) and 15th order approximation $C_m(j\omega)$ (dashed) for multiplicative uncertainty.

between gain and phase margin on the one hand and H_∞ robustness measures on the other hand are discussed in the textbook [33]. The gain margin for the continuous crystallization process with the 15^{th} order controller $C_m(s)$ is $a_m = 1/0.70 = 1.4$, the phase margin is $\alpha_m = 37.0°$. Typical values for a good design are given in [31]. The margins should be

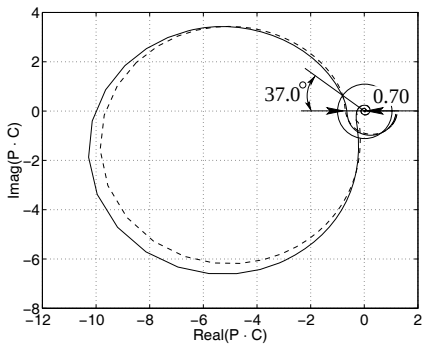

Figure 4.5: Nyquist plot of open loop transfer function $P(j\omega)C_{m,opt}(j\omega)$ (solid line) and $P(j\omega)C_m(j\omega)$ (dashed) along with unit circle (for the determination of gain and phase margins).

at least

$$a_m = 2.5 \dots 10 \tag{4.31-a}$$

$$\alpha_m = 30^\circ \dots 60^\circ. \tag{4.31-b}$$

According to these rules, the gain margin obtained with this controller design is not very good. This may be improved by asking for less disturbance attenuation, i.e. by making $|W_d(j\omega)|$ smaller, in the low frequency range. The frequency, at which the gain margin is obtained, is $\omega_0 = 0.40\ 1/\text{h}$.

4.4.3 Controller Design Based on Coprime Factor Uncertainty

In Chapter 4.3.2 a formulation of model uncertainty based on a coprime factorization of the plant transfer function is presented. Furthermore, it is shown that the resulting robust stabilization problem can be reformulated as a mixed sensitivity problem with the specific choice of weighting functions given in (4.17). However, since the plant factor $N_m(s)$ is infinite-dimensional, the choice of weighting function $W_m(s)$ according to (4.17) is in conflict with the requirement of finite-dimensional weights, which is a major requirement for the applicability of the H_∞ method presented in Chapter 4.3.3. This problem can be avoided by using a rational approximation of $N_m(s)$ in the definition of the weighting function

$$W_m(s) = N^{-1}_{m,appr}(s) = k \frac{(s+s_0)(s+s_1)\prod_{i=2}^{n_1}(s-s_i)}{\prod_{i=0}^{3}(s+z_i)\prod_{i=4}^{n_2}(s-z_i)}\,. \tag{4.32}$$

This approximation makes use of the first few poles s_i and zeros z_i of the plant P(s), where s_0, s_1 and z_i, $i = 0, \cdots 3$ are in the right half of the complex plane. In Figure 4.6, a Bode magnitude plot of $W_m(j\omega)$ from (4.32) and $N^{-1}(j\omega)$ is given, where 13 poles and 12 zeros of the plant are used in the definition of $N_{m,appr}(s)$. Since only the magnitude of the weighting function matters for the controller design, W_m can be chosen to be stable and minimum phase. This is achieved by reflecting the right half plane poles and zeros at the imaginary axis. This kind of controller design can be interpreted either as an 'approximate' coprime factor design or as a mixed sensitivity design with the choice of weighting functions $W_d(s)$ and $W_m(s)$ being inspired by the robust stabilization problem of coprime factor perturbed plants.

An optimal controller for this choice of weighting functions is obtained from (4.19). Again, a Fourier expansion as given in equations (4.21-4.23) is determined with the pa-

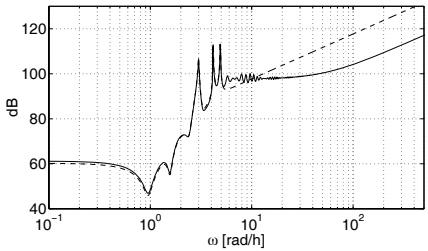

Figure 4.6: Magnitude plots of $N^{-1}(j\omega)$ (solid line) and weighting function $W_m(j\omega)$ (dashed line).

rameter values $M = 4096$, $N = 500$, $\lambda = 1.2$. Then, the resulting transfer function is reduced to 16^{th} order by balanced reduction.

In Figure 4.7 Bode plots of the frequency responses of the irrational optimal controller $C_{cf,opt}(s)$ and a 16^{th} order rational approximation $C_{cf}(s)$ are shown. Figure 4.8 presents the Nyquist plot of the frequency responses of the open loop transfer function $P(s)C_{cf}(s)$. Gain and phase margins are also included in the plot. The gain margin with the finite-dimensional controller $C_{cf}(s)$ is found to be $a_m = 1/0.30 = 3.3$, the phase margin is $\alpha_m = 67.7°$. Compared to the mixed-sensitivity design presented in the previous chapter, this controller design results in superior robustness properties in terms of the classical robustness measures. The controller designed in this chapter satisfies the rules given in (4.31-a) and (4.31-b).

4.5 Simulation Study

The uncontrolled process exhibits sustained oscillations. This means, after a transient phase the system ends up on a limit cycle. For controller design, this implies the following requirement. In order to be useful, a controller should not only stabilize the unstable steady state but the domain of attraction should include the limit cycle. Then, the controller can be switched on at any time while the crystallizer shows its natural oscillating behaviour and the controller will bring the system to its steady state.

To verify if the controllers designed in the previous chapter based on the linearized design model achieve this and in order to compare their performance and robustness properties,

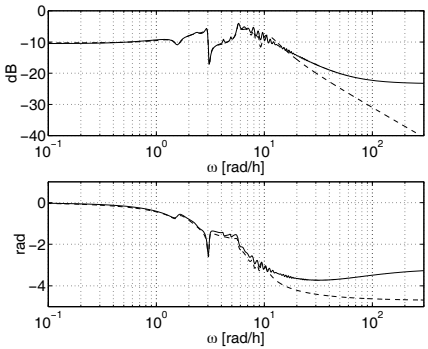

Figure 4.7: Bode plot of irrational optimal controller $C_{cf,opt}(j\omega)$) designed for coprime factor uncertainty (solid line) and 16th order approximation $C_{cf}(j\omega)$ (dashed.

they are tested in simulations with both the nonlinear simplified model derived in Chapter 3 and the original reference model presented in Chapter 2. For all simulations, the initial condition is chosen randomly on the limit cycle. The process is operated open loop with a constant fines flow rate $\dot{V}_{AZ,out} = 3l/h$ for 10 hours. Obviously, the crystallizer shows its characteristic oscillations. Then, at $t_0 = 10h$ the respective controller is switched on.

Figure 4.11 presents simulation results of the controller $C_m(s)$ designed for multiplicative

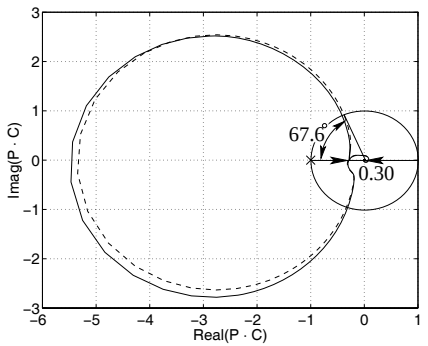

Figure 4.8: Nyquist plot of open loop transfer function $P(s)C_{cf,opt}(j\omega)$ (solid line) and $P(s)C_{cf}(j\omega)$ (dashed) for coprime factor uncertainty.

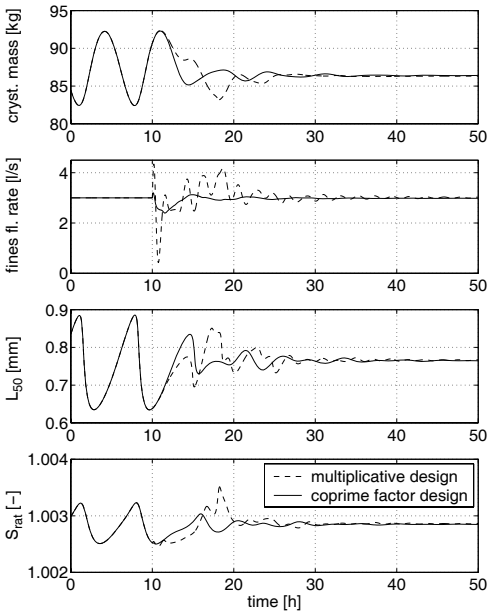

Figure 4.9: Simplified model simulation: controller started at $t_0 = 10h$. From top to bottom: Crystal mass in crystallizer (measured variable), fines flow rate (manipulated variable), mass median crystal size L_{50} and supersaturation S_{rat}.

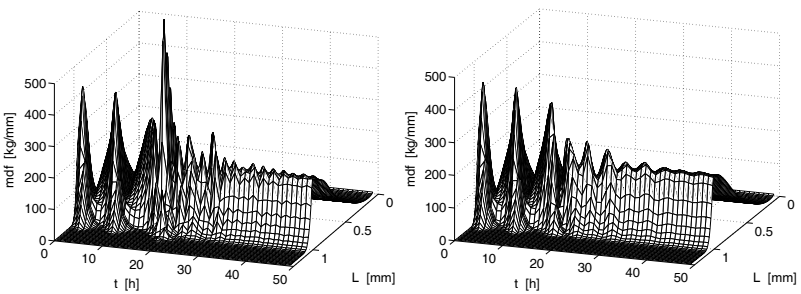

Figure 4.10: Simplified model simulation: mass density function with controller started at $t_0 = 10h$. Mixed sensitivity design 4.4.2 (left) and coprime factor design 4.4.3 (right).

uncertainty in Chapter 4.4.2 and the controller $C_{cf}(s)$ designed for coprime factor uncertainty in Chapter 4.4.3, both tested with the simplified model derived in Chapter 3. The first plot shows the overall crystal mass in the crystallizer, which is proportional to the third moment $m_3(t)$ of the size distribution, i.e. the measured variable. It is brought to its desired value in the time of about 3 cycle periods of the limit cycle. If only this variable is considered both controllers perform quite similar. They both stabilize the steady state and the speed of decay is comparable. However, the manipulated variable, i.e. the fines flow rate $\dot{V}_{AZ,out}(t)$, which is presented in the second plot, behaves quite differently for both controllers. The controller $C_m(s)$ uses much more control effort than $C_{cf}(s)$. Furthermore, there is a slightly damped oscillation in the manipulated variable plot for $C_m(s)$. This results from an almost pole-zero cancellation between plant and controller close to the imaginary axis. In the remaining plots, where the mass median crystal length $L_{50}(t)$ and the supersaturation $S_{rat}(t)$ are shown, this oscillation is also observed.

In Figure 4.12, the temporal evolution of the crystal size distribution in the form of the more intuitive mass density function

$$mdf(L,t) = k_V \rho_A F(t) L^3 \tag{4.33}$$

is shown as a quasi 3D plot. Obviously, not only the scalar measures in Figure 4.11 are brought to a constant value but also the mass density function $mdf(L,t)$ converges to its steady state distribution.

In simulations with the reference model, which was presented in Chapter 2, the difference between the two controllers becomes even more apparent. The controller $C_m(s)$ causes an oscillation of the same frequency as in the previous simulation but instead of being slightly damped the amplitude is slowly increasing. Hence, with the complex model the limit cycle does not belong to the domain of attraction any more. Simulation results for this case are not shown here.

In contrast, the controller $C_{cf}(s)$ designed for coprime factor uncertainty demonstrates its superior robustness. Just as in the simulation with the simplified model the steady state is stabilized although it takes somewhat longer to reach the steady state. As can be seen in Figure 4.11 the amplitude of the manipulated variable is, again, very acceptable. Figure 4.12 shows the convergence of the mass density function towards the steady state distribution.

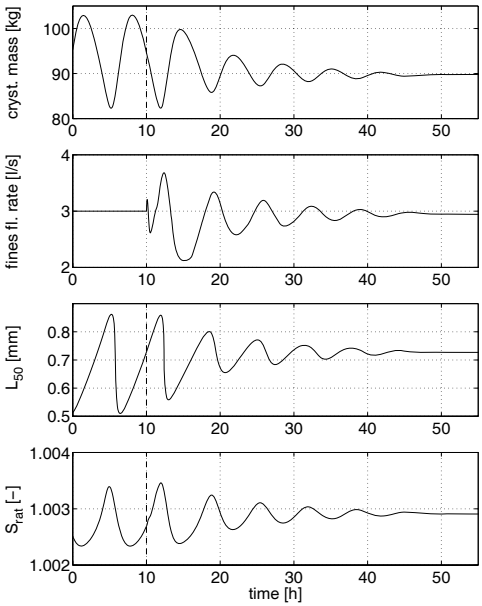

Figure 4.11: Reference model simulation: controller (coprime factor design) started at $t_0 = 10h$. Top to bottom: Crystal mass in crystallizer (measured variable), fines flow rate (manipulated variable), mass median crystal size L_{50} and supersaturation S_{rat}.

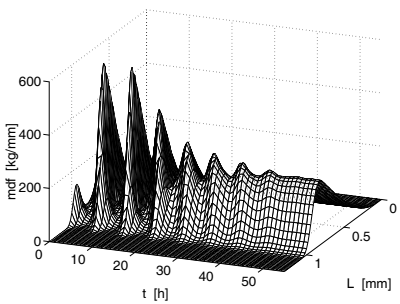

Figure 4.12: Reference model simulation: controller (coprime factor design) started at $t_0 = 10h$. Temporal evolution of mass density function.

4.6 Discussion

A controller design method for a continuous crystallizer has been presented. The controller design was based on the simplified model presented in the previous chapter. This model can be represented in the form of a transcendental transfer function. However, it is only an approximation of the original model. Therefore, controller design has to take into account robustness of the controller with respect to model uncertainties. H_∞-theory provides a framework for the formulation of robustness issues. Two different representations of model uncertainty were used, namely multiplicative uncertainty and coprime factor uncertainty.

Optimizing robustness with respect to multiplicative uncertainty leads to the mixed sensitivity minimization problem. This takes into account stability as well as disturbance attenuation of the closed loop system. By adjusting two weighting functions emphasis can be put on either of the properties, stability or disturbance attenuation. Also, optimization of robustness with respect to coprime factor uncertainty can be formulated as a mixed sensitivity problem, however, with a specific choice of weighting functions depending on the plant model.

A solution method for the mixed sensitivity problem for transcendental transfer functions from the literature has been presented and applied to the crystallizer control problem. In simulations with both the simplified design model and the reference model, the effectiveness of the controllers was tested. In the test with the simplified model both controllers behaved well. The situation was different with the reference model. With the multiplicative uncertainty approach, even after extensive trial-and-error, no choice of weighting functions was found which produced a controller stabilizing the reference model such that the limit cycle is in the domain of attraction. In contrast, with the coprime factor approach this design objective was achieved without any tuning of weighting functions.

Unlike other approaches to the problem of continuous crystallizer control this controller design is based on a distributed parameter model, i.e. an infinite-dimensional system. Only in the last step, after obtaining an optimal (transcendental) controller, it is approximated by a rational, i.e. finite-dimensional transfer function. Hence, the proposed controller design follows a late lumping philosophy.

An alternative procedure would be to approximate the transcendental plant transfer function by a rational transfer function first and subsequently do a standard H_∞ design with the same performance objective as used in the infinite-dimensional design. Padé approxi-

mations for the $e^{-\tau_i s}$-terms could be used, for example. In this case, care is to be taken that the unstable pair of poles, which is quite close to the imaginary axis, is not shifted to the left half plane. However, the major disadvantage of this "early lumping approach" is that one does not know how much better the controller could have been if it had been based on a better finite-dimensional approximation. In contrast, with the late lumping procedure, first the optimal solution is computed and then, in the last step, it is decided how much performance one is willing to sacrifice for the sake of a low-dimensional controller.

Chapter 5

Batch Crystallization – Flatness Analysis

5.1 Introduction to Batch Crystallization

Crystallization in batch mode is used for the production of smaller amounts of high-value-added fine chemicals and pharmaceuticals. The manufacturing of specialty products, such as biochemicals or food additives, becomes more and more important in the chemical industry. Batch operation enables a higher flexibility to allow for rapidly changing product specifications and quality requirements. Often, multi-purpose batch plants are used such that it is possible to quickly react to market demand and specific requests of costumers. Such demands can only be satisfied by employing advanced control strategies. The operation of one single plant in several different ways to obtain changing product specifications requires the ability of the plant operator to determine appropriate operation strategies which achieve prespecified product requirements. It is not desirable to determine these operation strategies from tedious test series for each new case, but it should be possible to quickly redetermine them, ideally on a batch-to-batch basis.

The batch-wise operation of crystallizers is quite different from the continuous mode. Consequently, the control problems arising from these two types of operation are also entirely different. Continuous crystallizers are operated without being changed for a long time. They have to be kept at a steady state such that a constant product quality is maintained. This may require the application of a stabilizing feedback controller as described in Chapter 4. Since the process is operated at a steady state, the controller can be designed

based on a linearized model. In contrast, batch crystallization is a transient process and does not achieve a steady state. Therefore, linearized models are not appropriate.

But not only the underlying model is different but also the reason for applying control differs from the continuous case. The main control objective is to achieve a desired product CSD at the end of the batch. The desired CSD may be specified in several different ways. It may either be entirely determined as a function of crystal length, or it may only be required to have certain properties (e.g. a certain mean crystal size). A third way to define a desired product CSD is to define an objective function which is to be optimized (e.g. maximize mean crystal size). Therefore, the control problem is to determine how to operate the crystallizer during a batch run such that a desired CSD is obtained at the end of the batch. This is, first of all, a problem of trajectory planning and feedforward control. In a second step, it may be desirable to incorporate feedback to be able to react to disturbances during the operation and to eliminate the effects of model uncertainties.

In the following, more specifically, batch *cooling* crystallization is considered, see Fig. 5.1. Cooling crystallization exploits the fact that solubility depends on temperature. The initially undersaturated hot solution is cooled during batch operation. Since solubility decreases with temperature the solution becomes supersaturated. Supersaturation is the driving force for nucleation and crystal growth, the main processes involved in crystallization. As the rates of nucleation and crystal growth depend on the degree of supersaturation and supersaturation, in turn, is a function of temperature, the final product CSD can be influenced by the temperature-time-profile during the batch. Consequently, crystallizer temperature serves as the manipulated variable for batch cooling crystallizers. The control problem is to determine a feedforward control, i.e. a temperature trajectory, which produces a desired CSD at the end of the batch.

Of course, in practice the temperature inside the crystallizer cannot actually be manipulated. Only the inlet temperature to the cooling jacket $T_c(t)$ can be influenced directly. Viewing $T_c(t)$ as the manipulated variable makes it necessary to augment the process model by an ODE for temperature $T(t)$ derived from an energy balance for the crystallizer. However, it is common practice in batch crystallization control to use a fast feedback controller that manipulates $T_c(t)$ and makes sure that the crystallizer temperature $T(t)$ tracks its desired value. Hence, temperature $T(t)$ can be pretended to be the manipulated variable. This approach has the advantage that uncertainties in the transfer behaviour from $T_c(t)$ to $T(t)$ are compensated by feedback. A common source for uncertainty is, e.g., the change of the heat transfer coefficient from cooling medium to crystallizer content due to fouling, i.e the deposition of crystal solids on the walls of the heat exchanger.

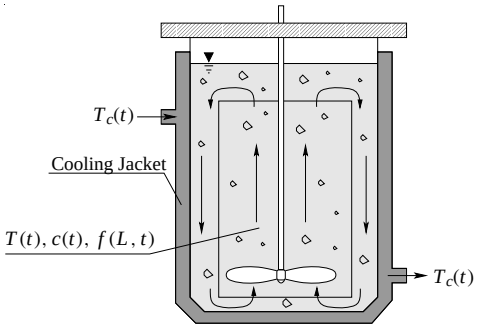

Figure 5.1: Sketch of a batch cooling crystallizer

A further means to influence the final CSD, besides the control of crystallizer temperature, is the addition of small seed crystals during the start of the batch. The amount and size distribution of seed crystals has a considerable effect on the achievable final CSD. The type of process treated in this study therefore is called *seeded batch cooling crystallization.*

As explained above, a *nonlinear* model has to be used as a basis for batch control design. Hence, the model is inherently more complex than the design model in the case of continuous crystallization. In order to keep the problem tractable we restrict ourselves to a population balance model with simpler constitutive relations for crystal growth and nucleation than in the model presented in Chapter 3. The population balance model considered here is of a standard type frequently used in the crystallization literature [86, 87]. The formulation used here is taken from [65] and is presented in Chapter 5.2. It is of a specific form such that a finite-dimensional moment model can be derived, which exactly describes the dynamics of a number of leading moments of the size distribution.

For the synthesis of control strategies the notion of *differential flatness* will be used. In Chapter 5.3 the definition of differential flatness is recapitulated. The idea of flatness has been introduced in [20, 22]. It is well known that flat systems possess a certain invertibility property and, therefore, trajectory planning and feedforward control design can be done in a very elegant way [94]. Therefore, in Chapter 5.4 flatness of the moment model is tested. It turns out that it is not flat but can be rendered flat by a state dependent time scaling. Such systems are called *orbitally flat* [21, 35, 89]. In Chapter 6 this property will be exploited for the design of feedforward and feedback control strategies for the batch crystallizer.

5.2 Batch Crystallizer Model

5.2.1 Population Balance Model

The investigations carried out in this and the following chapter are based on a – relatively simple – population balance model as, for example, described in the classical reference [86]. The specific formulation used here can be found in [65] where a model is presented describing crystallization of potassium nitrate (KNO_3) from water in a laboratory scale three litre batch cooling crystallizer. Differences compared to the continuous crystallizer model described in Chapter 2, on the one hand, are due to the different operation of the crystallizer and, on the other hand, they result from different modelling paradigms used. In batch mode there are, obviously, no feed and product removal streams. Furthermore, the crystallizer is not equipped with a fines dissolution unit. Consequently, the corresponding terms do not exist in the batch model. Concerning the modelling paradigm, in [65] the phenomena of nucleation, crystal growth and attrition are not described by detailed first principles models. Instead, empirical relations are used to describe nucleation and growth rates. The parameters involved in these equations have to be determined by parameter identification techniques from experimental data. The parameters summarize dependencies on the chemical system, the crystallizer type, size and geometry and the operating conditions such as temperature range or stirrer speed. Attrition is not modelled explicitly but the production of small fragments by attrition is contained implicitly in the nucleation rate. Consequently, the model is not expected to be able to *predict* the effects of, e.g., scale-up or changes in the operating conditions. But, as shown in [64], it is capable of *describing* the behaviour of a given process in the relevant operating range fairly well. To be appropriate for control design, a model needs to be descriptive but not necessarily predictive. Therefore, the type of model considered here has become and still is standard in batch crystallizer control [87].

Under the assumption that all crystals grow at the same rate, i.e. the growth rate G is independent of crystal size, and that nuclei are formed at negligible size, the temporal evolution of the CSD is described by the following population balance equation with boundary and initial condition

$$\frac{\partial f(L,t)}{\partial t} = -\frac{\partial (G(t) f(L,t))}{\partial L} \tag{5.1-a}$$

$$f(0,t) = \frac{B(t)}{G(t)} \tag{5.1-b}$$

$$f(L,0) = f_{seed}(L). \tag{5.1-c}$$

The rate of nucleation is denoted by $B(t)$ and the CSD of seed crystals added at the beginning of the batch is named $f_{seed}(L)$. A mole balance for the liquid phase yields an ordinary differential equation for the solute mass concentration $c(t)$ (in units of kg solute/kg solvent).

$$\begin{aligned} \frac{dc(t)}{dt} &= -3\rho_c k_v h \int_0^\infty L^2 G(t) f(L,t)\, dL, \\ \text{with } c(0) &= c_0 \end{aligned} \tag{5.2}$$

where ρ_c is the density of crystals, h is a conversion factor equal to the volume of slurry per mass of solvent and k_v is a volume shape factor defined such that the volume of a crystal with length L is $V_{crystal}(L) = k_v L^3$. Furthermore, an ODE for the temperature $T(t)$ is obtained from an energy balance of the crystallizer

$$\begin{aligned} \rho V c_p(t) \frac{dT(t)}{dt} &= -3\Delta H_c(t) \rho_c k_v V \int_0^\infty L^2 G(t) f(L,t)\, dL - U A_c (T(t) - T_c(t)) \\ \text{with } T(0) &= T_0. \end{aligned} \tag{5.3}$$

The heat of crystallization ΔH_c depends on the solution concentration. The dependence can be adequately represented by a quadratic fit to empirical data

$$\Delta H_c(t) = B_0 + B_1 c(t) + B_2 c(t)^2. \tag{5.4}$$

The heat capacity of the solution as a function of solution concentration can be expressed as

$$c_p(t) = C_0 + C_1 \left(\frac{c(t)}{1 + c(t)} \right) + C_2 \left(\frac{c(t)}{1 + c(t)} \right)^2. \tag{5.5}$$

Relative supersaturation, which can be defined as

$$S(t) := \frac{c(t) - c_{sat}(t)}{c_{sat}(t)}, \tag{5.6}$$

represents the driving force for crystallization. Hence, the growth rate

$$G(t) = k_g S(t)^g \tag{5.7}$$

is determined by supersaturation. Nucleation summarizes effects of primary and secondary nucleation (e.g. attrition) [86]. Therefore, the nucleation rate

$$B(t) = k_b S(t)^b k_v \int_0^\infty L^3 f(L,t)\, dL, \tag{5.8}$$

depends not only on supersaturation but also on the CSD. Both, the equations for nucleation and growth are of empirical nature. The parameters k_g, k_b, g and b have to be determined by parameter identification methods [65]. The saturation concentration c_{sat} depends on the temperature of the solution. A quadratic fit to solubility data gives

$$c_{sat}(t) = A_0 + A_1 T(t) + A_2 T(t)^2. \tag{5.9}$$

Thus, crystallizer temperature $T(t)$ determines saturation concentration and hence it influences the rates of nucleation $B(t)$ and growth $G(t)$ via supersaturation $S(t)$.

Equations (5.1-a) - (5.9) constitute an infinite-dimensional model for the batch crystallizer. It basically consists of a PDE (5.1-a) with boundary condition (5.1-b) coupled with two ODEs (5.2), (5.3). Values for all necessary parameters corresponding to the crystallization of KNO_3 from water are given in [64] and are summarized in Appendix B.

5.2.2 Moment Model

From the PDE (5.1-a) with boundary condition (5.1-b), a set of ODEs for the moments of the CSD

$$\mu_i(t) := \int_0^\infty L^i f(L,t)\, dL, \quad i = 0, 1, 2, \ldots \tag{5.10}$$

can be derived. The zeroth moment $\mu_0(t)$ gives the overall number of crystals. The second moment $\mu_2(t)$ is proportional to the overall crystal surface, and the third moment $\mu_3(t)$ is proportional to the volume of the crystalline material in the crystallizer. Since the duration of the batch t_{end} and the growth rate $G(t)$ are finite, i.e.

$$t_{end} < \infty \tag{5.11-a}$$

$$G(t) < \infty, \quad \forall t \tag{5.11-b}$$

it follows that the size of crystals is bounded. Hence, there is a maximum crystal length L_{max} such that the following is true

$$f(L,t) = 0, \quad \forall L > L_{max}. \tag{5.12}$$

Consequently, by partial integration it follows from (5.1-a), (5.1-b) that

$$\begin{aligned} \frac{d\mu_0(t)}{dt} &= B(t) \\ \frac{d\mu_i(t)}{dt} &= iG(t)\mu_{i-1}(t), \quad i = 1, 2, \ldots \end{aligned} \tag{5.13}$$

Since the overall mass of solute in the crystallizer is constant, an additional algebraic equation can be derived, relating the third moment $\mu_3(t)$ and the solute concentration $c(t)$

$$c(t) = c_0 + \rho_c k_v h(\mu_{3,Seed} - \mu_3(t)) \tag{5.14}$$

where c_0 is the initial solute concentration and $\mu_{3,Seed} := \int_0^\infty f_{seed}(L)\, dL$ is the third moment of the seed CSD. Hence, the ODE for the concentration (5.2) is redundant. Further, note that the integral expression in the nucleation law (5.8) is the third moment, i.e.

$$B(t) = k_b k_v S(t)^b \mu_3(t). \tag{5.15}$$

Because of (5.6),(5.7),(5.9) and (5.14), $B(t)$ and $G(t)$ are entirely determined by $\mu_3(t)$ and $T(t)$. Hence, the differential equations for the first four moments and the crystallizer temperature can be written as

$$\begin{aligned}
\frac{d\mu_0}{dt} &= B(\mu_3, T) && \text{(5.16-a)}\\
\frac{d\mu_1}{dt} &= G(\mu_3, T) \cdot \mu_0 && \text{(5.16-b)}\\
\frac{d\mu_2}{dt} &= 2G(\mu_3, T) \cdot \mu_1 && \text{(5.16-c)}\\
\frac{d\mu_3}{dt} &= 3G\left(\mu_3, T\right) \cdot \mu_2, && \text{(5.16-d)}\\
\frac{dT}{dt} &= -\frac{3\rho_c k_v}{\rho} \frac{\Delta H_c\left(\mu_3\right) G\left(\mu_3, T\right) \mu_2}{c_p\left(\mu_3\right)} - \frac{UA_c}{\rho V} \frac{(T - T_c)}{c_p\left(\mu_3\right)}, && \text{(5.16-e)}
\end{aligned}$$

with initial conditions

$$T(0) = T_0,\ \mu_i(0) = \mu_{i,Seed} = \int_0^\infty L^i f_{Seed}(L)\, dL, \quad i = 0, \ldots, 3.$$

This constitutes a simplified model for the batch crystallizer. It is clearly nonlinear, but finite-dimensional. The moments $\mu_0(t) \ldots \mu_3(t)$ and temperature $T(t)$ are the system states, and cooling medium temperature $T_c(t)$ is the control input. Viewing the temperature $T(t)$ as the control input by using a feedback tracking controller for the temperature as discussed in Chapter 5.1 eliminates equation (5.16-e), resulting in a model with only the moments as system states. The moment model (5.16-a)-(5.16-e) exactly describes the dynamics of the moments of the CSD but it does, of course, not describe the evolution of the entire CSD. As mentioned above, the moments have a clear physical meaning. For some applications they represent the most important aspects of the CSD, hence the exact shape of the CSD may not be of primary importance. Furthermore, as will be seen in the

following, the CSD at a certain point in time can be determined from the past trajectories of third moment and temperature. Hence, it is possible, on the basis of a moment model, to design control strategies to achieve given product CSDs.

5.3 Differential Flatness and Orbital Flatness

5.3.1 Introduction to Flatness

The notion of flatness can be mathematically defined in a differential algebra setting [22] or in the context of differential geometry of infinite jets and prolongations [23]. A finite dimensional dynamic system

$$\dot{x}(t) = f\left(x(t), u(t)\right), \quad x(t) \in I\!R^n,\, u(t) \in I\!R^m \tag{5.17}$$

is called *differentially flat*, or simply *flat*, if there exists a fictitious output $y(t) \in I\!R^m$ which satisfies the following conditions.

A The output $y(t)$ can be expressed as a function of the system states $x(t)$ and inputs $u(t)$ and finitely many time derivatives of the inputs

$$y(t) = \Phi\left(x(t), u(t), \dot{u}(t), \ldots u^{(\alpha)}(t)\right). \tag{5.18}$$

B Reversely, the system states and inputs can be expressed as functions of the output $y(t)$ and finitely many of its time derivatives

$$x(t) = \Psi_1\left(y(t), \dot{y}(t), \ldots, y^{(\beta)}(t)\right) \tag{5.19-a}$$

$$u(t) = \Psi_2\left(y(t), \dot{y}(t), \ldots, y^{(\beta+1)}(t)\right). \tag{5.19-b}$$

The fictitious output $y(t)$ is then called a *flat output*. It completely determines the dynamic behaviour of system (5.17). If a sufficiently smooth trajectory of the flat output is given, the trajectories of the entire system state $x(t)$ and the system input $u(t)$ are determined by (5.19-a) and (5.19-b), respectively. They can be computed without solving a differential equation. This can be interpreted as an invertibility property. Therefore, trajectory planning and feedforward control design can be done in a very elegant way for flat systems [94]. Since the flat output constitutes an algebraic parameterization of the system's dynamics, flatness is also a particularly useful property for the solution of dynamic optimization problems. Furthermore, flatness is closely related to linearizability of nonlinear

systems by feedback. For single-input systems, for example, flatness is equivalent to linearizability by static state feedback. In general, flat systems are exactly linearizable by endogenous feedback. Flatness based control has been applied to systems from a diverse range of application areas such as chemical processes [93], bio processes [58], electrical drives [42] and aircrafts [59]. Recently, the flatness concept is being extended to delay systems and to distributed parameter systems, see e.g. [95, 96].

5.3.2 Orbital Flatness

The advantages of flat systems can also be extended to a somewhat larger class of systems allowing an appropriate state-dependent time scaling ([21, 35, 89]). A new 'time'-variable τ is defined as follows:

$$\begin{aligned} [t_0 \quad t_{end}] &\mapsto [\tau_0 \quad \tau_{end}] \\ \frac{dt}{d\tau} &= s(x(t), u(t)), \quad \tau(t_0) = \tau_0. \end{aligned} \tag{5.20}$$

For the mapping of t to τ to be bijective, the scaling function $s(x(t), u(t))$ has to satisfy

$$0 < s(x(t), u(t)) < \infty, \quad \forall t. \tag{5.21}$$

This condition ensures that τ is a strictly monotonically increasing function in t and goes to infinity if and only if t goes to infinity, as intuitively expected from a proper notion of 'time'. Furthermore, (5.21) makes the time scaling invertible such that a control law $u(\tau)$ designed in new time τ can be transformed back and applied in real time t. In new 'time', the system (5.17) evolves according to

$$\frac{dx}{d\tau} = f(x(\tau), u(\tau))s(x(\tau), u(\tau)) \equiv g(x(\tau), u(\tau)). \tag{5.22}$$

If the time scaled system (5.22) is flat then the original system (5.17) is called *orbitally flat*. In the following, in a slight abuse of notation, the flat output of the time scaled system (5.22) will sometimes also be referred to as the flat output of the original system (5.17).

5.4 Orbital Flatness of Crystallizer Model

5.4.1 Flatness Test for Moment Model

First, it will be shown that the moment model (5.16-a) - (5.16-e) is *not* flat. For single-input systems flatness and input-state linearizability by feedback are equivalent [92]. A

single-input system which is affine in the control variable u

$$\dot{x} = f(x) + g(x)u, \quad x \in I\!R^n,\ u \in I\!R \tag{5.23}$$

is input-state linearizable at x_0 if and only if the following conditions hold locally around x_0 [41, 77]:

A the matrix $\mathcal{G}(x) = [g_0(x), g_1(x), \ldots, g_{n-1}(x)]$ with $g_i = \text{ad}_f^i g(x)$ has full rank n

B the distribution $\mathcal{D} = \text{span}\{g_0, g_1, \ldots, g_{n-2}\}$ is involutive.

The notation $\text{ad}_f g$ is standard to denote the Lie product of two vector fields f and g. For the moment model (5.16-a) - (5.16-e) the vector fields f and g are defined as follows

$$f(x) = \begin{pmatrix} B(\mu_3, T) \\ G(\mu_3, T)\mu_0 \\ 2G(\mu_3, T)\mu_1 \\ 3G(\mu_3, T)\mu_2 \\ -\frac{3\rho_c k_v}{\rho} \frac{\Delta H_c(\mu_3) G(\mu_3, T)\mu_2}{c_p(\mu_3)} - \frac{UA_c}{\rho V} \frac{T}{c_p(\mu_3)} \end{pmatrix}, \quad g(x) = \begin{pmatrix} 0 \\ 0 \\ 0 \\ 0 \\ \frac{UA_c}{\rho V c_p(\mu_3)} \end{pmatrix}, \tag{5.24}$$

where the state vector x is given by $x = (\mu_0, \ldots, \mu_3, T)^T$. To check condition B, i.e. involutivity of $\mathcal{D}$, a Matrix $D_{0,1}$ can be made up of all vectors spanning the distribution $\mathcal{D}$ and the Lie product $\text{ad}_{g_0} g_1(x)$ of the first two of these vectors

$$D_{0,1}(x) = [g_0(x) \quad g_1(x) \quad g_2(x) \quad g_3(x) \quad \text{ad}_{g_0} g_1(x)]\,. \tag{5.25}$$

It can be verified that this matrix has full rank for almost all $x \in I\!R^5$. Hence, the Lie product of the first two vector fields in the definition of $\mathcal{D}$ do not belong to $\mathcal{D}$

$$g_0 \in \mathcal{D}, \quad g_1 \in \mathcal{D}, \quad \text{but} \quad \text{ad}_{g_0} g_1 \notin \mathcal{D}. \tag{5.26}$$

Hence, distribution $\mathcal{D}$ is not involutive, condition B is violated, the moment model (5.16-a) - (5.16-e) is not input-state linearizable by feedback and therefore it is not flat.

5.4.2 Flatness of Time-Scaled Moment Model

In the following, it is shown that the system (5.16-a)-(5.16-e) is orbitally flat. Using the scaling function

$$s(t) = \frac{1}{G(\mu_3(t), T(t))}, \tag{5.27}$$

a new notion of time is introduced by

$$d\tau = G(\mu_3(t), T(t))dt, \quad \tau_0 = 0. \tag{5.28}$$

As G represents the crystal growth rate, the new 'time' τ is the length which a crystal has gained since the beginning of the batch. This is a very natural way to describe the progression of the batch. According to (5.21) the scaling function has to be strictly positive and finite. For the specific scaling function (5.27) used here this condition is equivalent to the crystal growth rate $G(\mu_3, T)$ being strictly positive and finite. Because of (5.7) and (5.6), this reduces to the requirement that the solution has to be kept supersaturated, i.e. $c(t) > c_{sat}(t), \forall t$. Since in a crystallizer crystals are to be grown rather than dissolved this condition makes eminent sense from a practical point of view. Using new time τ, the system (5.16-a)-(5.16-e) is transformed to

$$\frac{d\mu_0(\tau)}{d\tau} = \frac{B(\mu_3(\tau), T(\tau))}{G(\mu_3(\tau), T(\tau))} \tag{5.29-a}$$

$$\frac{d\mu_1(\tau)}{d\tau} = \mu_0(\tau) \tag{5.29-b}$$

$$\frac{d\mu_2(\tau)}{d\tau} = 2\mu_1(\tau) \tag{5.29-c}$$

$$\frac{d\mu_3(\tau)}{d\tau} = 3\mu_2(\tau) \tag{5.29-d}$$

$$\frac{dT(\tau)}{d\tau} = -\frac{3\rho_c k_v}{\rho}\frac{\Delta H_c\left(\mu_3\right)\mu_2}{c_p\left(\mu_3\right)} - \frac{UA_c}{\rho V}\frac{(T - T_c)}{G\left(\mu_3, T\right)c_p\left(\mu_3\right)}. \tag{5.29-e}$$

This can be written in short form as

$$\frac{dx}{d\tau} = \bar{f}(x) + \bar{g}(x)u, \text{ where } \bar{f}(x) = \frac{f(x)}{G(x)}, \bar{g}(x) = \frac{g(x)}{G(x)} \tag{5.30}$$

with vector fields f and g according to (5.24). It is easy to check that both conditions A and B for feedback linearizability in Chapter 5.4.1 are met. The matrix

$$\bar{\mathcal{G}}(x) = [\bar{g}_0(x) \quad \bar{g}_1(x) \quad \dots \quad \bar{g}_4(x)] \text{ with } \bar{g}_i = \mathrm{ad}_{\bar{f}}^i \bar{g}(x) \tag{5.31}$$

has full rank for all x in the physically meaningful range. The matrices

$$\bar{D}_{i,j}(x) = [\bar{g}_0(x) \quad \bar{g}_1(x) \quad \bar{g}_2(x) \quad \bar{g}_3(x) \quad \mathrm{ad}_{\bar{g}_i}\bar{g}_j(x)], \quad i, j = 0, \dots, 3 \tag{5.32}$$

are singular for all $x \in \mathbb{R}^5$. Hence, the corresponding distribution $\bar{\mathcal{D}} = \mathrm{span}\{\bar{g}_0(x) \quad \bar{g}_1(x) \quad \bar{g}_2(x) \quad \bar{g}_3(x)\}$ is involutive. Therefore, the time scaled system (5.29-a)-(5.29-e) is feedback linearizable and, consequently, it is flat. This

implies that the moment model in original time (5.16-a)-(5.16-e) is an orbitally flat system.

Exploiting flatness requires the knowledge of a flat output of the system. As in many cases, also for the batch crystallizer the flat output has a physical meaning. Intuitively speaking, the flat output of the crystallizer model is the element of the system state vector on which the influence of the system input T_c is the "least direct". The cooling temperature T_c, of course, directly affects the crystallizer temperature T (5.29-e). Temperature T determines the saturation concentration c_{sat} (5.9) and therefore has a direct effect on supersaturation S (5.6) and hence also on growth and nucleation rates G and B, see equations (5.7) and (5.8), respectively. According to (5.29-a), G and B determine the derivative of the zeroth moment μ_0. This, in turn, is the derivative of the first moment, and so on. Hence, in some sense, the influence of the input T_c on the third moment μ_3 is "least direct". With the third moment of the CSD as a flat output candidate, it is easy to verify the flat output conditions (5.18), (5.19-a) and (5.19-b). In the following, it is shown that for the output

$$y(\tau) = \mu_3(\tau) \tag{5.33}$$

both conditions A and B in the definition of flatness (see Chapter 5.3.1) hold. As $\mu_3(\tau)$ is a state variable, equation (5.18) and therefore requirement A hold trivially. Differentiating the output $y(\tau)$ five times with respect to τ along the system trajectories yields

$$\frac{dy(\tau)}{d\tau} = 3\mu_2(\tau) \tag{5.34-a}$$

$$\frac{d^2y(\tau)}{d\tau^2} = 6\mu_1(\tau) \tag{5.34-b}$$

$$\frac{d^3y(\tau)}{d\tau^3} = 6\mu_0(\tau) \tag{5.34-c}$$

$$\frac{d^4y(\tau)}{d\tau^4} = 6\frac{B(\mu_3(\tau),T(\tau))}{G(\mu_3(\tau),T(\tau))} \tag{5.34-d}$$

$$\frac{d^5y(\tau)}{d\tau^5} = \phi\big(\mu_3(\tau),\mu_2(\tau),T(\tau),T_c(\tau)\big) \tag{5.34-e}$$

where

$$\begin{aligned}&\phi\big(\mu_3,\mu_2,T,T_c\big)\\ &= 6\frac{G(\mu_3,T)(\frac{\partial B}{\partial T}\frac{dT}{d\tau}+\frac{\partial B}{\partial \mu_3}\frac{d\mu_3}{d\tau}) - B(\mu_3,T)(\frac{\partial G}{\partial T}\frac{dT}{d\tau}+\frac{\partial G}{\partial \mu_3}\frac{d\mu_3}{d\tau})}{G(\mu_3,T)^2}.\end{aligned} \tag{5.35}$$

with the expressions for $\frac{d\mu_3}{d\tau}$ and $\frac{dT}{d\tau}$ according to (5.29-d) and (5.29-e), respectively. Note

that $\phi(\mu_3, \mu_2, T, T_c)$ is affine with respect to the system input T_c, i.e. it is of the form

$$\phi(\mu_3, \mu_2, T, T_c) = \alpha(\mu_3, \mu_2, T) + \beta(\mu_3, T)T_c. \tag{5.36}$$

From (5.33), (5.34-a)-(5.34-c) it is immediately clear that the states $\mu_3(\tau) \dots \mu_0(\tau)$ can be computed from $y(\tau)$ and its first three derivatives. The state $T(\tau)$ can be determined from (5.34-d) by additionally using the fourth derivative. Finally, the computation of the input $T_c(\tau)$ from equation (5.34-e) also involves the fifth derivative of the flat output. Hence, equations (5.19-a), (5.19-b) and therefore requirement B also hold. Consequently, $y(\tau)$ is a flat output of the transformed system (5.29-a)-(5.29-e).

Note that the calculations presented in this chapter are - to a certain extend - independent of the specific dependence of growth and nucleation rate B and G on the system states. The flatness property of the system and the third moment μ_3 as a flat output are independent of the kinetics. The only requirement is that equation (5.34-d) must be solvable for $T(\tau)$.

As described in Chapter 5.1, it may desirable to interprete the crystallizer temperature T as the manipulated input and disregard equation (5.16-e) or (5.29-e), respectively. It can easily be verified that the resulting model (5.16-a) - (5.16-d) with the four leading moments $\mu_0, \dots, \mu_3$ as system states and T as input is also orbitally flat with the same time scaling function (5.27) and the same flat output (5.33).

If one is interested in higher moments beyond μ_3, ODEs of the form (5.13) have to be appended to the model (5.16-a) - (5.16-e). These higher order moment models are orbitally flat for any finite number of moments, again, with the same time scaling function. This can easily be checked by verifying that the highest moment which is taken into account is a flat output for the time scaled system.

5.5 Discussion

A standard population balance model taken from the literature was presented in this chapter. The model describes a lab-scale seeded batch cooling crystallizer. Its structure is relatively simple, e.g. assuming growth rate being independent of crystal size, such that a closed set of ODEs for the leading moments of the CSD can be derived.

The notion of differential flatness was introduced and it was shown that moment models are not flat but they possess the property of orbital flatness regardless of the model dimension, i.e. the number of moments being considered. These results are used in the

following Chapter for the design of control strategies. According to M. Fliess [19] this is the first practical example where orbital flatness proves to be useful.

The flatness based approach presented in this chapter heavily relies on the specific model structure under consideration. In particular, its applicability is restricted to population balance models which allow the derivation of finite-dimensional moment models. As in most cases, only a specific problem structure allows the use of powerful methods.

Chapter 6

Batch Crystallization – Flatness Based Control Synthesis

6.1 Introduction to Batch Crystallizer Control

Different cooling strategies lead to different product CSDs at the end of a batch. For a given temperature trajectory, it is obviously possible to determine the resulting CSD by running an experiment or by numeric simulation of a population balance model, such as the one given in Chapter 5.2. The solution of the reverse problem, i.e. the design of a temperature trajectory which produces a specific desired CSD defined as a function of crystal length, requires the inversion of the system model. See Figure 6.1 for a graphical illustration. This defines a feedforward control problem which, so far, had been unsolved.

Instead, in the literature, the problem of batch crystallizer control has been addressed

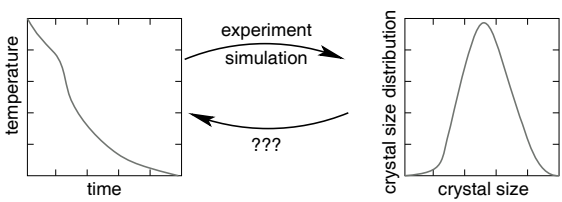

Figure 6.1: Illustration of inverse problem

mainly from an optimization point of view. A number of authors have considered the problem of finding a temperature trajectory which maximizes or minimizes a characteristic of the final CSD [1, 46, 51, 60, 65, 105]. These studies differ with respect to model assumptions, optimization methods, objective functions and the question whether or not constraints can be handled. The methods applied vary from Pontryagin's maximum principle to nonlinear dynamic optimization. Concerning the underlying process models, in actual case studies, moment models (or even simpler equations) have been used, although the more recent approaches could potentially handle more complex population balance based model formulations. Since an optimal temperature trajectory represents an open loop control law the positive effects may be lost due to plant-model mismatch or because of imperfect tracking of the desired optimal temperature trajectory. This issue is treated in [56]. Attempts to incorporate feedback in the optimal control of batch cooling crystallizers can be found in [8, 67, 115]. The influence of the distribution of seed crystals and its use as a further degree of freedom for optimization is studied in [12]. Optimization of a CSD over more than one characteristic crystal length has recently been considered in [57].

If the objective is to obtain large crystals it is beneficial to suppress nucleation as far as possible such that seed crystals grow up to larger sizes. Therefore, in [70] a temperature trajectory was derived to maintain nucleation at a constant low level. Because of the nonlinear dependence of nucleation and growth rates on supersaturation it is also possible to favour growth over nucleation by keeping the supersaturation at a constant low value. This is another popular approach, which has been pursued, e.g., in [48] in an open loop setting. In [113] a nonlinear feedback controller for the same purpose has been designed. The usage of fines dissolution as an additional manipulated variable for batch crystallizer control has been examined in [47, 91].

In this chapter, a considerably different approach is taken which is neither based on optimization nor does it just keep one process variable constant. The approach presented here rather uses methods from nonlinear control theory to analytically determine the feedforward control which steers the system into a desired final CSD. Differential flatness, which was introduced in the previous chapter, is exploited for control design. Based on this property, a procedure is developed which enables inversion of the system model and hence makes it possible to check whether a desired final CSD, according to the model, is physically possible and, if so, to compute the corresponding temperature trajectory. The flatness property is further exploited in Chapter 6.3 to facilitate the dynamic optimization of the CSD. In Chapter 6.4, trajectory planning is treated. It is shown how to design a trajectory which achieves certain CSD properties (expressed in terms of moments) at the end

of the batch. Finally, a feedback control scheme to track such a trajectory in the presence of uncertainty is presented in Chapter 6.5. Parts of the results presented in this Chapter have been published earlier in [112], [111].

6.2 Feedforward Control for Desired CSD

In the following, crystallizer temperature T is used as the manipulated input to control the final CSD. The object is to invert the batch crystallizer model (5.1-a)-(5.2) such that a desired final CSD $f_{end,d}(L)$ can be chosen and the corresponding desired temperature-time profile $T_d(t)$ be determined. This is illustrated in Figure 6.2 where Σ is the system (the batch crystallizer) and Σ^{-1} is the inverse system to be derived in this chapter.

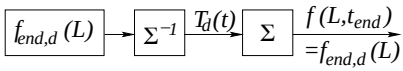

Figure 6.2: Illustration of feedforward control by system inversion

Two specific properties of the batch crystallizer model are exploited to facilitate system inversion and therefore feedforward control design. These properties are, on the one hand, the orbital flatness of the moment model and, on the other hand, the simple form of population balance equation (5.1-a) when rewritten in new time τ.

The system's characteristic lines in the $L-t$ domain, on which the CSD $f(L,t)$ is constant, are defined by

$$\frac{df(L,t)}{dt} = 0. \tag{6.1}$$

The total differential of f is given by

$$\frac{\partial f(L,t)}{\partial L}\frac{dL}{dt} + \frac{\partial f(L,t)}{\partial t} = 0. \tag{6.2}$$

With the PDE (5.1-a) this leads to the following expression for the characteristic lines

$$\frac{dL}{dt} = G(t). \tag{6.3}$$

See Figure 6.3 for an illustration.

Applying the time transformation (5.28) to the PDE (5.1-a) yields the simple transport equation

$$\frac{\partial f(L,\tau)}{\partial \tau} = -\frac{\partial f(L,\tau)}{\partial L}. \tag{6.4}$$

This implies that $f(L,\tau)$ is constant on straight lines in the (L,τ)-domain with $\frac{dL}{d\tau} = 1$, see Figure 6.4. Furthermore, the size distribution $f(L,\tau)$ can be split into two parts, where one part represents grown seed crystals

$$f_s(L,\tau) = \begin{cases} f(L,\tau) & \text{for } L \geq \tau \\ 0 & \text{else} \end{cases} \tag{6.5}$$

and the other part describes the distribution of crystals produced by nucleation

$$f_n(L,\tau) = \begin{cases} f(L,\tau) & \text{for } L < \tau \\ 0 & \text{else} \end{cases} . \tag{6.6}$$

Obviously, the distribution of grown seed crystals $f_s(L,\tau)$ cannot be influenced by control since it is equivalent to the initial seed distribution shifted in size by the length $\Delta L = \tau$

$$f_s(L,\tau) = f_{seed}(L+\tau). \tag{6.7}$$

In contrast, the distribution of particles created by nucleation $f_n(L,\tau)$ can be influenced by appropriate manipulation of the crystallizer temperature $T(\tau)$, since the nucleation rate $B(\tau)$ is temperature dependent. Consequently, a necessary condition for a desired CSD at the end of the batch $f_{end,d}(L)$ to be attainable is

$$f_{end,d}(L) = f_{seed}(L - \Delta L_{end}), \text{ for } L \geq \Delta L_{end}, \tag{6.8}$$

where $\Delta L_{end} = \tau_{end}$ is the increase in size which a crystal gains over the whole batch run.

Since $f(L,\tau)$ is constant on the characteristic lines $\frac{dL}{d\tau} = 1$, the values of a desired $f_{end,d}(L)$ in the size range $0 \leq L < \Delta L_{end}$ can be traced back to values of the CSD at the lower boundary of the size range $f(0,\tau)$ for $0 < \tau \leq \tau_{end}$. Consequently, if the CSD at the end of the batch is desired to be a certain desired distribution

$$f(L,\tau_{end}) = f_{end,d}(L), \tag{6.9}$$

then the time profile of the boundary condition which is necessary to produce the desired distribution $f_{end,d}(L)$ is determined by

$$f_d(0,\tau) = f_{end,d}(\tau_{end} - \tau), \quad 0 < \tau \leq \tau_{end}. \tag{6.10}$$

Note that τ_{end} is the maximum length of nucleated crystals, which is also fixed when choosing the desired final CSD $f_{end,d}(L)$. Equation (6.10) establishes the first step of a

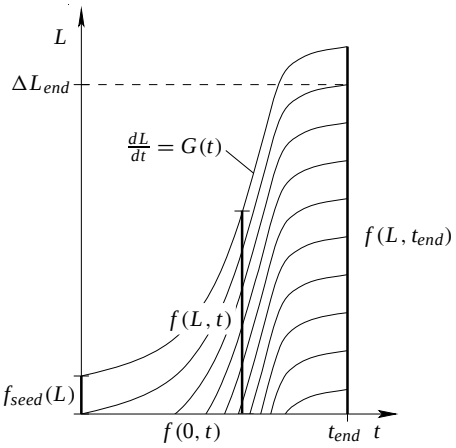

Figure 6.3: Evolution of CSD in the (L, t)-domain

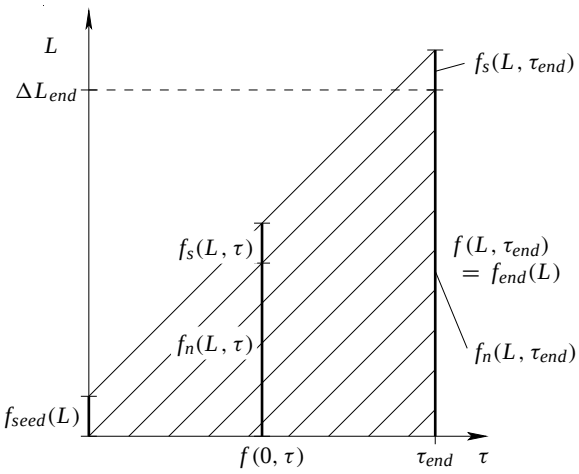

Figure 6.4: Evolution of CSD in the (L, τ)-domain

feedforward control design. If a desired final CSD $f_{end,d}(L)$ is chosen, (6.10) determines the corresponding time profile of the CSD at length $L = 0$ (the lower boundary of the length coordinate) required to produce $f_{end,d}(L)$. In a second step, flatness will be used to determine the desired crystallizer temperature $T_d(\tau)$, i.e. the feedforward control, from the desired trajectory of the left boundary of the CSD $f_d(0,\tau)$.

Because of boundary condition (5.1-b) and equation (5.34-d), the trajectory $f_d(0,\tau)$ determines the fourth derivative of the flat output

$$\frac{d^4 y_d(\tau)}{d\tau^4} = 6 f_{end,d}(\tau_{end} - \tau). \tag{6.11}$$

Integrating this expression four times yields the flat output as a function of new time τ. Integration constants are obtained from the initial condition, i.e. the seed CSD. The desired trajectory of the flat output, i.e. the third moment of the CSD, connecting the seed CSD $f_{seed}(L)$ with the desired final CSD $f_{end,d}(L)$ is

$$y_d(\tau) = 6 \int_0^{\tau}\int_0^{\tau}\int_0^{\tau}\int_0^{\tau} f_{end,d}(\tau_{end}-\theta)\, d\theta^4 + \mu_{3,Seed} + 3\mu_{2,Seed}\tau + 3\mu_{1,Seed}\tau^2 + \mu_{0,Seed}\tau^3. \tag{6.12}$$

According to the definition of flatness, all system states and the system input can be determined from the flat output and its derivatives. This means in particular that equation (5.19-b) determines a feedforward control $T_d(\tau)$ which produces the trajectory of the flat output defined by (6.12) and, therefore, creates the desired final CSD $f_{end,d}(L)$. To compute $T_d(\tau)$, in equation (5.34-d) all variables are replaced by their respective desired counterparts. The resulting equation

$$\frac{d^4 y_d(\tau)}{d\tau^4} = 6\frac{B(y_d(\tau), T_d(\tau))}{G(y_d(\tau), T_d(\tau))} \tag{6.13}$$

is solved for $T_d(\tau)$. Due to the quadratic dependence of saturation concentration c_{sat} on temperature T, see equation (5.9), this procedure yields two solutions for $T_d(\tau)$ of which at most one is physically meaningful. If for some τ both results are not meaningful, e.g. in the case of complex conjugate solutions, this implies that the desired CSD $f_{end,d}(L)$ is not compatible with the model, i.e. it cannot be produced by the given system from the given initial CSD $f_{seed}(L)$.

Eventually, the time transformation (5.28) has to be inverted to obtain the control $T_d(t)$ in original time. This requires the evaluation of the integral

$$t = \int_0^{\tau} \frac{1}{G(\mu_{3,d}(\theta), T_d(\theta))}\, d\theta \tag{6.14}$$

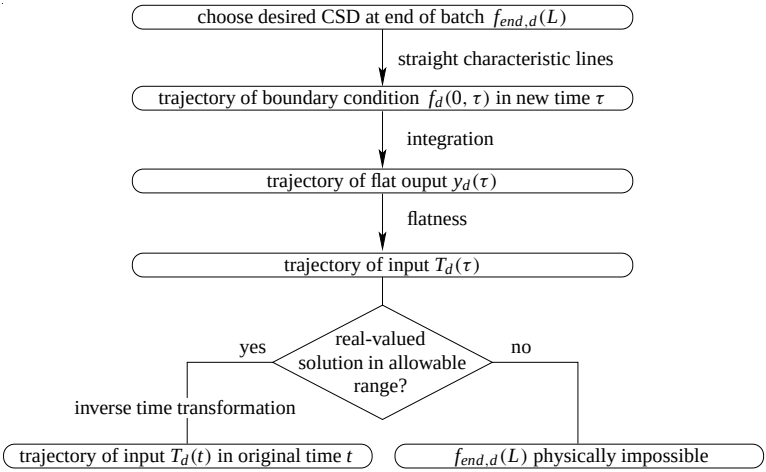

Figure 6.5: Open Loop Control Design Procedure

and the solution of the resulting equation for τ. Depending on the kinetic relations used for the growth and nucleation rate and the function chosen for the desired CSD $f_{end,d}(L)$, these computations may be done analytically or numerically. If the inversion of the time transformation can be done analytically an explicit functional dependence of temperature T_d on time t is obtained. Otherwise, the open loop control $T_d(t)$ can only be determined at a number of time instances. However, this is not a severe restriction for practical implementation.

In summary, the flatness property of the crystallizer model can be exploited for the following tasks: checking if a desired final CSD $f_{end,d}(L)$ is physically possible and computing the temperature trajectory $T_d(t)$ which produces this desired CSD. The corresponding procedure is summarized schematically in Figure 6.5.

The system inversion derived in this chapter involves three main steps. The first step uses the straight characteristic lines of the time scaled population balance model. The second step exploits flatness of the time scaled moment model. In the last step, the time scaling is reversed. This is illustrated as a block diagram in Figure 6.6.

Example

For illustration, the procedure is applied to a specific example. The batch crystallizer is supposed to be started with a solution of concentration

$$c_0 = 0.493 \, \frac{g_{KNO_3}}{g_{H_2O}} \tag{6.15}$$

which corresponds to a saturation temperature of $32°$C. A small amount ($m_{seed} = 0.05$g) of seed crystals of size $L_{seed} = 196\mu$m is added, i.e. the initial number density function is

$$f_{seed}(L) = \frac{N_{seed}}{V} \cdot \delta(L - L_{seed}), \tag{6.16}$$

where $\delta(\bullet)$ is the Dirac delta impulse and the number of seed crystals is

$$N_{seed} = \frac{m_{seed}}{\rho_c k_v L_{seed}^3}. \tag{6.17}$$

For a complete list of model parameter values and operating conditions see Appendix B.

As an example, the part of the desired final CSD which is to be generated by nucleation is chosen as an exponential function Ae^{-BL}, with two parameters A and B. The other part, which cannot be influenced by the cooling mode, results from seed crystals which have grown. This is described by the seed CSD shifted in the size domain by ΔL_{end}. The overall desired final CSD consequently is

$$\begin{aligned} f_{end,d}(L) &= \begin{cases} Ae^{-BL} & \text{for } L < \Delta L_{end} \\ f_{seed}(L - \Delta L_{end}) & \text{for } L \geq \Delta L_{end} \end{cases} \\ &= \begin{cases} Ae^{-BL} & \text{for } L < \Delta L_{end} \\ \frac{N_{seed}}{V} \cdot \delta(L - (L_{seed} + \Delta L_{end})) & \text{for } L \geq \Delta L_{end}. \end{cases} \end{aligned} \tag{6.18}$$

From the given desired final CSD $f_{end,d}(L)$ the corresponding time trajectory of the desired number density function at the lower boundary of the size range, $f_d(L = 0, \tau)$, can be obtained from equation (6.10)

$$f_d(0, \tau) = f_{end,d}(\tau_{end} - \tau) = Ae^{-B(\tau_{end} - \tau)}, \quad 0 < \tau \leq \tau_{end}. \tag{6.19}$$

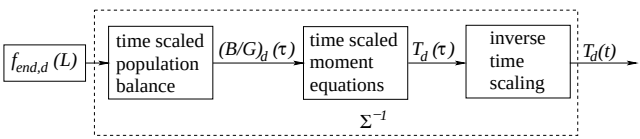

Figure 6.6: Steps Involved in the System Inversion

Because of boundary condition (5.1-b) and equation (5.29-a) this determines the derivative of the zeroth moment

$$\frac{d\mu_{0,d}(\tau)}{d\tau} = f_{end,d}(\tau_{end} - \tau) = Ae^{-B(\tau_{end}-\tau)}. \tag{6.20}$$

According to (5.29-a)-(5.29-d), the trajectories of all four moments can be obtained by essentially integrating the expression for the boundary condition (6.19) four times. The integration constants are determined by the initial conditions for the moments of the CSD, which in turn can be obtained from the seed CSD given in (6.16). This results in the following expressions for the first four moments

$$\mu_{0,d}(\tau) = \frac{Ae^{-B\tau_{end}}\left(e^{B\tau}-1\right)}{B} + \frac{N_{seed}}{V} \tag{6.21-a}$$

$$\mu_{1,d}(\tau) = \frac{Ae^{-B\tau_{end}}\left(e^{B\tau}-B\tau-1\right)}{B^2} + \frac{N_{seed}(L_{seed}+\tau)}{V} \tag{6.21-b}$$

$$\mu_{2,d}(\tau) = \frac{Ae^{-B\tau_{end}}\left(2e^{B\tau}-B^2\tau^2-2B\tau-2\right)}{B^3} + \frac{N_{seed}(L_{seed}+\tau)^2}{V} \tag{6.21-c}$$

$$\mu_{3,d}(\tau) = \frac{Ae^{-B\tau_{end}}\left(6e^{B\tau}-B^3\tau^3-3B^2\tau^2-6B\tau-6\right)}{B^4} + \frac{N_{seed}(L_{seed}+\tau)^3}{V}. \tag{6.21-d}$$

From equation (5.14), the corresponding desired trajectory for the solute concentration $c_d(\tau)$ can be obtained. In the next step, equation (5.1-b) with expressions for growth and nucleation rates from (5.7) and (5.15) is used to determine the temperature $T_d(\tau)$. The desired temperature trajectory $T_d(\tau)$ is obtained by inserting the desired trajectories for the boundary condition (6.19), the third moment (6.21-d) and concentration $c_d(\tau)$ into equation (5.1-b). Due to the quadratic dependence of $c_{sat}(T)$ on T (5.9), the resulting equation

$$c_{sat}(T_d(\tau)) = \frac{c_d(\tau)}{1+\left(\frac{k_g f_d(0,\tau)}{hk_b k_v \mu_{3,d}(\tau)}\right)^{\frac{1}{b-g}}} \tag{6.22}$$

has two solutions

$$T_d(\tau) = \frac{-A1 \pm \sqrt{A_1^2 - 2A_0A_2 + 4A_2c_d(\tau)\left(1+\left(\frac{k_g f_d(0,\tau)}{hk_b k_v \mu_{3,d}(\tau)}\right)^{\frac{1}{b-g}}\right)^{-1}}}{2A2} \tag{6.23}$$

of which only the positive solution is physically meaningful. Finally, the time scaling has to be inverted according to equation (6.14)

$$
\begin{aligned}
t &= \int_0^{\tau} \frac{1}{G(\mu_{3,d}(\theta), T_d(\theta))}\, d\theta \\
&= \int_0^{\tau} \Bigg[\Bigg(\frac{AB^4 e^{B\theta} k_g V}{h k_b k_v} \Big(B^4 e^{BL_{end}} N_{seed} (L_{seed} + \theta)^3 \\
&\qquad - AV(6(1 - e^{B\theta}) + 6B\theta + 3B^2\theta^2 + B^3\theta^3) \Big)^{-1} \Bigg)^{\frac{-g}{b-g}} \Big/ kg \Bigg]\, d\theta. \qquad (6.24)
\end{aligned}
$$

This integral has to be evaluated and the resulting equation has to be solved for τ. Inserting the function $\tau(t)$ in equation (6.23) yields the desired temperature trajectory in original time $T(t)$. However, the integral in (6.24) cannot be evaluated analytically. Hence, the temperature T cannot be obtained as an explicit function of time t but values at an arbitrary number of time instants can be determined by numerical evaluation of (6.24). Plots of the desired final CSD $f_{end,d}(L)$, the trajectory of the boundary condition $f_d(0, \tau)$, the third moment (i.e. the flat output of the system) $\mu_{3,d}(\tau)$, the temperature trajectory in scaled time $T(\tau)$ and the temperature trajectory in original time (i.e. the desired feedforward control) $T(t)$ are presented in Figure 6.7. The parameters for the desired CSD in (6.18) were chosen as follows: $A = 2 \cdot 10^7$ #(mm l)$^{-1}$, $B = 7.5$ mm^{-1}, $\Delta L_{end} = 0.9$ mm.

6.3 Optimization of CSD Properties

As pointed out in Chapter 5.1, quite a number of researchers have applied optimization techniques for the design of open loop control strategies for batch crystallizers. Commonly, dynamic optimization based on moment models is used to obtain a temperature trajectory which optimizes selected properties of the CSD. Typical objectives are the maximization of the maximum crystal size or the weight mean size of crystals. Since in some situations it is desirable to suppress nucleation as much as possible, another common optimization objective is the minimization of the ratio of the mass of crystals that have been produced by nucleation and the mass of grown seed crystals.

In [36], it was shown that exploiting the invertibility of (orbitally) flat systems, dynamic optimization problems can be facilitated significantly. As described in Chapter 5.3, a flat output completely parameterizes the corresponding dynamic system. If the flat output trajectory is known, the state and input trajectories - and hence any objective func-

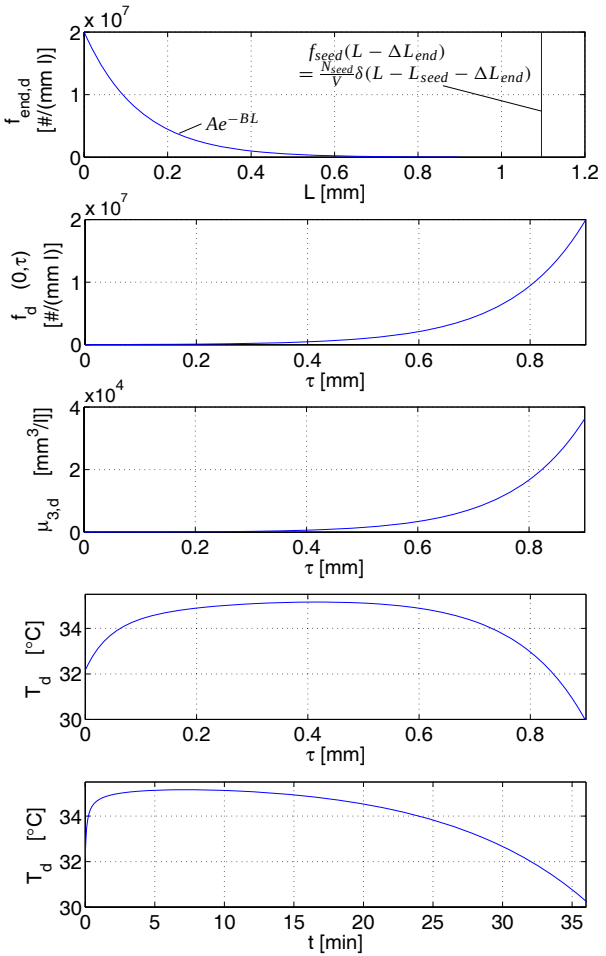

Figure 6.7: Desired final CSD and corresponding trajectories of boundary condition, third moment and temperature.

tion depending on the states - can be determined without solving a differential equation. Therefore, if the flat output is parameterized, e.g. via splines, the complete system is parameterized and the dynamic optimization problem is reduced to a parameter optimization problem.

For the problem of optimizing CSD properties, which is treated here, it is convenient to directly choose a parameterization of the final CSD $f(L, t_{end})$ rather than parameterizing the flat output trajectory. Then, any objective depending on $f(L, t_{end})$ can be easily expressed as an explicit function of the optimization parameters. Furthermore, as shown in Chapter 6.2, the trajectory of the flat output can be determined from $f(L, t_{end})$. Hence, because of the system being flat, path constraints and final time constraints on the moments of the distribution, on solute concentration and on crystallizer temperature can also be directly expressed in terms of the optimization parameters.

Figure 6.8 shows two block diagrams comparing standard dynamic optimization and flatness based optimization of final CSD properties. In standard dynamic optimization the system input, i.e. temperature $T(t)$, is parameterized (e.g. piece-wise linear) using n_{dyn} sampling values T_i, $i = 1, \ldots, n_{dyn}$. The system equations are solved numerically. For the resulting final CSD the objective function is evaluated. Furthermore, constraints may be checked. Based on these evaluations a new set of T_i is chosen, and so on. In contrast, in the flatness based procedure the system output, i.e. the final CSD $f(L, t_{end})$ is parameterized (e.g. using splines) with n_{flat} sampling values f_i, $i = 1, \ldots, n_{flat}$. Now, the cost function can be evaluated directly. If there are path constraints on the system input or the system states, the respective trajectories have to be computed as shown in Chapter 6.2. Then constraints can be evaluated and a new set of f_i is determined by the optimization algorithm. Note that all the calculations can be done analytically such that during run-time of the optimization procedure only the f_i values have to be inserted to obtain the value of the objective function and the trajectories of the system input and states. The only numerical calculation which might be necessary during run-time of the optimization procedure is the computation of t_{end} if the batch time is to be constrained. Hence, by eliminating the numerical solution of the system equations the optimization problem can be solved in a much more robust and efficient manner.

Example

The potential of this flatness based optimization approach is demonstrated by means of a specific example. The following case study is based on the model (5.16-a)-(5.16-d) with

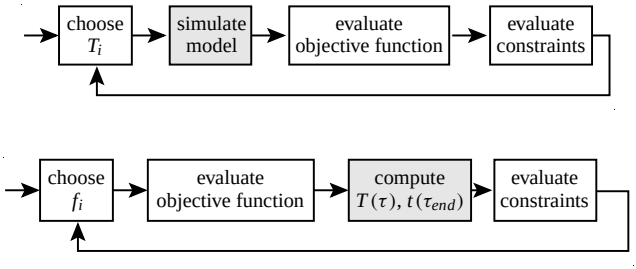

Figure 6.8: Block diagrams illustrating standard dynamic optimization (top) and flatness based optimization (bottom) of CSD properties

the initial condition defined in equations (6.15) - (6.17). An optimization problem taken from [65] is considered. The objective is to favour growth of seed crystals and suppress nucleation as far as possible. Therefore, the objective function to be minimized is defined as the ratio of crystal mass produced by nucleation to crystal mass produced by grown seed crystals at the end of the batch

$$\frac{m_n}{m_s} = \frac{\rho_c k_v V \int_0^{\Delta L_{end}} L^3 f_n(L, t_{end})\, dL}{\rho_c k_v V \int_0^{\Delta L_{end}} L^3 f_s(L, t_{end})\, dL} = \frac{V \int_0^{\Delta L_{end}} L^3 f_n(L, t_{end})\, dL}{N_{seed}(L_{seed} + \Delta L_{end})^3}. \tag{6.25}$$

The batch time

$$t_{end} = \int_0^{\tau_{end}} \frac{1}{G(\mu_3(\tau), T(\tau))}\, d\tau \tag{6.26}$$

is restricted to lie between 50 and 80 minutes. The yield, i.e. the mass of crystals at the end of the batch

$$m_{end} = m_n + m_s \tag{6.27}$$

has to be at least 100g. This is a final time constraint for the optimization. The crystallizer temperature $T(t)$ is not allowed to be smaller than 28° C over the whole batch run, which imposes a path constraint.

For the solution of this problem, the final CSD of nucleated crystals $f_{n,end}$ is parameterized via third order splines. Spline breaks are chosen to be at 0, 200, 380, 500, 600, 680, 750, 810, 860 μm and at the maximum length of nucleated crystals ΔL_{end}. The optimization parameters are the 10 function values f_i at the spline breaks and the maximum size

$\Delta L_{end} = \tau_{end}$. Hence, the following optimization problem has to be solved

$$\begin{aligned} & \min_{f_i, \tau_{end}} \quad \frac{m_n}{m_s} \\ \text{subject to:} \quad & 50min \leq t_{end} \leq 80min \\ & m_{end} \geq 100g \\ & T(\tau) \in I\!R \text{ and } T(\tau) \geq 28^{\circ}C, \, \forall \tau. \end{aligned} \tag{6.28}$$

This is a nonlinear optimization problem which, due to the path constraint on $T(\tau)$, is semi-infinitely constrained. Software packages such as the Matlab optimization toolbox provide techniques for the numerical solution of this type of problems.

Note, that the optimization problem (6.28) does not involve any differential equations. The objective function m_n/m_s, the yield m_{end} and the temperature profile $T(\tau)$ can be symbolically expressed as functions of the optimization parameters. The duration of the batch t_{end} has to be computed by numerical evaluation of the integral (6.26).

Results obtained with the Matlab optimization toolbox are presented in Figures 6.9 and 6.10. The trajectories of temperature and supersaturation as well as the final distribution of nucleated crystals are shown for linear cooling, which was used as the starting point of the optimization, and for optimized cooling. The shape of the temperature trajectory matches with the results obtained in [65] by dynamic optimization. The temperature is kept relatively high for the most part of the batch and drops sharply towards the end. This results in low supersaturation over 60 minutes, thus favouring growth over nucleation. Towards the end of the batch supersaturation rises sharply which results in a rapid growth of existing crystals but also in a burst of nuclei. However, as these nuclei do not have time to grow towards considerable sizes they do not contribute much to the mass of nucleated crystals, which is in the numerator of the objective function (6.25). Conversely, linear cooling leads to a peak in supersaturation and therefore the production of a large amount of nuclei at an early instant of time. Hence the nuclei have time to grow, which leads to a larger mass of nucleated crystals at the end of the batch. Furthermore, the final size of seed crystals is only 1057 μm compared to 1126 μm with optimized cooling. Therefore, the final mass of seed crystals (the denominator of the objective function) is smaller than in the optimized case. The decrease of nucleated crystal mass and the increase in final mass of seed crystals lead to an overall reduction of the cost (6.25) from 12.4 for linear cooling to 9.5 for optimal cooling. In Figure 6.11 the evolution of the mass density function is shown for linear and optimized cooling. These are simulation results where the linear and the optimized cooling curves shown in Figure 6.9 are applied,

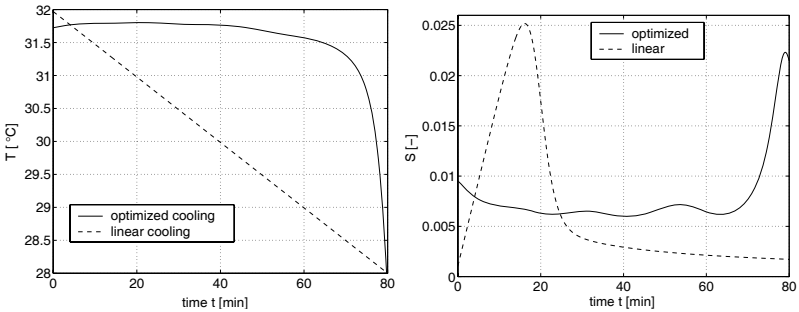

Figure 6.9: Trajectories of temperature and relative supersaturation for optimized cooling (solid) and linear cooling (dashed).

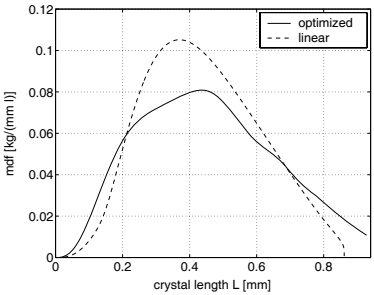

Figure 6.10: Mass density function obtained by optimized cooling (solid) and linear cooling (dashed)

but in the initial condition the Dirac impulse at $L_{Seed} = 196\mu$m has been replaced by a quadratic function between 180 and 212μm with maximum at 196 μm. This is done because a Dirac impulse cannot be represented properly in a plot. This difference in the initial condition can be interpreted as an initial disturbance. The simulation results do not deviate perceivably from the undisturbed case.

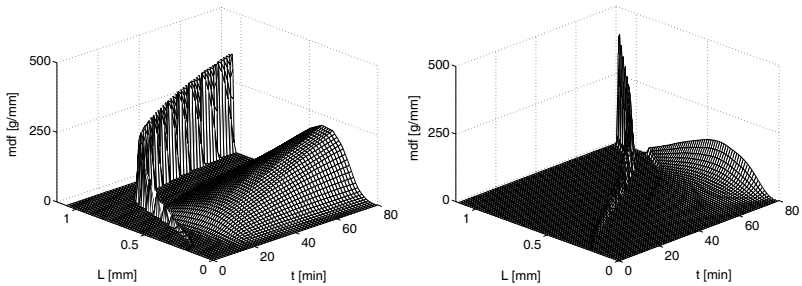

Figure 6.11: Mass density function for linear (left) and optimized (right) cooling

6.4 Feedforward Control for Desired CSD Properties

In cases where CSD properties which can be formulated in terms of the moments of the CSD are desired to assume prescribed values rather than being optimized, a more direct way to design a feedforward control may be used. The flat output trajectory can be parameterized, e.g. by a polynomial, in new time τ. The coefficients are determined such that the trajectory is compatible with given initial conditions and with the desired properties of the final CSD. Due to equation (5.19-b) in the definition of flatness it is then, again, straightforward to compute the corresponding feedforward control $T(\tau)$.

As an example, in the following a trajectory is designed that steers the system from the initial condition (6.15), (6.16) to a size distribution with prescribed weight mean size

$$L_{wm} := \frac{\mu_4}{\mu_3}, \tag{6.29}$$

overall crystal mass $m_{end} = k_v \rho_c V \mu_3$ and maximum length of nucleated crystals, ΔL_{end}. Since the definition of the weight mean size L_{wm} involves the fourth moment μ_4, the equation

$$\frac{d\mu_4}{dt} = 4G(\mu_3, T) \cdot \mu_3 \tag{6.30}$$

has to be added to the model (5.16-a)-(5.16-e). Similarly, the time scaled model (5.29-a)-(5.29-e) is augmented by the equation

$$\frac{d\mu_4}{d\tau} = 4\mu_3. \tag{6.31}$$

As mentioned in Chapter 5.4.2 the resulting sixth order model is orbitally flat with flat output $y = \mu_4$. In a first step, it is now shown how to invert this system model, i.e.

how to determine the system input trajectory from the flat output and its time derivatives. Afterwards, in a second step it is shown how to determine an appropriate flat output trajectory.

Similar to equations (5.34-a)-(5.34-e), differentiating the flat output y six times with respect to new time τ yields

$$\frac{dy(\tau)}{d\tau} = 4\mu_3(\tau) \tag{6.32-a}$$

$$\frac{d^2y(\tau)}{d\tau^2} = 12\mu_2(\tau) \tag{6.32-b}$$

$$\frac{d^3y(\tau)}{d\tau^3} = 24\mu_1(\tau) \tag{6.32-c}$$

$$\frac{d^4y(\tau)}{d\tau^4} = 24\mu_0(\tau) \tag{6.32-d}$$

$$\frac{d^5y(\tau)}{d\tau^5} = 24\frac{B(\mu_3(\tau),T(\tau))}{G(\mu_3(\tau),T(\tau))} \tag{6.32-e}$$

$$\frac{d^6y(\tau)}{d\tau^6} = 4\phi\big(\mu_3(\tau),\mu_2(\tau),T(\tau),T_c(\tau)\big) \tag{6.32-f}$$

where ϕ is defined by equation (5.35). If temperature T is used as the control input the sixth derivative (6.32-f) is not needed for system inversion. In this case, equation (6.32-e) is solved for the input T, using (6.32-a) to replace μ_3. This is done in the following way. Using the expressions for growth and nucleation rates given in equations (5.7) and (5.15), equation (6.32-e) is solved for supersaturation

$$S(\tau) = \left(\frac{k_g y^{(5)}(\tau)}{6hk_b k_v y'(\tau)}\right)^{\frac{1}{b-g}}. \tag{6.33}$$

Then the definition of supersaturation (5.6) together with the expression for the saturation concentration (5.9) is solved for temperature T. Due to the quadratic dependence in (5.9) this, as in (6.23), yields two solutions for T of which only the positive one is physically meaningful

$$T(\tau) = -\frac{A_1}{2A_2} + \frac{\sqrt{A_1^2(1+S(\tau)) - 4A_2(A_0 - c(\tau) + A_0S(\tau))}}{2A_2\sqrt{1+S(\tau)}}. \tag{6.34}$$

In this solution, $S(\tau)$ can be replaced by a function of the flat output $y(\tau)$ and its derivatives using (6.33) and $c(\tau)$ is replaced using (5.14) and (6.32-a). Hence, this constitutes the desired system inversion. For any desired trajectory of the flat output $y_d(\tau)$, the corresponding input trajectory $T_d(\tau)$ can be calculated. If the open loop control is to be applied

in "real" time t, the time scaling has to be inverted by (numerically) integrating (6.14) and solving for τ.

In a second step, the problem of trajectory planning is treated. The flat output trajectory is determined such that the system moves from the initial state to the desired final condition. For this purpose, the desired flat output trajectory $y_d(\tau)$ is parameterized by an eighth order polynomial in new time τ

$$y_d(\tau) = \sum_{i=0}^{8} a_i \tau^i. \tag{6.35}$$

The six leading coefficients $a_0 \dots a_5$ are determined such that the desired trajectory $y_d(\tau)$ is consistent with the initial values for the moments $\mu_0 \dots \mu_4$ and supersaturation S, which is determined by the initial values for solute concentration c_0 and temperature T_0

$$\begin{aligned}
y_d(0) &= a_0 = \mu_4(0) && \text{(6.36-a)}\\
y_d'(0) &= a_1 = 4\mu_3(0) && \text{(6.36-b)}\\
y_d''(0) &= 2a_2 = 12\mu_2(0) && \text{(6.36-c)}\\
y_d'''(0) &= 6a_3 = 24\mu_1(0) && \text{(6.36-d)}\\
y_d^{(4)}(0) &= 24a_4 = 24\mu_0(0) && \text{(6.36-e)}\\
y_d^{(5)}(0) &= 120a_5 = 24B/G. && \text{(6.36-f)}
\end{aligned}$$

The prime in y_d' denotes differentiation with respect to τ. Furthermore, the following desired final time conditions are to be met

$$\begin{aligned}
L_{wm}(\tau_{end}) &= \frac{\mu_4(\tau_{end})}{\mu_3(\tau_{end})} = \frac{4y_d(\tau_{end})}{y_d'(\tau_{end})} = 500\mu\text{m}, && \text{(6.37-a)}\\
m(\tau_{end}) &= k_v\rho_c V\mu_3(\tau_{end}) = \frac{k_v\rho_c V}{4} y_d'(\tau_{end}) = 50\text{g} && \text{(6.37-b)}\\
\Delta L_{end} &= \tau_{end} = 800\mu\text{m}. && \text{(6.37-c)}
\end{aligned}$$

This, overall, constitutes nine equations for the determination of ten unknown parameters (the 9 coefficients $a_0, \dots, a_8$ and final time τ_{end}). Hence, a family of solutions is obtained of which one can be chosen, e.g., such that supersaturation, crystallizer temperature or batch time remain within certain bounds. In Figure 6.12, trajectories resulting from different choices of the free coefficient a_8 are shown. From the requirements (6.37-a) and (6.37-b) it follows that all trajectories reach the same value of weight mean size L_{wm} and fourth moment μ_4 (i.e. flat output y) at final time t_{end}. The final values of temperature T and supersaturation S may differ. As can be seen from the figure, batch time t_{end}

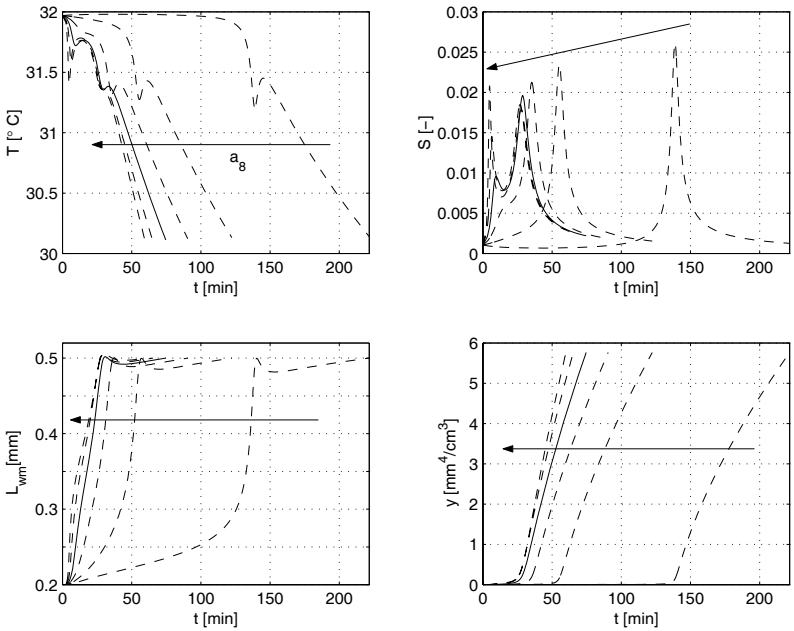

Figure 6.12: Desired trajectories for temperature T, supersaturation S, weight mean size L_{wm} and flat output $y = \mu_4$ (top left – bottom right) for different values of coefficient a_8.

decreases with a_8. Also, the maximum temperature gradient observed during the batch changes. For very small and very large values of a_8 the maximum temperature gradient is unrealistically high. Hence, these trajectories have to be ruled out. A good choice for the free parameter is, e.g., $a_8 = 30mm^{-4}cm^{-3}$, corresponding to the solid curves in Figure 6.12. For this choice all the variables remain in a reasonable range.

In the following chapter, a feedback tracking controller is designed to stabilize the system around the desired trajectory resulting from this choice.

6.5 Feedback Tracking Control

Beside their invertibility property, which can be exploited for trajectory planning and design of feedforward controls, flat systems possess a further advantage. They are linearizable by feedback. Based on this property it is possible to synthesize feedback controllers for the stabilization of batch crystallization processes around desired trajectories for the moments of the CSD and the crystallizer temperature. Such desired trajectories may, for example, be designed by one of the procedures presented in Chapter 6.2, 6.3 or 6.4.

In the following, as an example, a tracking controller is designed to stabilize the crystallizer around the trajectory designed in the previous Chapter 6.4 such that the system is steered from a given initial condition to a final CSD of which the weight mean size $L_{wm}(t_{end})$, crystal mass m_{end} and final size of seed crystals ΔL_{end} is prespecified. Since a *feedback* controller is to be synthesized, the argument given in the introduction 5.1 for the use of the crystallizer temperature T as a manipulated variable is not valid any more. Consequently, the cooling jacket temperature T_c is used as the manipulated variable for feedback control of the batch crystallizer.

Since the definition of weight mean size L_{wm} involves the fourth moment μ_4 the crystallizer model (5.16-a)-(5.16-e), again, is augmented by equation (6.31). As explained in Chapter 6.4, $y = \mu_4$ is a flat output of the augmented model.

As the function ϕ defined in (5.35) occurring in the sixth derivative $y^{(6)}(\tau)$ in (6.32-f) is affine in T_c the feedback law

$$T_c = \frac{v - \alpha(\mu_3, \mu_2, T)}{\beta(\mu_3, T)} \tag{6.38}$$

with α and β according to (5.35),(5.36) exactly linearizes the nonlinear batch crystallizer model. Using (6.32-f) the feedback linearized system

$$\frac{d^6 y}{d\tau^6} = v \tag{6.39}$$

with the fictitious input v and flat output y is obtained. Asymptotic tracking of desired trajectories $y_d(\tau)$ is accomplished by a simple linear control law for the input v

$$v = y_d^{(6)} - \sum_{i=0}^{5} \left(q_i (y^{(i)} - y_d^{(i)}) \right) \tag{6.40}$$

where the coefficients q_i are chosen such that the tracking error dynamics are stable. Equations (6.38) and (6.40) form a nonlinear tracking controller for the batch crystallizer.

The flat output and its derivatives occurring in the control law (6.40) can be replaced by system states of the original crystallizer model using (6.32-a)-(6.32-f). Thus, (6.38), (6.40) form a nonlinear static state feedback controller. The complete system state needs to be measured (or estimated by an observer).

Note that the speed of convergence of the tracking error defined by the coefficients q_i in (6.40) is with respect to new time τ. Since τ is associated with crystal size L, in real time t the tracking error decays fast when growth rate G is large, the decay is slow when G is low.

For a simulation study, a controller as defined in (6.38), (6.40) is implemented with the coefficients q_i chosen such that all six poles of the tracking error dynamics in new time are at $\lambda_k = 20\text{mm}^{-1},\ k = 1, \ldots, 6$.

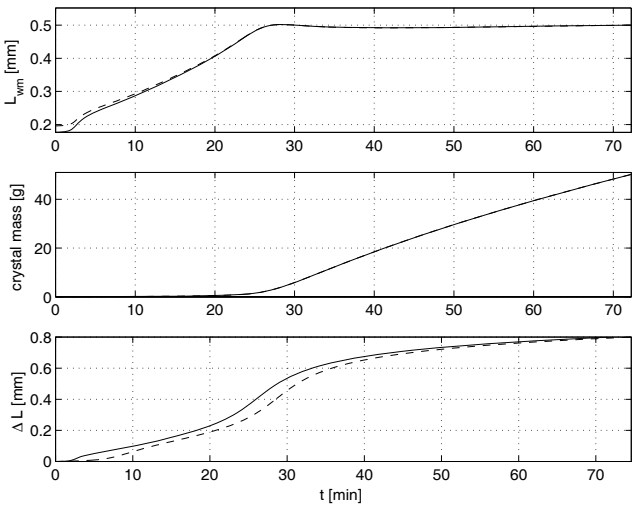

Figure 6.13: Weight mean size $L_{wm}(t)$, crystal mass $m(t)$, and size increase of crystals $\Delta L(t)$, actual (solid line) and desired (dashed line) trajectory.

In a first simulation, an initial error is considered. The desired trajectory starts from the initial condition (6.15), (6.16) with the exception that the actual initial value of the fourth moment μ_4 is decreased by 10 %. Figure 6.13 shows the time trajectories of weight mean size $L_{wm}(t)$, crystal mass $m(t)$, and size increase of crystals $\Delta L(t)$. These are

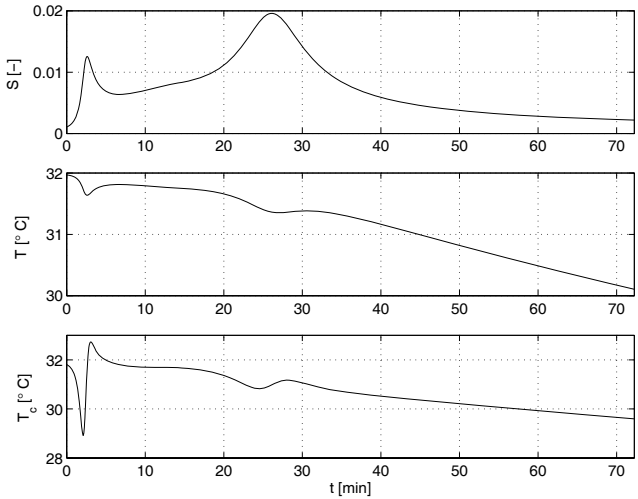

Figure 6.14: Supersaturation $S(t)$, crystallizer temperature $T(t)$ and cooling jacket temperature $T_c(t)$.

the quantities involved in the final time requirements for the desired trajectory (6.37-a)-(6.37-c). Figure 6.14 presents the corresponding time trajectories of supersaturation $S(t)$, crystallizer temperature $T(t)$ and temperature of cooling jacket $T_c(t)$. In Figure 6.15, the tracking error is plotted versus original time t and new time τ. It can be seen that in

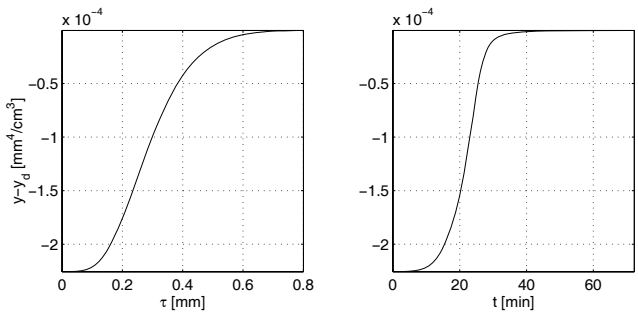

Figure 6.15: Tracking error $y - y_d$ vs. new time τ and vs. original time t.

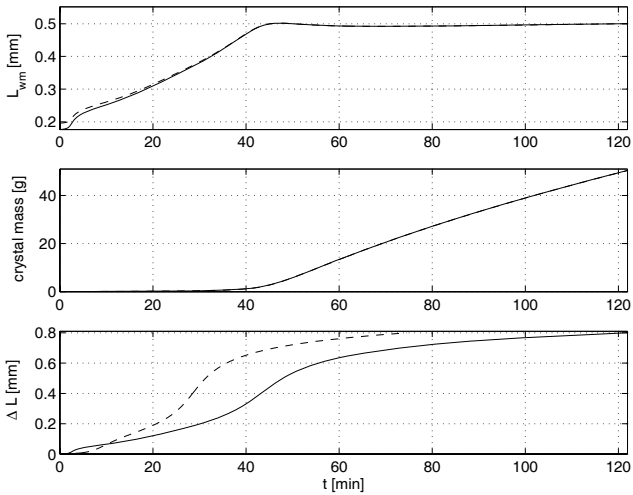

Figure 6.16: Weight mean size $L_{wm}(t)$, crystal mass $m(t)$, and size increase of crystals $\Delta L(t)$, actual (solid line) and desired (dashed line) trajectory, with model error.

new time τ the error dynamics exhibits the expected sixth order linear decay behaviour whereas in original time t the error decays quickly during the time span 20 min$< t <$30 min, i.e. when the supersaturation (and therefore growth rate) is large.

In a second simulation, in addition to the initial error a model error is taken into account. The most uncertain part of the model is the nucleation rate as defined in equation (5.8). Nucleation is hard to capture since several mechanisms contribute to this phenomenon, furthermore it is heavily influenced by impurities in the solution. Therefore, to demonstrate the performance of the tracking controller in the presence of model errors, the nucleation rate parameter k_b is increased by 20%.

Again, the same plots are presented as for the previous simulation. In Figure 6.16, it can be seen that the final time requirements on weight mean size $L_{wm}(t_{end})$, crystal mass $m(t_{end})$ and length increase $\Delta L(t_{end})$ are met quite precisely. The trajectories of supersaturation $S(t)$, crystallizer temperature $T(t)$ and cooling jacket temperature $T_c(t)$ in Figure 6.17 are changed only slightly compared to the case without model error (see Figure 6.14) . However, there are two main differences.

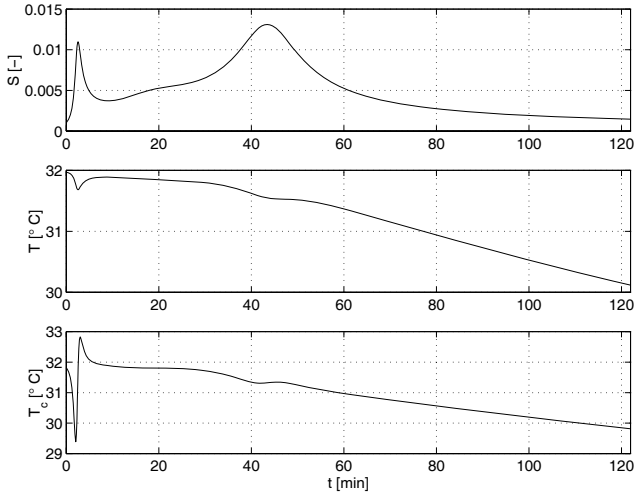

Figure 6.17: Supersaturation $S(t)$, crystallizer temperature $T(t)$ and cooling jacket temperature $T_c(t)$, with model error.

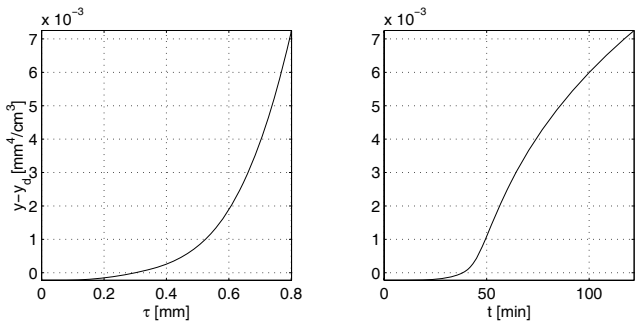

Figure 6.18: Tracking error $y - y_d$ vs. new time τ and vs. original time t, with model error.

First, the absolute tracking error $y(t) - y_d(t)$ in Figure 6.18 obviously does not converge to 0 any more. It can be shown that instead of the nominal error dynamics resulting from (6.39) and (6.40) a modified error equation is obtained with the modified nucleation rate $\bar{B} = k_{err} \cdot B$

$$y^{(6)} = k_{err} \left(y_d^{(6)} - q_5 \left(\frac{1}{k_{err}} y^{(5)} - y_d^{(5)} \right) - \sum_{i=0}^{4} q_i (y^{(i)} - y_d^{(i)}) \right) \tag{6.41}$$

or equivalently

$$\begin{aligned} (k_{err} - 1)(y_d^{(6)} + y_d^{(5)}) &= (y^{(6)} - y_d^{(6)}) + q_5 (y^{(5)} - y_d^{(5)}) + k_{err} \sum_{i=0}^{4} q_i (y^{(i)} - y_d^{(i)}) \\ &= e^{(6)} + q_5 e^{(5)} + k_{err} \sum_{i=0}^{4} q_i e^{(i)} \end{aligned} \tag{6.42}$$

where $e := y - y_d$. The left hand side of equation (6.42) is a third order polynomial in τ. If k_{err} is small enough the error dynamics is still stable and the tracking error $e(t)$ converges to a third order polynomial. However, as the desired trajectory is an eighth order polynomial it grows faster than the tracking error, such that the relative tracking error $(y(t) - y_d(t))/y_d(t)$ converges to 0. This also explains the excellent tracking of $L_{wm}(t)$ and $m(t)$ in Figure 6.16.

The second major difference is that the batch time t_{end} is increased considerably. The desired trajectory in the control law (6.40) is implemented in new time τ and it is assumed that τ, which is equivalent to the length increase ΔL, is measurable in the process. Hence, the duration of the batch is not fixed in original time t but in new time τ, i.e. the batch runs until $\tau = \tau_{end} = \Delta L_{end}$ is reached. With the model error in the nucleation rate, nucleation is increased. To stay close to the desired trajectory, supersaturation has to be lower than it had to be with the unperturbed model. Hence, the growth rate is lower and, therefore, the duration of the batch has to be longer to achieve the desired length increase ΔL_{end}.

6.6 Discussion

In this chapter, the control of batch crystallization processes was treated in the framework of differential flatness. It was shown that the time scaling involved in the verification of orbital flatness of the process model transforms the population balance equation into a

very simple form, namely a simple transport equation whose characteristics are straight lines. These two characteristic features of the batch crystallizer model - orbital flatness of the moment model and the simple structure of the time scaled population balance equation - allows a very elegant design of feedforward and feedback control laws.

Several control problems were solved using this approach. First, it was shown that for any given desired final CSD it can be decided whether this CSD is attainable and, if so, the corresponding temperature-time profile can be determined analytically. This problem was so far unsolved. A popular way to solve the feedforward control problem for batch crystallization processes is the use of dynamic optimization, where some *properties* of the CSD are optimized, rather than determining the entire shape of the CSD. In this context, it was shown that flatness can be used to simplify the optimization problem considerably by eliminating the differential equations describing the system dynamics. Finally, flatness was used to design feedforward *and* feedback controllers which make sure that given trajectories of the moments are tracked in the presence of uncertainties. For the feedback controller design the fact is exploited that flat systems are linearizable by feedback. The solution to each of these problems has been illustrated by an example. Hence, it was shown that batch control problems can be solved in a very elegant, model-based way using orbital flatness.

Chapter 7

Conclusion

7.1 Summary

Research in control of crystallization processes essentially focuses on two main problems resulting from the two ways to operate a crystallization plant, continuous or batch-wise. Continuous crystallizers are operated at steady state. Product quality is determined by the steady state CSD, which can be influenced by fines dissolution. Continuously operated DTB crystallizers have been reported to exhibit oscillatory behaviour especially if fines dissolution is employed. In this case, the desired steady state, at which one intends to operate the process, is unstable. This poses a stabilization problem which can be addressed using feedback control. In batch crystallization, product quality is determined by the CSD obtained at the end of the batch, which is influenced by the operation of the process during the entire batch-run. In batch cooling crystallization, the cooling rate is manipulated to shape the final CSD. This poses a problem of trajectory planning and feedforward control. In this thesis, new methods for the solution of both problems are presented. Both approaches are based on population balance models.

In their excellent review article, Rawlings et al. [87] asserted that, at that time, no attention had been paid to robustness issues in continuous crystallizer control. They identified this lack of up-to-date robust control theory as one of the major shortcomings in the area of continuous crystallizer control. This problem is addressed in this thesis by applying H_∞ robust control theory for infinite-dimensional systems developed by Foias et al. [24]. A relatively complex, detailed population balance model [66] is approximated by a population balance model with simpler kinetic expressions. Furthermore, since the process

is to be kept at its steady state, it is justified to linearize the model at this steady state. The structure of the simplified model is chosen such that it allows the derivation of a (transcendental) transfer function from manipulated input to measured output. For this transfer function the H_∞ mixed sensitivity problem is solved. This yields robustly stabilizing controllers for the simplified model. In simulation studies it is shown that, with a proper choice of weighting functions during the design process, controllers can be designed to stabilize also the original, more complex model. Apart from the robustness issues, the distinguishing feature of this approach is its late lumping philosophy, which does not involve discretization of the process model prior to controller synthesis.

The batch crystallizer control problem is addressed using a standard population balance model with empiric kinetic expressions [65], which allows the derivation of a moment model. The notion of differential flatness introduced in Fliess et al. [20] is very useful in the context of feedforward control problems. For flat systems, trajectory planning and design of feedforward control strategies can be solved in a very elegant way. It is shown that the moment model is not differentially flat but can be made flat by an appropriate time scaling, i.e. it is orbitally flat. The time scaled model does not answer the question "what is the state of the crystallizer after x minutes" but rather " what is its state after the crystals have been increased in length by x μm". This establishes a very natural notion of timing for a batch crystallizer. The same time scaling which renders the moment model flat makes the characteristics of the population balance model straight lines in the length – "time" domain. Due to this simple structure of the time scaled model it is possible to analytically determine the corresponding temperature trajectory in new time for any given desired final CSD. Only the last step of feedforward control design, i.e. inversion of the time scaling, may have to be done numerically. Based on these results, it can easily be checked whether a given final CSD can be attained under the given conditions. Furthermore, flatness can be used to significantly simplify dynamic optimization of final CSD, which has been the most common approach to batch crystallizer control. Finally, nonlinear feedback tracking controllers can be designed by feedback linearization to stabilize the system around a desired trajectory of moments.

7.2 Perspectives

For the future, there are several ways to continue and extend the work presented in this thesis. First, the control strategies, which have only been tested in simulations, should

be implemented in experiments. Of course, this requires a model for the specific process to be controlled. The derivation of a model, in turn, requires the availability of on-line measurements. In the area of measurement techniques for supersaturation and CSD, work at the Max-Planck-Institute is going on at present.

Second, it would be desirable to extend the results obtained for the batch case to less restrictive models. There is strong evidence, that this is possible for a class of systems with size dependent growth, where the growth law is a product of a size dependent term and a term depending on supersaturation. Then, analogous to the time scaling a length scaling can be used to transform the population balance equation to the same simple form as in the case of length independent growth. A remaining problem to be solved is that concentration c is a function of the third moment in original length coordinates but in general is not a function of moments in the new length.

Furthermore, the use of the distribution and amount of seed crystals to influence the final CSD could be investigated systematically using the flatness based approach. In the trajectory planning problem treated in Chapter 6.4, there would remain more parameters to be chosen freely than in the present case, where the seed distribution, i.e. the initial condition, is given.

Moreover, the start-up of continuously operated plants remains a challenge. Just as in the batch control problem, the system does not stay close to a steady state. The objective is to find suitable trajectories and control strategies to steer the system along these trajectories. It appears promising to investigate the use of the flatness based methods presented in Chapters 5 and 6 to the start-up problem.

Finally, other particulate processes exhibit similar problems as the ones encountered in crystallization. For example, sustained oscillations have been observed in granulation [38] or fermentation of cell cultures [117]. Both processes can be described by population balance models. Therefore, the approaches developed for crystallization in this thesis are potentially useful for other particulate processes as well.

Appendix A

Continuous Crystallizer

Two models for a continuous crystallizer are used in this thesis. This appendix summarizes the technical details for the detailed reference model presented in Chapter 2 as well as all parameter values for both the reference model and the simplified design model derived in Chapter 3. Parameter values correspond to the evaporative crystallization of Ammonium Sulphate $(NH_4)_2S0_4$ from aqueous solution in a draft tube baffled crystallization plant operated at the Laboratory for Process Equipment at Delft University of Technology [28, 43, 74].

A.1 Details for Reference Model

In the following, a complete list of expressions occurring in the reference model in Chapter 2 is given. In particular, this comprises the terms needed in the growth and attrition kinetics. For detailed derivations see [66] and the references therein.

Mass transfer coefficient for growth law:

$$\begin{aligned} k_d(L) &= \frac{D_{AB}}{L}\left(0.8\left(\frac{\bar{\varepsilon}L^4}{\nu_L^3}\right)^{1/5}\left(\frac{\nu_L}{D_{AB}}\right)^{1/3}+2\right) \\ \nu_L &= \frac{\eta_L}{\rho_L} \\ \rho_L &= c_L M_L \\ M_L &= x_{L,A}M_A + (1-x_{L,A})M_B \end{aligned}$$

Molar concentrations:

$$
\begin{aligned}
c_S &= \frac{\rho_A}{M_A} \\
c_B &= \frac{\rho_B}{M_B} \\
c_L &= \frac{n_L}{V_L} = \frac{\rho_A \rho_B}{x_{L,A} M_A \rho_B + (1 - x_{L,A}) M_B \rho_A} \\
c_{Feed,L} &= c_{L,sat} = \frac{\rho_A \rho_B}{x_{L,A,sat} M_A \rho_B + (1 - x_{L,A,sat}) M_B \rho_A} \\
c_{FD,L} &= \frac{\rho_A \rho_B}{x_{FD,L,A} M_A \rho_B + (1 - x_{FD,L,A}) M_B \rho_A} \\
x_{Feed,L,A} &= x_{L,A,sat} \\
c_{L,A,sat,ideal} &= \frac{x_{L,A,sat} \rho_A \rho_B}{x_{L,A,sat} M_A \rho_B + (1 - x_{L,A,sat}) M_B \rho_A} \\
n_{AZ,L} &= \frac{V_{AZ,L} \rho_A \rho_B}{x_{AZ,L,A} M_A \rho_B + (1 - x_{AZ,L,A}) M_B \rho_A} \\
c_{AZ,L} &= \frac{n_{AZ,L}}{V_{AZ,L}}
\end{aligned}
$$

Critical particle length for dissolution:

$$
\begin{aligned}
L_{crit} &= \frac{2 \gamma_{SL} M_A}{RT \ln(S_{rat}) \rho_A} \\
S_{rat} &= \frac{c_{L,A}}{c_{L,A,sat}} \\
\gamma_{SL} &= 0.414 k_B T (c_S N_A)^{2/3} \ln \frac{c_S}{c_{L,A}}
\end{aligned}
$$

Attrition kinetics:

$$
\begin{aligned}
\bar{\beta}(L,r) &= \frac{\dot{V}_{pump}}{V}\left(\eta_{geo,edge}(r)\eta_{tar,edge}(L,r)+\eta_{geo,blade}(r)\eta_{tar,blade}(L,r)\right)\\
\eta_{geo,edge/blade}(r) &= \frac{L_{tar,edge/blade}(r)a_{st}}{\pi R_{dt}^2}\\
L_{tar,edge/blade} &= b_{edge/blade}\frac{\eta_{edge/blade}}{\sin(\alpha(r))}\\
\eta_{edge}(r) &= \cos(\alpha(r)-\beta)\\
\eta_{blade}(r) &= |\sin(\alpha(r)-\beta)|\\
\alpha(r) &= \arctan\frac{w_{ax}}{w_{st}(r)}\\
w_{st}(r) &= 2\pi r\omega_{st}\\
w_{ax} &= \frac{\dot{V}_{pump}}{\pi R_{dt}^2}\\
\dot{V}_{pump} &= N_{pump}R_{st}^3\omega_{st}\\
\eta_{tar,edge/blade}(L,r) &= \left(\frac{\Psi_{edge/blade}(L,r)}{0.32+\Psi_{edge/blade}(L,r)}\right)^{2.1}\\
\Psi_{edge/blade}(L,r) &= \frac{(\rho_A-\rho_L)L^2w_\infty(r)}{18\eta_L L_{tar,edge/blade}(r)}\\
w_\infty(r) &= \sqrt{w_{ax}^2+w_{st}^2(r)}\\
V_{attr,edge/blade}(L,r) &= \frac{2H_V^{2/3}K_r}{3\mu_{shear}\Gamma}E_{kin,edge/blade}^{4/3}(L,r)\\
E_{kin,edge/blade}(L,r) &= \frac{\rho_A k_V L^3 w_{coll,edge/blade}^2(L,r)}{2}\\
w_{coll,edge/blade}(L,r) &= w_\infty(r)\eta_{tar,edge/blade}(L,r)\eta_{edge/blade}\\
f_{frag,edge/blade}(L',L,r) &= \left(h(L-L_{frag,min})-h(L-L_{frag,max,edge/blade}(L',r))\right)\\
&\quad\cdot\frac{2.25L^{-3.25}}{L_{frag,min}^{-2.25}-L_{frag,max,edge/blade}(L',r)}\\
L_{frag,min} &= \frac{48\mu_{shear}\Gamma}{\pi^{4/3}K_r H_V^2}\\
L_{frag,max,edge/blade}(L',r) &= \frac{3\cdot 2^{4/3}K_r^{1/3}E_{kin,edge/blade}^{4/9}(L',r)}{\pi^{4/3}\mu_{shear}^{1/3}\Gamma^{1/3}H_V^{1/9}}
\end{aligned}
$$

Volumetric flow rates:

$$\begin{aligned}
\dot{V}_{Product,L} &= \varepsilon_L \dot{V}_{Product} \\
\varepsilon_L &= \frac{V_L}{V} \\
\dot{V}_{Feed} &= \dot{V}_{Product} + \dot{V}_{vap} \\
\dot{V}_{AZ,out} &= \dot{V}_{FD,out} \\
\dot{V}_{AZ,in} &= \dot{V}_{AZ,out} + \dot{V}_{AZ,back} \\
\dot{V}_{AZ,back} &= k_V \int_0^\infty L^3 \dot{F}_{AZ,back}\, dL \\
\dot{V}_{AZ,L,in} &= \varepsilon_L \dot{V}_{AZ,in} \\
\dot{V}_{AZ,L,out} &= \varepsilon_{AZ,L} \dot{V}_{AZ,out} \\
\varepsilon_{AZ,S} &= \frac{V_{AZ,S}}{V_{AZ}} \\
\varepsilon_{AZ,L} &= \frac{V_{AZ,L}}{V_{AZ}}
\end{aligned}$$

Particle sink velocity in annular zone:

$$\begin{aligned}
v_s(L, \varepsilon_{AZ,S}) &= \frac{1-\varepsilon_{AZ,S}}{(1+\varepsilon_{AZ,S}^{1/3}) \exp\left(\frac{5\varepsilon_{AZ,S}}{3(1-\varepsilon_{AZ,S})}\right)} \left(-\frac{A(L)}{2} + \sqrt{\left(\frac{A(L)}{2}\right)^2 + B(L)} \right)^2 \\
A(L) &= \frac{4.8\sqrt{\eta_L}}{0.63\sqrt{L\rho_L}} \\
B(L) &= \frac{1}{0.63} \sqrt{\frac{4L(\rho_A - \rho_L)g}{3\rho_L}}
\end{aligned}$$

Annular zone volumes:

$$\begin{aligned}
V_{AZ} &= h_{AZ} \cdot A_{AZ} \\
V_{AZ,S} &= k_V \int_0^\infty L^3 F_{AZ}(L)\, dL
\end{aligned}$$

A.2 Parameters for Reference Model

The reference model has been developed in [66]. The corresponding parameter values and their original sources, where appropriate, can also be found there. For completeness, these values are listed here.

Description	Symbol	Value	Unit
General physical constants:			
ideal gas constant	R	8.314	$\frac{\text{J}}{\text{mol K}}$
Boltzmann's constant	k_B	$1.38 \cdot 10^{-23}$	$\frac{\text{J}}{\text{K}}$
Avogadro's number	N_A	$6.022 \cdot 10^{23}$	$\frac{1}{\text{mol}}$
Mechanical properties of ammonium sulphate crystals:			
shear modulus	μ_{shear}	$8.90 \cdot 10^{9}$	$\frac{\text{N}}{\text{m}^2}$
fraction resistance	Γ/K_r	2.8	$\frac{\text{J}}{\text{m}^2}$
vickers hardness	H_V	$3.55 \cdot 10^{8}$	$\frac{\text{N}}{\text{m}^2}$
Physical properties of ammonium sulphate and water			
density of solute (substance A, crystals)	ρ_A	$1.769 \cdot 10^{3}$	$\frac{\text{kg}}{\text{m}^3}$
density of solvent (substance B)	ρ_B	$0.987 \cdot 10^{3}$	$\frac{\text{kg}}{\text{m}^3}$
molecular weight solute (substance A)	M_A	$132.1 \cdot 10^{-3}$	$\frac{\text{kg}}{\text{mol}}$
molecular weight solvent (substance B)	M_B	$18.015 \cdot 10^{-3}$	$\frac{\text{kg}}{\text{mol}}$
volume shape factor (sphere)	k_V	0.524	–
diffusion coefficient	D_{AB}	$0.83 \cdot 10^{-9}$	$\frac{\text{m}^2}{\text{s}}$
dynamic viscosity of liquid phase	η_L	$2.1 \cdot 10^{-3}$	$\frac{\text{Ns}}{\text{m}^2}$
mole fraction at saturation	$x_{L,A,sat}$	0.10268	–
Physical properties related to crystal growth			
integration coefficient	k_r	$1.0 \cdot 10^{-5}$	$\frac{\text{m}^4}{\text{mol s}}$
surface related energy increase	Γ_S	$1.22 \cdot 10^{-4}$	$\frac{\text{J m}}{\text{mol}}$

Continued on next page

Continued from previous page

Description	Symbol	Value	Unit
Operation conditions			
temperature of slurry	T	323.15	K
volume of slurry	V	1.1	m^3
mean specific power input	$\bar{\varepsilon}$	2.3	$\frac{W}{kg}$
stirrer radius	R_{st}	0.2425	m
pumping capacity	N_{pump}	2.56	–
stirrer revolution speed	ω_{st}	370	$\frac{1}{min}$
number of stirrer blades	a_{st}	3	–
height of stirrer blade	b_{edge}	0.006	m
width of stirrer blade	b_{blade}	0.18	m
angle of stirrer blades	β	25	°
draft tube radius	R_{dt}	0.5	m
product removal flow rate (slurry)	$\dot{V}_{Product}$	880	$\frac{l}{h}$
volume loss due to evaporation	$\dot{V}_{vap}$	185.0	$\frac{l}{h}$
Operation conditions related to fines dissolution			
fines removal flow rate	$\dot{V}_{FD,out}$	10800	$\frac{l}{h}$
annular zone cross sectional area	A_{AZ}	0.761	m^2
annular zone height	h_{AZ}	1.018	m
residence time in fines dissolution	τ_{FD}	200	s

A.3 Parameters for Design Model

The design model is derived in Chapter 3. There, it is also discussed how appropriate parameter values are determined. These values are listed in the following table.

Description	Symbol	Value	Unit
in- and outflow rate	$\dot{V}_{Product}$	14.667	$\frac{\text{l}}{\text{min}}$
crystallizer volume	V	1100.0	l
annular zone volume	V_{AZ}	775.0	l
fines dissolution cut size	L_{FD}	100	μm
fines dissolution rate	$\dot{V}_{AZ,out}$	180.0	$\frac{\text{l}}{\text{min}}$
large crystal dissolution factor	$k_{FD,large}$	0.2	–
large crystal dissolution cut size	$L_{FD,large}$	950	μm
growth rate constant	k_g	$6.774 \cdot 10^3$	$\frac{\mu\text{m}}{\text{min}} \left(\frac{\text{l}}{\text{mol}}\right)^{1.6}$
growth rate exponent	g	1.6	–
growth rate corner size	L_{growth}	100	μm
negative growth rate constant	$k_{g,attr}$	$-2.111 \cdot 10^{-3}$	$\frac{\text{l}}{\text{min}}$
negative growth rate corner size	$L_{g,attr}$	550.0	μm
nucleation rate constant	k_b	$2.931 \cdot 10^{-11}$	$\frac{1}{\mu\text{m}^4\text{min}}$
nucleation rate exponent	b	4	–
crystal density	ρ_A	1769	$\frac{\text{g}}{\text{l}}$
mole mass	M_A	132.1	$\frac{\text{g}}{\text{mol}}$
volumetric shape factor	k_V	$\pi/6$	–
saturation concentration	$c_{L,A,sat}$	4.273	$\frac{\text{mol}}{\text{l}}$
inlet concentration	$c_{Feed,L,A}$	5.171	$\frac{\text{mol}}{\text{l}}$

Continued on next page

Continued from previous page

Description	Symbol	Value	Unit
smallest crystal length	L_0	16.5	μm
largest crystal length	L_{end}	1100	μm

Appendix B

Batch Crystallizer

The batch crystallizer model is presented in Chapter 5. The control design examples in Chapter 6 are worked out for the laboratory scale crystallization of potassium nitrate KNO_3 from water as described in [64]. The corresponding parameter values and their original sources, where appropriate, can also be found there. For completeness, these values are listed here.

Description	Symbol	Value	Unit
growth coefficient	k_g	$6.97 \cdot 10^3$	$\frac{\mu\text{m}}{\text{min}}$
growth exponent	g	1.32	–
nucleation coefficient	k_b	$3.47 \cdot 10^7$	$\frac{1}{\text{cm}^3\text{min}}$
nucleation exponent	b	1.78	–
volume shape factor	k_v	$1{\cdot}10^{-12}$	$\frac{\text{cm}^3}{\mu\text{m}^3}$
density of crystals	ρ_c	2.11	$\frac{\text{g}}{\text{cm}^3}$
conversion factor	h	1.246	$\frac{\text{cm}^3}{\text{g}_{\text{H}_2\text{O}}}$
heat transfer coefficient · area	UA_c	903.74	$\frac{\text{J}}{\text{min K}}$

Continued on next page

Continued from previous page

Description	Symbol	Value	Unit
volume of slurry	V	2056	cm^3
saturation parameters	A_0	0.1286	$\frac{\mathrm{g}_{\mathrm{KNO}_3}}{\mathrm{g}_{\mathrm{H_2O}}}$
	A_1	$5.88 \cdot 10^{-3}$	$\frac{\mathrm{g}_{\mathrm{KNO}_3}}{\mathrm{g}_{\mathrm{H_2O}}{}^{\circ}\mathrm{C}}$
	A_2	$1.721 \cdot 10^{-4}$	$\frac{\mathrm{g}_{\mathrm{KNO}_3}}{\mathrm{g}_{\mathrm{H_2O}}{}^{\circ}\mathrm{C}^2}$
parameters for heat of crystallization	B_0	-358.78	$\frac{\mathrm{J}}{\mathrm{g}_{\mathrm{KNO}_3}}$
	B_1	388.36	$\frac{\mathrm{J}\mathrm{g}_{\mathrm{H_2O}}}{\mathrm{g}^2_{\mathrm{KNO}_3}}$
	B_2	-418.27	$\frac{\mathrm{J}\mathrm{g}^2_{\mathrm{H_2O}}}{\mathrm{g}^3_{\mathrm{KNO}_3}}$
parameters for heat capacity	C_0	4.172	$\frac{\mathrm{J}}{\mathrm{g}_{\mathrm{solution}}\mathrm{K}}$
	C_1	-4.435	$\frac{\mathrm{J}}{\mathrm{g}_{\mathrm{solution}}\mathrm{K}}$
	C_2	4.213	$\frac{\mathrm{J}}{\mathrm{g}_{\mathrm{solution}}\mathrm{K}}$

Appendix C

Computations for the Derivation of Plant Transfer Function

As mentioned in Chapter 3.2.5, the PBE (3.24), the boundary condition (3.9) and the mole balance (3.26) are linearized with respect to the desired steady state with the fines flow rate $\dot{V}_{AZ,out}$ considered to be the system input. This leads - after some restructuring - to the following linear process model:

population balance

$$\begin{aligned}(V + V_{AZ})\frac{\partial \Delta f(L,t)}{\partial t} = \\ -V\left(\left.\frac{\partial^2 G(L,\sigma)}{\partial L\,\partial c_{L,A}}\right|_{ss} f_{ss}(L) + \left.\frac{\partial G(L,\sigma)}{\partial c_{L,A}}\right|_{ss} \frac{df_{ss}(L)}{dL}\right)\Delta\sigma(t) \\ -\left(V\frac{\partial G_{eff}(L,\sigma_{ss})}{\partial L} + \dot{V}_{out} + h_{FD}(L)\dot{V}_{FD,ss}\right)\Delta f(L,t) \\ -h_{FD}(L) f_{ss}(L)\Delta\dot{V}_{FD}(t) - VG_{eff}(L,\sigma_{ss})\frac{\partial \Delta f(L,t)}{\partial L}\end{aligned} \tag{C.1}$$

boundary condition

$$\begin{aligned}\Delta f(L = L_0, t) = \\ \frac{\Delta B(t)}{G_{eff}(L_0,\sigma_{ss})} - \frac{B_{ss}}{G_{eff}(L_0,\sigma_{ss})^2}\left.\frac{\partial G(L_0,\sigma)}{\partial c_{L,A}}\right|_{ss}\Delta\sigma(t)\end{aligned} \tag{C.2}$$

mole balance

$$\begin{aligned}\frac{d\Delta\sigma}{dt} = & \\ & \frac{\dot{V}_{out}}{V+V_{AZ}}\Delta\sigma(t) + \frac{3k_V\rho_A V}{\varepsilon_{ss}M_A(V+V_{AZ})}\int_{L_0}^{L_\infty} G_{attr}(L)L^2\Delta f(L,t)dL \\ & - \left(\frac{\dot{V}_{out}(M_A c_{Feed,L,A}-\rho_A)+3k_V\rho_A V\int_{L_0}^{L_\infty} G_{attr}(L)L^2 f_{ss}(L)dL}{\varepsilon_{ss}M_A(V+V_{AZ})}\right)\Delta\varepsilon \\ & + \frac{\rho_A - M_A c_{L,A,ss}}{\varepsilon_{ss}M_A}\frac{d\Delta\varepsilon(t)}{dt} \end{aligned} \tag{C.3}$$

The symbols $\Delta f(L,t)$, $\Delta\sigma(t)$, $\Delta B(t)$, $\Delta\dot{V}_{FD}(t)$ and $\Delta\varepsilon(t)$ denote the deviations of time dependent functions from their respective steady state values $f_{ss}(L,t)$, $\sigma_{ss}(t)$, B_{ss}, $\dot{V}_{FD,ss}(t)$ and $\varepsilon_{ss}(t)$. The time derivative of the volume fraction $\Delta\varepsilon(t)$ can be computed as follows

$$\frac{d\Delta\varepsilon(t)}{dt} = -k_V\int_{L_0}^{L_\infty}\frac{\partial\Delta f(L,t)}{\partial t}L^3 dL \tag{C.4}$$

with $\frac{\partial\Delta f(L,t)}{\partial t}$ according to (C.1). This linear model is then Laplace transformed. Thus, a first order ordinary differential equation with non-constant parameters with independent variable L is obtained from the linear PBE (C.1). This equation can be solved analytically which yields the following expression for the crystal size distribution

$$\begin{aligned}\Delta f(L,s) = & \\ & e^{A(L,s)}\left(\frac{\Delta B(s)}{G_{eff}(L_0,\sigma_{ss})} - \frac{B_{ss}}{G_{eff}(L_0,\sigma_{ss})^2}\left.\frac{\partial G(L_0,\Delta c)}{\partial c_{L,A}}\right|_{ss}\Delta\sigma(s)\right. \\ & - \int_{L_0}^{L}\frac{e^{A(\xi,s)}}{VG_{eff}(\xi,\sigma_{ss})}\left(h_{FD}(\xi)f_{ss}(\xi)\Delta\dot{V}_{FD}(s)\right. \\ & \left.\left. + V\left(\left.\frac{\partial^2 G(\xi,\sigma)}{\partial\xi\,\partial c_{L,A}}\right|_{ss} f_{ss}(\xi) + \left.\frac{\partial G(\xi,\sigma)}{\partial c_{L,A}}\right|_{ss}\frac{df_{ss}(\xi)}{d\xi}\right)\Delta\sigma(s)\right)\right)d\xi \end{aligned} \tag{C.5}$$

where s is the complex Laplace variable and

$$A(L,s) = \int_{L_0}^{L}\frac{s(V+V_{AZ}) + V\left.\frac{\partial G_{eff}(\xi\Delta c)}{\partial\xi}\right|_{ss} + \dot{V}_{out} + h_{FD}(\xi)\dot{V}_{FD,ss}}{VG_{eff}(\xi\sigma_{ss})}d\xi. \tag{C.6}$$

With the piecewise linear expressions for the growth rates (3.1) and (3.3) the integrals in the above equations can be computed analytically. This is done with a computer algebra

system and leads to rather lengthy expressions that are therefore omitted here. However, the solution for the crystal size distribution is of the form

$$\Delta f(L,s) = \Phi_1(L,s)\Delta\sigma(s) + \Phi_2(L,s)\Delta B(s) + \Phi_3(L,s)\Delta\dot{V}_{FD}(s). \tag{C.7}$$

The measured output is the third moment of the distribution, i.e.

$$\begin{aligned} \Delta m_3(s) &= \int_{L_0}^{L_\infty} L^3 \Delta f(L,s) dL \\ &= \Psi_{3,1}(s)\Delta\sigma(s) + \Psi_{3,2}(s)\Delta B(s) + \Psi_{3,3}(s)\Delta\dot{V}_{FD}(s). \end{aligned} \tag{C.8}$$

The nucleation rate is proportional to the fourth moment of the size distribution (3.10)

$$\begin{aligned} \Delta B(s) &= k_b \int_{L_0}^{L_\infty} L^4 \Delta f(L,s) dL \\ &= k_b(\Psi_{4,1}(s)\Delta\sigma(s) + \Psi_{4,2}(s)\Delta B(s) + \Psi_{4,3}(s)\Delta\dot{V}_{FD}(s)), \end{aligned} \tag{C.9}$$

where the functions $\Psi_{k,i}(s)$ are defined as

$$\Psi_{k,i}(s) = \int_{L_0}^{L_\infty} L^k \Phi_i(L,s) dL, \; i = 1 \cdots 3, \; k = 3,4. \tag{C.10}$$

Inserting the expression for the size distribution $\Delta f(L,s)$ (C.7) in the Laplace transformed version of the linearized mole balance (C.3) and solving it for the concentration $\Delta\sigma(s)$ leads to an equation of the form

$$\Delta\sigma(s) = \Gamma_1(s)\Delta B(s) + \Gamma_2(s)\Delta\dot{V}_{FD}(s). \tag{C.11}$$

Finally, a transfer function from manipulated input $\Delta\dot{V}_{FD}(s)$ to measured output $\Delta m_3(s)$ can be obtained from equations (C.8), (C.9) and (C.11) by eliminating $\Delta\sigma(s)$ and $\Delta B(s)$. This concludes the derivation of the plant transfer function $P(s)$ in (3.31).

Appendix D

Notation

Abbreviations

CSD	crystal size distribution
DTB	draft tube baffled
PBE	population balance equation
PDE	partial differential equation
ODE	ordinary differential equation

D.1 Continuous Crystallization, Chapters 2-4

Latin Symbols

$A(L)$	auxiliary variable for particle sink velocity	$\sqrt{m/s}$
A_{AZ}	cross sectional area of annular zone	m^2
a_m	gain margin in controller design	-
a_{st}	number of stirrer blades	-
$B(L)$	auxiliary variable for particle sink velocity	m/s
$B(t)$	birth (nucleation) rate (design model)	1/s
b	nucleation rate exponent (design model)	-
b_{blade}	width of stirrer blade	m
b_{edge}	width of stirrer edge	m
C	constant in expression for steady state size distribution	1/m
$C(s)$	controller transfer function	$(m^3/s)/m^3$
c	molar concentration	mol/m^3

Continued on next page

Continued from previous page

D_{AB}	diffusion coefficient	m^2/s
D_{dis}	dissolution rate	1/s
$E(s)$	auxiliary function in controller design	-
E_{kin}	kinetic energy	J
F	number density function	1/m
$\dot{F}$	number density flux	1/(m s)
$F(s)$	auxiliary function in controller design	-
f_{frag}	volume based number density function	$1/(m\ m^3)$
$G(\sigma, L)$	growth rate	m/s
g	acceleration of gravity	m/s^2
g	growth rate exponent (design model)	-
H_V	Vicker's hardness	N/m^2
$H(s)$	auxiliary function in controller design	-
h_{AZ}	height of annular zone	m
$h_{FD}(L)$	fines dissolution classification function (design model)	-
K_r	crack efficiency	-
k_B	Boltzmann constant	J/K
k_b	nucleation rate constant (design model)	$1/(\mu m^4\ min)$
k_d	mass transfer coefficient	m/s
k_g	growth rate constant (design model)	$\mu m/min\ (l/mol)^{1.6}$
$k_{g,attr}$	negative growth rate constant (design model)	m
$k_{FD,large}$	large crystal dissolution factor (design model)	-
k_r	integration coefficient	$m^4/(mol\ s)$
k_V	volume shape factor	-
L	characteristic crystal length	m
L_0	smallest crystal length (design model)	m
L_{50}	mass median crystal length	m
L_{crit}	critical crystal length for dissolution	m
L_{end}	largest crystal length (design model)	m
L_{growth}	growth rate corner size (design model)	m
L_{tar}	projected length of stirrer edge	m
$L(s)$	auxiliary function in controller design	-
M	molar mass	kg/mol
$M(s)$	plant transfer function factor	

Continued on next page

Continued from previous page

m_3	third moment of size distribution	m^3
$mdf(L,t)$	mass density function	kg/m
N	amount (number)	-
$N(s)$	plant transfer function factor	
N_A	Avogadro constant	1/mol
N_{pump}	pumping capacity	-
n	number of moles	mol
$\dot{n}$	molar flux	mol/s
$P(s)$	plant transfer function	$m^3/(m^3/s)$
$\mathcal{P}$	set of transfer functions	
R	ideal gas constant	J/(mol K)
R_{dt}	radius of draft tube	m
R_{st}	stirrer radius	m
r	radial position on stirrer	m
$S(s)$	closed loop sensitivity transfer function	-
S_{rat}	supersaturation (ratio of concentrations)	-
s	Laplace variable	1/s
$s_k,\ k = 1, 2, \ldots$	transfer function poles	1/s
T	temperature	K
t	time	s
V	volume	m^3
$\dot{V}$	volumetric flow rate	m^3/s
v_s	particle sink velocity	m/s
$W_d(s)$	weighting function in controller design	-
$W_m(s)$	weighting function in controller design	-
w	velocity	m/s
x	mole fraction	-
z	discrete frequency variable	-
$z_k,\ k = 1, 2, \ldots$	transfer function zeros	1/s

Greek Symbols

$\alpha(r)$	approach angle of crystal towards stirrer	$^\circ$
α_m	phase margin in controller design	$^\circ$
β	stirrer blade angle	$^\circ$

Continued on next page

Continued from previous page

$\bar{\beta}(L,r)$	stirrer radius based attrition rate	1/(s m)
$\beta(L)$	attrition rate	1/s
Γ	fracture resistance	J/m^2
Γ_S	surface related energy increase	J m/mol
γ	performance index in H_∞ controller design	-
γ_{SL}	surface tension	J/m^2
Δ	deviation from steady state	
$\Delta(s)$	model uncertainty	
ε	volume fraction	-
$\bar{\varepsilon}$	mean specific power input	W/kg
η_L	dynamic viscosity	N s/m^2
η_{geo}	effective fractional area	-
η_{tar}	collision probability between crystal and stirrer	-
λ	parameter in bilinear transform	1/s
μ_{shear}	shear modulus	N/m^2
ν_L	kinematic viscosity	m^2/s
ρ	density	kg/m^3
σ	absolute supersaturation	mol/m^3
τ	residence time	s
Ψ	stokes separation number	-
ω	angular frequency	rad/s
ω_{st}	stirrer rotational velocity	1/s

Subscripts

A	component A (solute)
AZ	annular settling zone
$attr$	attrition
B	component B (solvent)
b	birth (nucleation)
cf	coprime factor uncertainty
dis	dissolution
dt	draft tube
eff	effective
FD	fines dissolution

Continued on next page

Continued from previous page

$frag$	fragment
g	growth
L	liquid
m	multiplicative uncertainty
opt	optimal
P	particle
S	solid
sat	saturation
ss	steady state
st	stirrer
vap	vapour
Δ	with uncertainty

D.2 Batch Crystallization, Chapters 5-6

Latin Symbols

$a_i,\ i = 1, 2..8$	coefficients for trajectory planning	
B	birth (nucleation) rate	1/(m m^3)
c	solute mass concentration	(kg solute)/(kg solvent)
c_p	heat capacity of slurry	J/K
f	volume based number density function	1/(m m^3)
f_s	part of CSD originating from seeds	1/(m m^3)
f_n	part of CSD originating from nucleation	1/(m m^3)
G	growth rate	m/s
ΔH_c	heat of crystallization	J/kg
h	conversion factor	(m^3 slurry)/(kg solvent)
k_b	birth (nucleation) rate coefficient	1/(m^3 s)
k_{err}	model error parameter	-
k_g	growth rate coefficient	m/s
k_v	volume shape factor	-
L	characteristic crystal length	m
L_{wm}	mean crystal size (mass based)	m
ΔL_{end}	length increase of crystals over complete batch	m

Continued on next page

Continued from previous page

m	mass (of crystals)	kg
N	number (of crystals)	-
$q_i,\ i = 1, 2..5$	coefficients for closed loop error dynamics	
S	relative supersaturation	-
$s(t)$	time scaling function	s/m
T	slurry temperature	°C
T_c	coolant temperature	°C
t	time	s
t_{end}	duration of batch	s
UA_c	heat transfer coefficient · heat transfer area	J/(s K)
V	volume of slurry	m^3
v	new input in flatness based feedback control	
y	flat output	

Greek Symbols

μ_i	ith moment of CSD	m^i/m^3
ρ_c	crystal density	kg/m^3
ρ	density of slurry	kg/m^3
τ	scaled time	m

Subscripts

0	initial condition
d	desired value
n	resulting from nucleation
s	resulting from seeds
sat	saturation

Bibliography

[1] M.B. Ajinkya and W.H. Ray. On the optimal operation of crystallization processes. *Chem. Eng. Comm.*, 1:181–186, 1974.

[2] B.E. Anshus and E. Ruckenstein. On the stability of a well mixed isothermal crystallizer. *Chem. Eng. Sci*, 28:501–513, 1973.

[3] Aristotle. *The Nicomachean Ethics, Book I, 3*. Oxford University Press, 1925. translated by W.D. Ross.

[4] S. Arunsawatwong. Stability of retarded delay differential systems. *Int J. Contr.*, 65(2):347–364, 1996.

[5] J.R. Beckmann and A.D. Randolph. Crystal size distribution dynamics in a classified crystallizer: Part II. Simulated control of crystal size distribution. *AIChE J.*, 23(4):510–520, 1977.

[6] S.K. Bermingham, A.M. Neumann, P.J. Verheijen, and H.J.M Kramer. Measuring and modeling the classification and dissolution of fine crystals in a dtb crystallizer. In *Proc. 14th Int. Symp. Ind. Cryst.*, Cambridge, UK, Sept. 1999.

[7] Y.A. Buyevich, V.V. Mansurov, and I.A. Natalukha. Instability and unsteady processes of the bulk continuous crystallization - i. linear stability analysis. *Chem. Eng. Sci.*, 46(10):2573–2578, 1991.

[8] C-T. Chang and M.A. Epstein. Simulation studies of a feedback control strategy for batch crystallizers. *AIChE Symp. Series*, 83:110–119, 1987.

[9] T. Chiu and P.D. Christofides. Nonlinear control of particulate processes. *AIChE J.*, 45(6):1279, 1999.

[10] T. Chiu and P.D. Christofides. Robust nonliner control of a continuous crystallizer. *Comp. Chem. Eng.*, Supplement:S257–S260, 1999.

[11] T. Chiu and P.D. Christofides. Robust control of particulate processes using uncertain population balances. *AIChE J.*, 46(2):266–280, 2000.

[12] S.H. Chung, D.L. Ma, and R.D. Braatz. Optimal seeding in batch crystallization. *Can. J. Chem. Eng.*, 77:590–596, 1999.

[13] D.D. Dunuwila and K.A. Berglund. ATR FTIR spectroscopy for in situ measurement of supersaturation. *J. Crystal Growth*, 179(1-2):185–193, 1997.

[14] R.A. Eek. *Control and Dynamic Modelling of Industrial Suspension Crystallizers*. PhD thesis, TU Delft, 1995.

[15] R.A. Eek and O.H. Bosgra. Controllability of particulate processes in relation to the sensor characteristics. *Powder Technology*, 108:137–146, 2000.

[16] R.A. Eek, S. Dijkstra, and G.M. van Rosmalen. Dynamic modeling of suspension crystallizers, using experimental data. *AIChE J.*, 41(3):571–584, 1995.

[17] R.A. Eek, H.A.A. Pouw, and O.H. Bosgra. Design and experimental evaluation of stabilizing feedback controllers for continuous crystallizers. *Powder Technology*, 82:21–35, 1995.

[18] M.A.F. Epstein and L. Sowul. Phase space analysis of limit cycle development in cmsmpr crystallizers using three-dimensional computer graphics. *AIChE Symp. Series*, 76(193):6–17, 1980.

[19] M. Fliess. Oral statement at the course "Flatness based control of distributed parameter systmes", Magdeburg, Feb. 2003.

[20] M. Fliess, J. Lévine, P. Martin, and P. Rouchon. On differentially flat nonlinear systems. In *Nonlinear Control Systems Design*, pages 408–412. Pergamon Press, 1992.

[21] M. Fliess, J. Lévine, P. Martin, and P. Rouchon. Design of trajectory stabilizing feedback for driftless flat systems. In *Proc. 3rd European Control Conference ECC '95*, pages 1882–1887, 1995.

[22] M. Fliess, J. Lévine, P. Martin, and P. Rouchon. Flatness and defect of nonlinear systems: Introductory theory and examples. *Int. J. Contr.*, 61:1327–1361, 1995.

[23] M. Fliess, J. Lévine, P. Martin, and P. Rouchon. A Lie-Bäcklund approach to equivalence and flatness of nonlinear systems. *IEEE Trans. Automatic Control*, 44: 922–937, 1999.

[24] C. Foias, H. Özbay, and A. Tannenbaum. *Robust Control of Infinite Dimensional Systems*. Springer, 1996.

[25] B.A. Francis. *A Course in H_∞ Control*. Number 88 in Lecture Notes in Control and Information Sciences. Springer-Verlag, Berlin, 1987.

[26] C. Gahn and A. Mersmann. Brittle fracture in crystallization processes. part A. Attrition and abrasion of brittle solids. *Chem. Eng. Sci.*, 54(9):1273–1282, 1999.

[27] C. Gahn and A. Mersmann. Brittle fracture in crystallization processes. part B. Growth of fragments and scale-up of suspension crystallizers. *Chem. Eng. Sci.*, 54 (9):1283–1292, 1999.

[28] J.H. Gerla. *Modelling, measurement and manipulation of crystallizers*. PhD thesis, TU Delft, 1995.

[29] A. Gerstlauer, A. Mitrović, S. Motz, and E.-D. Gilles. A population model for crystallization processes using two independent particle properties. *Chem. Eng. Sci.*, 56(7):2553–2565, 2001.

[30] A. Gerstlauer, S. Motz, A. Mitrović, and E.-D. Gilles. Development, analysis and validation of population models for continuous and batch crystallizers. *Chem. Eng. Sci.*, 57:4311–4327, 2002.

[31] E.D. Gilles and U. Knöpp. Skriptum zur Vorlesung Regelungstechnik I. Universität Stuttgart, Institut für Systemdynamik und Regelungstechnik, 1988.

[32] K. Glover and D. McFarlane. Robust stabilization of normalized coprime factor plant descriptions with H_∞ bounded uncertainty. *IEEE Trans. Automatic Control*, 34(8), 1989.

[33] M. Green and D.J.N. Limebeer. *Linear Robust Control*. Prentice Hall, 1995.

[34] G. Gu, P. Khargonekar, and E. B. Lee. Approximation of infinite-dimensional systems. *IEEE Trans. Automatic Control*, 34(6):610–618, 1989.

[35] M. Guay. An algorithm for orbital feedback linearizaton of single-input control affine systems. *Systems Control Lett.*, 38:271–281, 1999.

[36] M. Guay, S. Kansal, and J.F. Forbes. Trajectory optimization for flat dynamic systems. *Ind. Eng. Chem. Res.*, 40(9):2089–2102, 2001.

[37] R. Hashemi and M.A. Epstein. Observability and controllability considerations in crystallization process design. *AIChE Symp. Ser.*, 78(215):81–90, 1982.

[38] S. Heinrich, M. Peglow, M. Ihlow, M. Henneberg, and L. Mörl. Analysis of the start-up process in continuous fluidized bed spray granulation by population balance modelling. *Chem. Eng. Sci.*, 57:4369–4390, 2002.

[39] K. Heiskanen. On the difficulties of implementing particle size control in particulate processes. *Powder Technology*, 82:13–19, 1995.

[40] H.M. Hulburt and S. Katz. Some problems in particle technology. a statistical mechanical formulation. *Chem. Eng. Sci.*, 19:555–574, 1964.

[41] A. Isidori. *Nonlinear Control Systems*. Springer-Verlag, 3rd edition, 1995.

[42] F. Jadot, Ph. Martin, and P. Rouchon. Industrial sensorless control of induction motors. In A. Isidori, F. Lamnabhi-Lagarrigue F, and W. Respondek, editors, *Nonlinear Control in the Year 2000, Vol. 1*, pages 535–544. Springer-Verlag, 2001.

[43] J. Jager. *Control of industrial crystallizers*. PhD thesis, TU Delft, 1990.

[44] J. Jager, H.J.M Kramer, E.J. de Jong, S. de Wolf, O.H. Bosgra, A. Boxman, H.G. Merkus, and B. Scarlett. Control of industrial crystallizers. *Powder Technology*, 69:11–20, 1992.

[45] G.R. Jerauld, Y. Vasatis, and M.F. Doherty. Simple conditions for the appearance of sustained oscillations in continuous crystallizers. *Chem. Eng. Sci.*, 38:1673–1681, 1983.

[46] A.G. Jones. Optimal operation of a batch cooling crystallizer. *Chem. Eng. Sci.*, 29: 1075–1087, 1974.

[47] A.G. Jones and A. Chianese. Fines destruction during batch crytsallization. *Chem. Eng. Comm.*, 62:5–16, 1987.

[48] A.G. Jones and J.W. Mullin. Programmed cooling crystallization of potassium sulphate solutions. *Chem. Eng. Sci.*, 29:105–118, 1974.

[49] M. Kind and U. Nieken. On the dynamic simulation of mass crystallization with fines removal. *Chem. Eng. Process.*, 34:323 – 328, 1995.

[50] B.G. Lakatos. Stability and dynamics of continuous crystallizers. *Comp. Chem. Eng.*, 18(Suppl.):S427–S431, 1994.

[51] Y. Lang, A.M. Cervantes, and L.T. Biegler. Dynamic optimization of a batch cooling crystallization process. *Ind. Eng. Chem. Res.*, 38:1469–1477, 1999.

[52] S.-J. Lei, R. Shinnar, and S. Katz. The regulation of a continuous crystallizer with fines trap. *Chem. Eng. Prog. Symp. Ser.*, 67(110):129–144, 1971.

[53] S.-J. Lei, R. Shinnar, and S. Katz. The stability and dynamic behavior of a continuous crystallizer with a fines trap. *AIChE J.*, 17(6):1459–1470, 1971.

[54] F. Lewiner, J.P. Klein, F. Puel, and G. Fevotte. On-line ATR FTIR measurement of supersaturation during solution crystallization processes. Calibration and applications on three solute/solvent systems. *Chem. Eng. Sci.*, 56(6):2069–2084, 2001.

[55] M. Löffelmann and A. Mersmann. How to measure supersaturation? *Chem. Eng. Sci.*, 57(20):4301–4310, 2001.

[56] D.L. Ma and D. Braatz. Worst-case analysis of finite-time control policies. *IEEE Trans. Automatic Control*, 9:766–774, 2001.

[57] D.L. Ma and D. Braatz. Robust identification and control of batch processes. *Comp. Chem. Eng.*, 27(8-9), 2003.

[58] R. Mahadevan, S.K. Agrawal, and F.J. Doyle. Differential flatness based nonlinear predictive control of fed-batch bioreactors. *CONTROL ENG PRACT*, 9:889–899, 2001.

[59] Ph. Martin, S. Devasia, and B. Paden. A different look at output tracking: Control of a vtol aircraft. *Automatica*, 32:101–107, 1996.

[60] B. Mayrhofer and J. Nyvlt. Programmed cooling of batch crystallizers. *Chem. Eng. Process.*, 24:217–220, 1988.

[61] R.O. Meadhra. *Modelling of the Kinetics of Suspension Crystallizers*. PhD thesis, TU Delft, 1995.

[62] A. Mersmann, editor. *Crystallization Technology Handbook*. Dekker, New York, 1995.

[63] A. Mersmann, M. Angelhöfer, T. Gutwald, R. Sangl, and S.Wang. General prediction of median crystal sizes. *Sep. Technol.*, 2:85–97, 1992.

[64] S.M. Miller. *Modelling and Quality Control Strategies for Batch Cooling Crystallizers*. PhD thesis, University of Texas, Austin, 1993.

[65] S.M. Miller and J.B. Rawlings. Model identification and control strategies for batch cooling crystallizers. *AIChE Journal*, 40(8):1312–1327, 1994.

[66] A. Mitrović. *Population Balance Based Modelling, Simulation, Analysis and Control of Crystallization Processes*. PhD thesis, ISR, Universität Stuttgart, 2002. VDI-Fortschritt-Berichte 3/749, VDI-Verlag.

[67] S. Motz, J.Eggers, and E.D. Gilles. Model-based operation of batch crystallizers. In *Proc. 15th Int. Symp. Ind. Cryst.*, volume 3, pages 1173–1179, 2002.

[68] S. Motz, A. Mitrović, E.-D. Gilles, U. Vollmer, and J. Raisch. Modeling, simulation and stabilizing H_∞-control of an oscillating continuous crystallizer with fines dissolution. *Chem. Eng. Sci.*, 58:3473–3488, 2003.

[69] J.W. Mullin. *Crystallization*. Butterworth-Heinemann, Oxford, 3rd edition, 1997.

[70] J.W. Mullin and J. Nývlt. Programmed cooling of batch crystallizers. *Chem. Eng. Sci.*, 26, 1971.

[71] A.S. Myerson, editor. *Handbook of Industrial Crystallization*. Butterworth-Heinemann, Boston, 2nd edition, 2002.

[72] A.S. Myerson, S. Rush, F.J. Schork, and J.L. Johnson. Control of crystallization processes. In J. Nývlt and S. Žáček, editors, *Industrial Crystallization 87*, pages 407–410, 1987.

[73] J.A. Nelder and R. Mead. A simplex method for function minimization. *Computer Journal*, 7:308–313, 1965.

[74] A.M Neumann. *Characterizing industrial crystallizers of different scale and type*. PhD thesis, TU Delft, 2001.

[75] A.M. Neumann, S.K. Bermingham, H.J.M. Kramer, and G.M. van Rosmalen. Modeling industrial crystallizers of different scale and type. In *Proc. 14th Int. Symp. Ind. Cryst.*, Cambridge, UK, Sept. 1999.

[76] A.M. Neumann and H.J.M. Kramer. A comparative study of various size distribution measurement systems. *Part. Part. Syst. Char.*, 19(1):17–27, 2002.

[77] H. Nijmeijer and A.J. van der Schaft. *Nonlinear Dynamical Control Systems*. Springer-Verlag, 1990.

[78] H. Özbay. H_∞ optimal controller design for a class of distributed parameter systems. *Int J. Contr.*, 58(4):739–782, 1993.

[79] H. Özbay. A matlab based program for H_∞ optimal/suboptimal controller design. *http://eewww.eng.ohio-state.edu/∼ozbay/HINFCON.txt*, 1998.

[80] R.-Y. Qian and G.D. Botsaris. Laboratory simulation of industrial crystallizer cycling. *Ind. Eng. Chem. Res.*, 35(4):1163–1172, 1996.

[81] D. Ramkrishna. The status of population balances. *Rev. in Chem. Eng.*, 3:49–95, 1985.

[82] D. Ramkrishna. *Population balances: theory and applications to particulate systems in engineering*. Academic Press, 2000.

[83] A.D. Randolph, J.R. Beckmann, and Z.I. Kraljevich. Crystal size distribution dynamics in a classified crystallizer: Part I. Experimental and theoretical study of cycling in a potassium chloride crystallizer. *AIChE J.*, 23:500–509, 1977.

[84] A.D. Randolph, L. Chen, and A. Tavana. Feedback control of csd in a kcl crystallizer with a fines dissolver. *AIChE J.*, 33(4):583–591, 1987.

[85] A.D. Randolph and M.A. Larson. A population balance for countable entities. *Can. J. Chem. Eng.*, 42:280–281, 1964.

[86] A.D. Randolph and M.A. Larson. *Theory of Particulate Processes*. Academic Press, Inc., 1988.

[87] J.B. Rawlings, S.M. Miller, and W.R. Witkowski. Model identification and control of solution crystallization processes: A review. *Ind. Eng. Chem. Res.*, 32:1275–1296, 1993.

[88] T.P. Redman, S. Rohani, and G. Strathdee. On-line control of supersaturation in a continuous cooling kcl crystallizer. *Can. J. Chem. Eng.*, 73:725–733, 1995.

[89] W. Respondek. Orbital feedback linearization of single-input nonlinear control systems. In *Proc. of IFAC NOLCOS'98*, pages 499–504, Enschede, The Netherlands, 1998.

[90] S. Rohani, M. Haeri, and H.C. Wood. Modelling and control of a continuous crystallization process, part 1 and 2. *Comp. Chem. Eng.*, 23(3):263–277, 1999.

[91] S. Rohani, N.S. Tavare, and J. Garside. Control of crystal size distribution in a batch cooling crystallizer. *Can. J. Chem. Eng.*, 68:260–267, 1990.

[92] R. Rothfuß. *Anwendung der flachheitsbasierten Analyse und Regelung nichtlinearer Mehrgrößensysteme*. PhD thesis, ISR, Universität Stuttgart, 1997. VDI-Fortschritt-Berichte 8/664, VDI-Verlag.

[93] R. Rothfuß, J. Rudolph, and M. Zeitz. Flatness based control of a nonlinear chemical reactor model. *Automatica*, 32(10):1433–1439, 1996.

[94] P. Rouchon, M. Fliess, J. Lévine, and P. Martin. Flatness and motion planning: the car with n trailers. In *Proc. 2nd European Control Conference ECC '93*, pages 1518–1522, 1993.

[95] J. Rudolph. Boundary control of heat exchangers with spatially distributed parameters: a flatness-based approach. *Automatisierungstechnik*, 48(8):399–402, 2000.

[96] J. Rudolph and H. Mounier. Trajectory tracking for pi -flat nonlinear delay systems with a motor example. In A. Isidori, F. Lamnabhi-Lagarrigue F, and W. Respondek, editors, *Nonlinear Control in the Year 2000, Vol. 2*, pages 339–351. Springer-Verlag, 2001.

[97] A. Ruf, J. Worlitschek, and M. Mazzotti. Modeling and experimental analysis of PSD measurements through FBRM. *Particle and Particle Systems Characterization*, 17(4), 2000.

[98] D. Semino and W.H. Ray. Control of systems described by population balance equations – I. controllability analysis. *Chem. Eng. Sci.*, 50(11):1805–1824, 1995.

[99] M.B. Sherwin, R. Shinnar, and S. Katz. Dynamic behavior of the well-mixed isothermal crystallizer. *AIChE J.*, 13(6):1141 – 1153, 1967.

[100] Y.H. Song and J.M. Douglas. Self-generated oscillations in continuous crystallizers: Part II. An experimental study of an isothermal system. *AIChE J.*, 21:924–930, 1975.

[101] G. Strathdee T. Redman T, S. Rohani S. Control of the crystal mean size in a pilot plant potash crystallizer. *Chem. Eng. Res. Des.*, 75(2):183–192, 1997.

[102] A. Tadayyon and S. Rohani. Extended kalman filter-based nonlinear model predictive control of a continuous KCl-NaCl crystallizer. *Can. J. Chem. Eng.*, 79(2): 255–262, 2001.

[103] N.S. Tavare. *Industrial Crystallization : Process Simulation, Analysis and Design*. Plenum Press, New York, 1995.

[104] S. Tsuruoka and A.D. Randolph. State space representation of the dynamic crystallizer population balance. application to csd controller design. *AIChE Symp. Series*, 83(253):104–109, 1987.

[105] M. Ulrich. Optimization of batch solution crystallization. *Ger. Chem. Eng.*, 4: 195–200, 1979.

[106] B. van Keulen. *H_∞-Control for Infinite-Dimensional Systems: A State-Space Approach* . PhD thesis, Rijksuniversiteit Groningen, 1993.

[107] U. Vollmer and J. Raisch. Stabilizing control of an oscillatory crystallizer. In *4th Topical Conference on Separations Science and Technology*, Dallas, USA, 1999. AIChE.

[108] U. Vollmer and J. Raisch. H_∞-control of a continuous crystallizer. *Cont. Eng. Prac.*, 9(8):837–845, 2001.

[109] U. Vollmer and J. Raisch. Controller design for an oscillatory dtb crystallizer based on a population balance model. In A. Chianese, editor, *Proceedings of 15th International Symposium on Industrial Crystallization*, pages 1233–1239, Sorrento, Italy, 2002.

[110] U. Vollmer and J. Raisch. Population balance modelling and H_∞- controller design for a crystallization process. *Chem. Eng. Sci.*, 57:4401–4414, 2002.

[111] U. Vollmer and J. Raisch. Control of batch cooling crystallisers based on orbital flatness. *Int. J. Contr.*, 76(16):1635–1643, 2003.

[112] U. Vollmer and J. Raisch. Feedforward control of batch crystallisers - an approach based on orbital flatness. In *ADCHEM International Symposium on Advanced Control of Chemical Processes, Preprints*. IFAC, 2003.

[113] W. Xie, S. Rohani, and A. Phoenix. Dynamic modeling and operation of a seeded batch cooling crystallizer. *Chem. Eng. Comm.*, 187:229–249, 2001.

[114] D. Youla, H. Jabr, and J. Bongiorno. Modern Wiener-Hopf design of optimal controllers, Part 2: the multivariable case. *IEEE Trans. Automatic Control*, 21:319–338, 1976.

[115] G.P. Zhang and S. Rohani. On-line optimal control of a seeded batch crystallizer. *Chem. Eng. Sci.*, 58:1887–1896, 2003.

[116] K. Zhou, J.C. Doyle, and K. Glover. *Robust and optimal control*. Prentice Hall, 1996.

[117] G.-Y. Zhu, A. Zamamiri, M. Henson, and M. Hjortsø. Model predictive control of continuous yeast bioreactors using cell population balance models. *Chem. Eng. Sci*, 55:6155–6167, 2000.